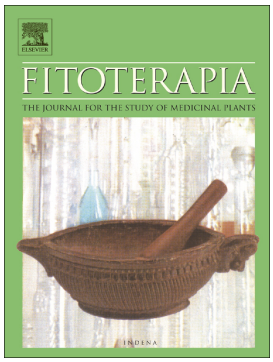

Antileishmanial, antitrypanosomal and anti-coronavirus activities of benzophenanthridine alkaloids and other specialized metabolites isolated from the root bark of Zanthoxylum zanthoxyloides (Lam.) B.Zepernick & Timler

Abda Ba, Vincent Roumy, Malak Al Ibrahim, Kristelle Hughes, Thierry Hennebelle, Jennifer Samaillie, Sevser Sahpaz, Mehdi A. Beniddir, Marie-France Hérent, Karin Séron, Joëlle Quetin Leclercq, Matar Seck, Céline Rivière

PII: S0367-326X(24)00415-5

DOI: https://doi.org/10.1016/j.fitote.2024.106232

Reference: FITOTE 106232

To appear in: *Fitoterapia*

Received date: 1 July 2024

Revised date: 23 August 2024

Accepted date: 21 September 2024

Please cite this article as: A. Ba, V. Roumy, M. Al Ibrahim, et al., Antileishmanial, antitrypanosomal and anti-coronavirus activities of benzophenanthridine alkaloids and other specialized metabolites isolated from the root bark of Zanthoxylum zanthoxyloides (Lam.) B.Zepernick & Timler, *Fitoterapia* (2024), https://doi.org/10.1016/j.fitote.2024.106232

Antileishmanial, antitrypanosomal and anti-coronavirus activities of benzophenanthridine alkaloids and other specialized metabolites isolated from the root bark of *Zanthoxylum zanthoxyloides* (Lam.) B.Zepernick & Timler

Abda Ba,[a,b] Vincent Roumy,[a] Malak Al Ibrahim,[a,c,†] Kristelle Hughes,[d,†] Thierry Hennebelle,[a] Jennifer Samaillie,[a] Sevser Sahpaz,[a] Mehdi A. Beniddir,[e] Marie-France Hérent,[d] Karin Séron,[c] Joëlle Quetin Leclercq,[d] Matar Seck,[b] and Céline Rivière[a,*]

[a] *Joint Research Unit 1158 BioEcoAgro, Univ. Lille, Junia, INRAE, Univ. Liège, UPJV, Univ. Artois, ULCO, F-59650 Villeneuve d'Ascq, France*

[b] *Laboratoire de Chimie Organique et Thérapeutique, Faculté de Médecine, de Pharmacie et d'Odontologie de l'Université Cheikh Anta Diop de Dakar, BP 5005, Dakar-Fann, Sénégal*

[c] *Univ. Lille, CNRS, Inserm, CHU Lille, Institut Pasteur de Lille, U1019 – UMR9017 – Center for Infection and Immunity of Lille (CIIL), F-59000 Lille, France*

[d] *Pharmacognosy Research Group, Louvain Drug Research Institute, Université catholique de Louvain (UCLouvain), Avenue E. Mounier, 72, B B01.72.03-1200 Brussels, Belgium*

[e] *Equipe Chimie des Substances Naturelles, BioCIS, CNRS, Université Paris-Saclay, 17 Avenue des Sciences, 91400, Orsay, France*

Corresponding Author

Céline Rivière - *Joint Research Unit 1158 BioEcoAgro, Laboratory of pharmacognosy, UFR3S Pharmacy, University of Lille, 3 rue du Professeur Laguesse, 59000 Lille; orcid.org/0000-0002-8618-5530; E-mail:* celine.riviere@univ-lille.fr

[†] These authors contributed equally to this work.

ABSTRACT

Strong antileishmanial and antitrypanosomal activities were highlighted for the crude methanolic extract (IC_{50} = 0.61 and 2.15 µg/mL, respectively) of *Zanthoxylum zanthoxyloides* (Lam.) B.Zepernick & Timler root bark, as well as for its apolar partitions (cyclohexane: IC_{50} = 0.66 and 5.17 µg/mL, respectively and dichloromethane: IC_{50} = 0.07 and 0.22 µg/mL, respectively), with a good selectivity index (SI) towards WI-38 cells. In addition, cyclohexane and dichloromethane extracts exhibited a dose-dependent inhibition of human coronavirus HCoV-229E infection in hepatoma Huh-7 cells expressing or not the cellular protease TMPRSS2 (IC_{50} values of 5.29 µg/mL and 4.87 µg/mL, respectively). Fractionation of these active extracts led to the isolation of a new racemic benzophenanthridine alkaloid named zanthoxyloithrine (**1**), together with 13 known compounds. Their structures were elucidated by spectroscopic techniques including IR, UV, HR-MS, 1D and 2D NMR and electronic circular dichroism. In parallel, HR-ESI-MS/MS based dereplication and molecular networking analysis were performed to identify unpurified compounds in cyclohexane and dichloromethane extracts. Zanthoxyloithrine (**1**) showed strong antileishmanial (IC_{50} = 0.14 µM, SI = 52.0) and antitrypanosomal (IC_{50} = 0.36 µM, SI = 20.8) activities. In addition, compound (**1**) demonstrated a high antiviral activity against HCoV-229E with IC_{50} value of 6.70 µM in presence of TMPRRS2 and without significant toxicity on Huh-7 cells. Other purified benzo[c]phenanthridine alkaloids also showed anti-coronavirus and antiparasitic activities.

Keywords: *Zanthoxylum zanthoxyloides* (Lam.) B.Zepernick & Timler; Root bark; Benzophenanthridine alkaloids; Antileishmanial; Antitrypanosomal; Anti-coronavirus

1. Introduction

The genus *Zanthoxylum* L. (Rutaceae), consisting of trees and shrubs, includes 234 accepted species distributed throughout the world in tropical and temperate regions (Plants of the World Online). In Africa, this genus is represented by 35 species mainly distributed in West African countries (Zepernick and Timler, 1981). Different plant parts of *Zanthoxylum* species are widely used in traditional medicine in the treatment of many infectious diseases, but also in the management of sickle cell anemia or some cancers (Misra et al., 2013; Guetchueng et al., 2018; Okagu et al., 2021).

In Senegal, different organs of the small tree *Zanthoxylum zanthoxyloides* (Lam.) B.Zepernick & Timler, including root bark, are widely used in traditional medicine for their antiparasitic properties (Kerharo, 1971; Pousset, 2004). However, the antileishmanial and antitrypanosomal activities of this species are not well investigated. Leishmaniasis, an infectious zoonotic disease distributed worldwide with 1.3 million people infected per year, is caused by approximately twenty species of protozoa belonging to the genus *Leishmania* transmitted by a bite from a female sand fly vector, and manifested by visceral or cutaneous symptoms (Vila-Nova et al., 2013; Castillo et al., 2014; Dofuor et al., 2019a; Rinaldi et al., 2019). Human African trypanosomiasis (HAT) or Chagas disease, endemic in Africa and South America, respectively, which affects between 300,000 and 500,000 people per year, is caused by protozoa of the genus *Trypanosoma* after the bite of an infested tsetse fly and can in some cases attack the central nervous system (Fotie et al., 2007; Bero et al., 2011). Without effective treatments, both diseases are usually fatal (Chappuis et al., 2007; Alotaibi et al., 2021). Currently, existing drugs for these two diseases, depending on the stage of infection, cause many adverse effects related to their toxicity. In addition, the complexity of their administration (intramuscular or intravenous for most of them) and their high costs strongly limit their effectiveness (Fotie et al., 2007; Vila-Nova et al., 2013; Castillo et al., 2014).

At the beginning of the COVID-19 pandemic caused by severe acute respiratory syndrome coronavirus 2 (SARS-CoV-2), many countries promoted the use of plants by local populations for the management of symptoms of the infection without scientific verification (Chakraborty et al., 2022; Wasilewicz et al., 2024), including species belonging to the Rutaceae family such as *Z. zanthoxyloides* (Bafandeh et al., 2023; Houeze et al., 2023). In Senegal, some traditional practitioners recommended that patients infected with the coronavirus take an infusion or decoction of *Z. zanthoxyloides* root bark. HCoV-229E is a virus primarily responsible for respiratory infections, including the common cold in humans, and may serve as a model for highly pathogenic coronaviruses such as SARS-CoV-2. From a phytochemical perspective, previous studies have reported that *Z. zanthoxyloides* is a source of benzophenanthridine and quinoline alkaloids that have antibacterial (Miao et al., 2011), antiparasitic (Hu et al., 2017), anti-inflammatory (Danielewski et al., 2022), antiviral (Latarissa et al., 2021), and anti-tumoral (Couillerot et al., 1994; Yang et al., 2020) properties. In this context, we investigated the chemical composition of the root bark of *Z. zanthoxyloides* and evaluated the antiparasitic and anti-coronavirus activities of this plant. This paper describes the isolation and structural elucidation of one new racemic benzophenanthridine alkaloid along with thirteen known compounds. All these compounds were evaluated for their antiparasitic activities against *Leishmania mexicana mexicana* and *Trypanosoma brucei brucei* and their anti-coronavirus activity against human coronavirus HCoV-229E. The cytotoxicity of the purified compounds was also evaluated on normal human pulmonary fibroblast WI-38 cells and on hepatoma Huh-7 cells.

2. Results and discussion

2.1. Preliminary antiparasitic and antiviral assays

The crude methanolic extract of *Z. zanthoxyloides* root bark (ZZM) and its four partitions, cyclohexane (ZZC), dichloromethane (ZZD), ethyl acetate (ZZE), aqueous (ZZA),

were evaluated in dose-response experiments for their antiparasitic activities (IC_{50}) against *Leishmania mexicana mexicana* (Lmm) and *Trypanosoma brucei brucei* (Tbb), as well as for their cytotoxic activity (CC_{50}) on WI-38 cells (Table 1). ZZD demonstrated excellent antileishmanial activity against Lmm (IC_{50} = 0.07 µg/mL, SI = 252.4) and particularly good antitrypanosomal activity against Tbb (IC_{50} = 0.22 µg/mL, SI = 81.5) associated with good selectivity indexes (Table 1). The extract ZZD exhibited more potent antiparasitic activities than those of ZZC on Lmm (IC_{50} = 0.66 µg/mL, SI = 62.8) and on Tbb (IC_{50} = 5.17 µg/mL, SI = 8.0). ZZE and ZZA, although active against parasitic strains, were overall less active than ZZD and ZZC. The antiviral activities of the crude extract and the four partitions were further evaluated against the human coronavirus HCoV-229E-Luc possessing a luciferase reporter gene for the quantification of infection (Fig. 1a and 1b). Huh-7 hepatoma cell line, as well as Huh-7 cells transduced with a lentivirus encoding TMPRSS2 (Huh-7/TMPRSS2), a cellular protease that allows fusion of the virus to the host cell surface, have been used for HCoV-229E-Luc infection assays. In the absence of this TMPRSS2 protease, responsible for cleavage of the spike protein, the virus only uses the endosomal pathway for entry. ZZD and ZZC, tested at 25 µg/mL, showed the best activities against the human coronavirus HCoV-229E in Huh-7 and Huh-7/TMPRSS2 cells (Fig. 1b) but also a significant decrease of cell viability at 100 µg/mL for both ZZD and ZZC, and at 25 µg/mL for ZZD (Fig. 1a). Dose-response experiments were performed (Fig. 1c-f) and the concentrations decreasing the viability by 50% (CC_{50}), as well as the concentrations inhibiting 50% of the infection (IC_{50}) were determined for the two active extracts. The extracts ZZD (Huh-7/TMPRSS2: IC_{50} = 4.87 µg/mL, Huh-7: IC_{50} = 4.36 µg/mL) and ZZC (Huh-7/TMPRSS2: IC_{50} = 5.29 µg/mL, Huh-7: IC_{50} = 6.24 µg/mL) showed similar antiviral activities against the human coronavirus HCoV-229E in Huh-7 cells expressing or not the protease TMPRSS2 (Fig. 1e and 1f). The CC_{50} obtained on Huh-7 cells (Fig. 1c and 1d) for ZZD (CC_{50} = 23.91 µg/mL) and ZZC (CC_{50}

= 51.11 µg/mL) confirmed that the antiviral activity was not due to cytotoxicity. The different antiparasitic and antiviral activities, associated with the non-toxicity of ZZC and ZZD, at active concentrations, led to the choice of these extracts for the phytochemical study. UPLC-HR-ESI-MS/MS analysis was also carried out to perform putative identification of other compounds by HR-MS and MS/MS molecular networking dereplication.

2.2. Structural elucidation

Fractionation of the antiparasitic and antiviral active extracts of *Z. zanthoxyloides* root bark (ZZC and ZZD) was performed by preparative chromatographic techniques and led to the isolation of 14 compounds (Fig. 2), including a new racemic benzophenanthridine alkaloid named zanthoxyloithrine (**1**) and 13 previously known compounds. The structures of these compounds were established based on different spectroscopic data (HR-ESI-MS/MS, UV, 1D and 2D NMR) and by comparison with those described in the literature (Table 2 and Supplementary data, Fig. S21-S31). The known compounds (Supplementary data, Fig. S32-S120) were identified as dihydrochelerythrine (**2**) (Miao et al., 2011), *trans*-fagaramide (**3**) (Dofuor et al., 2019b), arnottianamide (**4**) (Ishii et al., 1976), pellitorine (**5**) (Adesina and Reisch, 1988; Queiroz et al., 2006), γ-sanshool (**6**) (Xia and Toy, 2014), chelerythrine (**7**) (Miao et al., 2011), evodiamide (**8**) (Shoji et al., 1988; Yang et al., 2016), decarine (**9**) (Zeng et al., 2022), 6-oxochelerythrine (**10**) (Miao et al., 2011), scoparone (**11**) (Ma et al., 2006; Vila-Nova et al., 2013), 4-methoxy-1-methylquinolin-2-one (**12**) (Min et al., 2007), skimmianine (**13**) (Chakravarty et al., 1999; Zeng et al., 2022), and γ-fagarine (**14**) (Min et al., 2007).

Compound **1** was obtained as a brown powder (m.p: 215-216 °C). The HR-ESI-MS in positive mode at *m/z* 593.1907 $[M+H]^+$ (calcd for 593.1895) supported its molecular formula as $C_{34}H_{28}N_2O_8$, indicating 22 degrees of unsaturation. The IR spectrum showed absorptions corresponding to an N-H band (υ_{max} = 3400 cm^{-1}), several methyls bands (υ_{max} = 3000, 2944,

2893, 2838 and 2810 cm^{-1}), a C=O band (υ_{max} = 1634 cm^{-1}), aromatic ring bands (υ_{max} = 1573, 1522, 1492, 1460 and 1415 cm^{-1}) and stretches of N-CH_3 (υ_{max} = 1361 cm^{-1}) and C-O-C (υ_{max} = 1265, 1238, 1072 and 1039 cm^{-1}). The ^{13}C NMR spectrum showed 34 carbon signals that are assigned based on the HSQC-Dept and HMBC experiments as five methyls, including four methoxy groups (δ_C 61.2, 61.0, 56.1, 55.8), one methylene (δ_C 101.0), ten methines including one carbon sp^3 (δ_C 55.3), eighteen quaternary carbons with one carbonyl (δ_C 173.6), eight oxygenated sp^2 carbons (δ_C 154.7, 153.1, 152.1, 150.2, 148.1, 147.5, 146.4 and 134.7) and nine single sp^2 carbons. ^1H NMR spectrum obtained in $CDCl_3$ (Table 2) combined with ^1H-^1H-COSY spectrum showed an N-H proton signal (δ_H 9.06), four methoxy signals (δ_H 3.99, 3.97, 3.95 and 3.91), one *N*-methyl (δ_H 2.80), nine signals in the aromatic region including three singlets (δ_H 7.76, 7.07 and 6.25) and three pairs of doublets [δ_H 8.02 and 6.90 (J = 9.1 Hz), 7.61 and 7.08 *(J* = 8.6 Hz) and 7.69 and 7.43 (J = 8.6 Hz)] corresponding to AB systems of three 1,2,3,4-tetrasubstituted benzene rings. The ^1H NMR spectrum also underlined the presence of a signal at δ_H 6.06 ppm (2H) corresponding to a -CH_2- belonging to a methylenedioxy group, as well as a signal at δ_H = 5.83 ppm integrating 1H corresponding to a methine adjacent to a nitrogen according to the HSQC-Dept experiment. The proton at δ_H = 5.83 was carried by a sp^3 hybridized carbon (δ_C 55.3) linked to the benzene ring, which suggested the absence of a double bond C=N and therefore confirmed the presence of a side chain attached to this carbon. Comparison of these spectroscopic data with those of benzo[c]phenanthridine alkaloids (Fotie et al., 2007; Oechslin et al., 1991; Miao et al., 2011; Wei et al., 2020) attested that **1** was structurally similar to dihydrochelerythrine (**1**) whose difference would therefore be the presence of a side chain in the C-6 position, suggesting that **1** was a dihydrochelerythrine derivative. The attachment of the side chain to C-6 was confirmed by the HMBC experiment which showed the correlations between the H-6 proton (δ_H 5.83) and the carbon C-6a (δ_C 124.5 ppm), 5-*N*-CH_3 (δ_C 42.2), C-4b (δ_C 139.6), C-7 (δ_C

146.4), C-2' (δ_C 150.2) and C-3' (δ_C 104.9) (Fig. 3). The HSQC and HMBC correlations underlined that the aromatic protons (δ_H 6.90 and 8.02), the furan methine (δ_H 6.26), the methoxy groups (δ_H 3.97 and 3.95) and the proton of the *N*-H group (δ_H 9.06) as well as the carbonyl group (C=O) (δ_C 173.6) were localized on the C-6 substituted unit of the dihydrochelerythrine. The mass spectrum obtained by HR-ESI-MS in positive mode showed a fragment at *m/z* 348,1224 $[M-244]^{\bullet+}$ corresponding to an ion resulting from the loss of the -$C_{13}H_{10}NO_4$ group (contributing to 9 unsaturations) at position C-6. The NMR data obtained for this part of the molecule **1** are similar to those of skimmianine (**13**) and γ-fagarine (**14**) also isolated in this study from the plant, as well as those found in the literature for iso-skimmianine and iso-γ-fagarine with the presence of an N-H instead of an *N*-methyl (Nayar et al., 1971; Mbaze et al., 2009; Yang et al., 2012). The spectroscopic data were consistent with a 4,9-dihydro-7,8-dimethoxy-4-oxofuro[2,3-b]quinolin-2-yl moiety at position C-6. The lack of optical activity and of any Cotton effect established the racemic status of **1.** The new compound **1** was thus characterized as 2-[1,2-dimethoxy-12-methyl-13*H*-[1,3]benzodioxolo[5,6-c]phenanthridine-13-yl]-7,8-dimethoxyfuro[2,3-b]quinolin-4(9*H*)-one and named zanthoxyloithrine.

2.3. HR-ESI-MS/MS based dereplication and molecular networking analysis

ZZC and ZZD were also analyzed by UHPLC-UV-MS and HR-ESI-MS/MS (Supplementary data, Fig. S1-S6) to putatively identify non-isolated compounds. The MS/MS data of the two extracts, first processed with MZmine, were exported to Global Natural Product Social (GNPS) to create a feature-based molecular network (Fig. 4). Dereplication of the ZZC and ZZD was performed by comparing MS/MS fragmentations to those present in the GNPS (Wang et al., 2016), PubChem (Kim et al., 2023) and KEGG (Kanehisa et al., 2023) databases. During this annotation process, several levels of confidence were assigned: level 1 (unambiguously identified metabolite, confirmed by at least two parameters of an

authentic standard, such as retention time and MS/MS spectrum, purified compounds in the case of our study), level 2 (putatively annotated metabolite), level 3 (putatively annotated metabolite class) and level 4 (unidentified metabolite) (Kodra et al., 2022). A putative identification was performed based on the analysis of the molecular network (Fig. 4) and MS/MS fragmentations (Supplementary data, Table S1). These approaches showed that these extracts consisted mainly of unsaturated and polyunsaturated amides (cluster A), as well as benzo[c]phenanthridine (cluster B), indolopyridoquinazolinone, isoquinoline and quinoline alkaloids. Only one coumarin, scoparone, was identified and purified in this study. The profiling process revealed that ZZD was highly enriched in benzo[c]phenanthridine and quinoline alkaloids while cyclohexane contained mainly amides. HR-ESI-MS/MS data made it possible to putatively identify (level 2), by using PubChem and KEGG databases, other alkaloids, such as edulitine (Rt 4.51 min, *m/z* 206.0807, $C_{11}H_{11}NO_3$), glaucine (Rt 4.56 min, *m/z* 356.1850, $C_{21}H_{25}NO_4$), ochotensine (Rt 5.24 min, *m/z* 352.1538, $C_{21}H_{21}NO_4$), evodiamine (Rt 7.82 min, *m/z* 304.1443, $C_{19}H_{17}N_3O$), and rutaecarpine (Rt 8.19 min, *m/z* 288.1129, $C_{18}H_{13}N_3O$) not previously described in the species *Z. zanthoxyloides*. Evodiamide (Rt 7.54 min, *m/z* 308.1756, $C_{19}H_{21}N_3O$), and decarine (Rt 7.91 min, *m/z* 320.0914, $C_{19}H_{13}NO_4$) purified in our study were also described for the first time in this plant. On the other hand, new polyunsaturated amides including hazaleamide (Rt 10.58, *m/z* 276.2319, $C_{18}H_{29}NO$) have been potentially identified in *Z. zanthoxyloides.* Among the 31 alkaloids detected, 12 were benzo[c]phenanthridines. Numerous chelerythrine derivatives (cluster B), including chelerythrine, 6-oxochelerythrine, norchelerythrine and dihydrochelerythrine, were identified (level 1) in ZZC and ZZD. The MS spectra of the chelerythrine compounds produced very characteristic daughter ions at *m/z* 348, 334/333, 332, 321/320, 319/318, 304 and 290 (Klejdus et al., 2007; Lin et al., 2020). Quinoline and its derivatives were considered as a preferred structure in drug research due to their broad spectrum of bio-response, mainly

antibacterial (Miao et al., 2011), antiparasitic (Hu et al., 2017), anti-COVID-19 (Latarissa et al., 2021), and anti-inflammatory (Danielewski et al., 2022). Therefore, given the high content of these compounds in ZZD, this could explain the good antiparasitic and anti-coronavirus activities described in this study.

2.4. Antileishmanial, antitrypanosomal and cytotoxic activities

The antiparasitic activity of compounds isolated from *Z. zanthoxyloides* root bark was evaluated against *Trypanosoma brucei brucei* and *Leishmania mexicana Mexicana* (Table 1). All compounds tested exhibited antileishmanial activity against *L. mexicana mexicana* in a dose-dependent manner with IC_{50} values ranging from 0.03 to 92.87 μM. IC_{50} values obtained against *T. brucei brucei* varied between 0.18 and 68.19 μM. Only arnottianamide (**4**), 6-oxochelerythrine (**10**) and γ-fagarine (**14**) did not show antitrypanosomal activity at the tested concentrations. No compound was found to be toxic on WI-38 cells at 50% inhibitory concentrations of parasite growth (IC_{50}). Dihydrochelerythrine (**2**) showed the best activities against both *L. mexicana mexicana* (IC_{50} = 0.03 μM, SI = 168.7) and *T. brucei brucei* (IC_{50} = 0.18 μM, SI = 32.0). Chelerythrine (**7**) also demonstrated good antiparasitic activity against *L. mexicana mexicana* (IC_{50} = 0.06 μM, SI = 271.7) and *T. brucei brucei* (IC_{50} = 0.49 μM, SI = 35.3) with the best selectivity indexes. The new alkaloid (**1)** was also highly active against *L. mexicana mexicana* (IC_{50} = 0.14 μM, SI = 52.0) and *T. brucei brucei* (IC_{50} = 0.36 μM, SI = 20.8) with a cytotoxic concentration on WI-38 cells 52 and 20 times higher than the IC_{50} on both parasites, respectively (Table 1). Compounds **2** and **7** showed better antiparasitic activity against *L. mexicana mexicana* than the positive controls pentamidine (IC_{50} = 0.23 μM) and amphotericin B (IC_{50} = 0.09 μM). The antileishmanial activity of compound **1** was also greater than that of pentamidine. The only isolated coumarin, scoparone (**11**), was also very active against *L. mexicana mexicana* (IC_{50} = 2,56 μM, SI = 37.2) and *T. brucei brucei* (IC_{50} = 9,54 μM, SI = 10.0). Chelerythrine and dihydrochelerythrine, two benzo[c]phenanthridine

alkaloids, are known to have a wide range of pharmacological activities, including antibacterial, antitumor, and antiparasitic ones (Malhotra et al., 2016). Antileishmanial and antitrypanosomal activities of benzophenanthridine alkaloids including dihydrochelerythrine (**2**) (Fotie et al., 2007; Fuchino et al., 2010), as well as the antileishmanial activity of chelerythrine (**7**) (Castillo et al., 2014) against different species of *Leishmania* sp., have been previously described in the same range of values. Additionally, another study showed good activity of dihydrochelerythrine against *L. donovani* (2.0 ± 0.8 µM) and *T. brucei brucei* (0.8 ± 0.2 µM) with good selectivity indexes (Fotie et al., 2007). The study of structure-activity relationship carried out on dihydrochelerythrine (**2**), chelerythrine (**7**), decarine (**9**), 6-oxochelerythrine (**10**) and zanthoxyloithrine (**1**) showed that the presence of a carbonyl group on C-6 (i.e., oxidation of C-6; **10**) or C-6 substitution (**1**) has significantly ($p < 0.05$) reduced antileishmanial activity. It also appeared that the unsaturation between C-6 and N-5 was necessary to maintain this high activity. The substitution of the nitrogen atom by a methyl on the B ring as well as the presence of methoxy groups at C-7 and C-8 seem favorable to an increase in activity (**9**). On the other hand, in the case of **1**, the presence of the large group -[4,9-dihydro-7,8-dimethoxy-4-oxofuro[2,3-b]quinolin-2-yl]- in position C-6 strongly attenuated the activity compared to dihydrochelerythrine and conferred slightly higher activity than chelerythrine against *T. brucei brucei* ($p < 0.05$). These observations were consistent with studies on the structure-activity relationship of benzo[c]phenanthridines previously described against *Leishmania* sp. and *Trypanosoma* sp (Fotie et al., 2007; Fuchino et al., 2010). However, the mechanisms of action of dihydrochelerythrine and its derivatives on *L. mexicana mexicana* and *T. brucei brucei* have not yet been elucidated. A previous study suggested that the primary antibacterial mechanism of chelerythrine may be attributed to the destruction of channels in bacterial membranes, causing protein leakage outside the cell, as well as inhibition of protein biosynthesis (He et al., 2018).

2.5. Anti-coronavirus and cytotoxic activity

The anti-coronavirus activity of the isolated compounds was evaluated on a recombinant HCoV-229E-Luc human coronavirus as described before. Each compound was added during the infection phase. The cytotoxic activity of the compounds was previously assessed on Huh-7 cells using the MTS assay and CC_{50} values were determined when possible (Supplementary data, Fig. S121). Only dihydrochelerythrine (**2**), *trans*-fagaramide (**3**), chelerythrine (**7**), 6-oxochelerythrine (**10**) and zanthoxyloithrine (**1**) showed antiviral activity against HCoV-229E. The best activity was observed for the new alkaloid (**1**) which strongly inhibited infection of cells by the virus, whether or not they express protease TMPRSS2 with IC_{50} values of 6.70 µM (Huh-7/TMPRSS2) and 5.40 µM (Huh-7) (Fig. 5a). The other benzo[c]phenanthridine alkaloids, dihydrochelerythrine (**2**), chelerythrine (**7**) and 6-oxochelerythrine (**10**), also showed antiviral activity in the presence of the protease TMPRSS2 (IC_{50} 12.95, 11.36 and 25.84 µM, respectively) or not (IC_{50} 10.38, 19.43 and 19.08 µM, respectively) (Fig. 5b, 5d and 5e). However, dihydrochelerythrine (**2**) and chelerythrine (**7**) exhibited mild toxicity to hepatoma Huh-7 cells with CC_{50} of 40.89 and 47.92 µM, respectively. By contrast, the compounds **1**, **3**, and **10** appeared non-toxic up to 100 µM. On the other hand, without toxicity on Huh-7 cells, *trans*-fagaramide (**3**) moderately inhibited viral infection but we were not able to determine its IC_{50} because it was higher than the maximum concentration tested. This is the first time that the anti-coronavirus activity of these compounds has been evaluated. The fact that these different compounds inhibited the viral infection caused by HCoV-229E, in Huh-7 cells expressing or not the TPMRSS2 protease is interesting because it suggests that they may inhibit infection after entry of the virus by any of the pathways (fusion at the cell surface and endosomal fusion) used by the virus to enter and infect cells. The structure-activity relationship study of dihydrochelerythrine (**2**), *trans*-fagaramide (**3**), chelerythrine (**7**), 6-oxochelerythrine (**9**) and zanthoxyloithrine (**1**) against

viral infection, underlined some differences compared to that carried out against the two parasites tested. The presence of the 4,9-dihydro-7,8-dimethoxy-4-oxofuro[2,3-b]quinolin-2-yl group at the C-6 (**1**) position strongly increased the antiviral activity by about a factor of two compared to dihydrochelerythrine (**2**), without toxicity on Huh-7 cells. The compound **1** was also found to be more active than compound **7**, although there was no iminium group in the molecule. Considering the presence of the benzodioxol group in all compounds inhibiting viral infection, this structural pattern appears to have a positive impact on antiviral activity (Papi et al., 2017). In the case of respiratory viral infection, the activation of protein kinase C (PKC) plays a key role in the nuclear transport of viral ribonucleoproteins in infected cells and their subsequent development at the cell membrane (Peng et al., 2021; Valipour et al., 2021). Several studies have already underlined that chelerythrine causes blockade of the NF-κB pathway and eliminates the effects of the serum hepatitis B core antigen (HBcAg) on different levels (Liu et al., 2018; Valipour et al., 2021). Another study showed that dihydrochelerythrine exhibited a potent activity against HBsAg and HBeAg secretions of the Hep G 2.2.15 cell line with $IC_{50} < 0.05$ µM, SI > 3.5 (Wu et al., 2007). Sanguinarine, another benzophenanthridine alkaloid, has also been shown to attenuate the proliferation of porcine reproductive and respiratory syndrome virus (PRRSV) by targeting the internalization, replication and release stages of the viral life cycle (Ke et al., 2023). Finally, chelerythrine chloride was identified as an inhibitor of Zika virus (ZIKV) infection in five cell lines ($0.25 < IC_{50} < 0.61$ µM, $11.4 < SI < 93.9$) by targeting the viral NS4B protein (Loe et al., 2023). The good anti-coronavirus activities of these chelerythrine analogues, dihydrochelerythrine (**2**), chelerythrine (**7**), 6-oxochelerythrine (**10**) and zanthoxyloithrine (**1**) could be explained by their ability to regulate critical signaling pathways involved in HCoV-229E infection.

3. Conclusions

A chemical investigation of *Zanthoxylum zanthoxyloides* root bark guided by antileishmanial, antitrypanosomal, and anti-coronavirus activities isolated a novel benzo[c]phenanthridine alkaloid, along with thirteen known compounds. Dereplication and molecular network analyses of the cyclohexane and dichloromethane extracts identified many specialized metabolites not previously described in this species, including alkaloids and polyunsaturated amides. The benzophenanthridine alkaloids zanthoxyloithrine, dihydrochelerythrine, and chelerythrine showed good antileishmanial, antitrypanosomal, and anti-coronavirus activities. This is the first time that these compounds have been tested against the HCoV-229E coronavirus. The very promising antileishmanial and antiviral activities of the new compound named zanthoxyloithrine, as well as its non-toxicity on hepatoma Huh-7 cells, make this compound a good candidate in the management of leishmaniosis and human coronavirus HCoV-229E infections. It would be also relevant to study its mechanism of action on these pathogens.

4. Materials and Methods

4.1. General experimental procedures

Melting points were determined by using an electrothermal IA9100 digital melting point apparatus (Thermo Scientific). The optical rotations were measured in CH_2Cl_2 at 25 °C on a Polaar 32 polarimeter. ECD spectra were measured at 25 °C on a JASCO J-810 spectropolarimeter. An ALPHA-P FT/IR-480 spectrometer (BRUKER Optics) was used to measure the IR spectra. The 1D (^{1}H and ^{13}C) and 2D (COSY, HSQC-DEPT, HMBC) NMR spectra were recorded in deuterated chloroform ($CDCl_3$) (99.96% D, D029T, EurisoTop®, France) or in dimethylsulfoxide (99.96% D, D034T, EurisoTop®, France) on a 500 MHz Bruker® spectrometer (NEO AVANCE console), operating at 500 MHz for proton (^{1}H) and 125.77 MHz for carbon-13 (^{13}C). Measurements were made with a 5 mm TXI probe at 25 °C. The data were processed with Bruker TopSpin software (4.1.4). UHPLC-UV-HR-ESI-MS

were performed on a Accela UHPLC system from Fisher Scientific (Thermo Fisher Scientific, Bremen, Germany) associated to a photodiode array (PDA) detector, an autosampler, a tray compartment cooler (set to 20 °C), a quaternary pump and a Thermo Fisher Scientific LTQ orbitrap XL mass spectrometer with ESI source. The UHPLC system and the mass spectrometry system were piloted by Xcalibur software. UHPLC-UV-MS analyses were carried out on a Waters ACQUITY equipment (Waters® Acquity UPLC® H-Class, Guyancourt, France) consisting of two independent pumps, an automatic injector, a controller, a diode array UV detector (PDA) and a quadrupole (QDA) mass spectrometer with ESI as ionization source. The preparative HPLC was performed on a Shimadzu chain equipped with two LC-20AP pumps, a 500 µL injection loop, a Shimadzu® SPD-M20A diode array UV detector and a CBM-20A control system. The column was an Interchim C18-HQ column (5 µm, 250 mm x 21.2 mm, Interchim™, France) preceded by a pre-column C18-HQ (7.5 mm x 21.2 mm). Mobile phase was composed of two solvents (A) ultrapure water + 0.1% formic acid and (B) acetonitrile. The centrifugal partition chromatography (CPC) was performed using a 250 ml rotor (SCPC-250 L) provided by ARMEN Instrument®, Saint-Avé, France). This CPC chain was equipped with the same pumps, the same UV detector, and the same control system as the preparative HPLC chain. The system was controlled by LC Solution software and an automatic collector (Gilson®, France) made it possible to recover the different fractions. Analytical thin-layer chromatography (TLC) was performed on precoated silica gel 60 F254 (AluGRAM® XtraSil G/UV254, Germany) and the spots were visualized at two wavelengths (254 and 365 nm) before being sprayed with a solution of sulfuric anisaldehyde and heating at 120°C for 10 min or with Dragendorff's reagent. The elution system used consisted of a mixture C_6H_{12}:$C_4H_8O_2$ with different conditions (9:1; 8:2; 7:3; 4:6 and 3:7). Silica gel 60 (63–200 µm, Macherey–Nagel, Germany) was used for preparative column chromatography. Extraction solvents (methanol, cyclohexane, dichloromethane, and ethyl

acetate), acetonitrile and formic acid for UHPLC-UV-MS analysis were purchased from Carlo Erba Reagents® (Val de Reuil, France). Ultrapure water was obtained after filtration on a system Millipore Integral 5 Milli-Q (Merck™, Germany).

4.2. Plant material

The plant material, *Z. zanthoxyloides*, was harvested in December 2021 in Niayes, in the Keur Massar department (14°47'59" N et 17°18'35" O) (Dakar region) in Senegal, and identified by Dr William Diatta, botanist at the Pharmacognosy Laboratory of the Faculty of Medicine, Pharmacy and Dentistry of the Cheikh Anta Diop University in Dakar. A voucher specimen was deposited in the Dakar Herbarium (Department of Plant Biology of the Faculty of Science and Technology of Cheikh Anta Diop University) and in the laboratory of Pharmacognosy of the University of Lille under the N° BA25. The root, very stiff with a brown colored bark and a yellowish pigment, was then separated from the rest of the plant and the root bark was dried at room temperature. When crushed, the roots give off a very aromatic, peppery, lemony smell (Supplementary data, Fig. S122).

4.3. Extraction and isolation

The root bark powder of *Z. zanthoxyloides* (300 g) was subjected to a solid-liquid (S/L) extraction with methanol (6 L, 5 x 24 h) using an orbital agitator (GFL 3015, Germany). The methanolic extract (ZZM, 32 g, 10.7% *w/w*) was solubilized in distilled water (500 mL) to be fractionated by liquid-liquid extraction (*v/v*) with organic solvents of increasing polarity (cyclohexane (1 L), dichloromethane (1.5 L), and ethyl acetate (1 L)). The aqueous residual partition was frozen and then freeze-dried using a freeze dryer (Telstar Cryodos™, Spain). The organic partitions were dried using a rotary evaporator between 30-35°C (Heidolph™, Schwabach, Germany). The dried cyclohexane (ZZC, 7.60 g, 23.75% *w/w*), dichloromethane (ZZD, 2.75 g, 8.6% *w/w*), ethyl acetate (ZZE, 1.16 g, 3.6% *w/w*) and aqueous (ZZA, 19.06 g, 59.6% *w/w*) extracts were obtained. The isolation of pure compounds was achieved by

different chromatographic procedures. ZZC (340 mg) was fractionated by chromatography on an open silica gel column (column 1.6 x 14 cm; normal phase 63-200 µm; 12 g) using a binary gradient of cyclohexane-EtOAc (90:10 to 0:100, *v/v*, 1 L) as elution system. The pure compounds **2** (11.7 mg, Dragendorff positive) and **3** (11.5 mg), as well as twelve fractions (FC1-FC12) were obtained based on their TLC behaviour and UHPLC-UV-MS chromatographic profile. From the fraction FC3 (23.9 mg), the compound **2** (5.2 mg) and the compound **4** (1.7 mg) were obtained by preparative HPLC using an Interchim C18-HQ column (5 µm, 250 mm x 21.2 mm, Interchim^{TM}, France) as stationary phase. The mobile phase was made up of (A) H_2O + 0.1% formic acid and (B) ACN. The gradient used was: [0-5 min (10-40% B).5-40 min (40-100% B) followed by 40-50 min (100% B), with a flow rate of 15 mL/min. The FC8 fraction (75.7 mg) was fractionated by silica gel open column chromatography (column 1 x 11 cm; normal phase 63-200 µm; 4.5 g) to give the compounds **5** (32.9 mg) and **6** (3.6 mg). In parallel, ZZD (2 g) was fractionated by CPC with the Arizona M system (heptane/EtOAc/MeOH/H_2O 5/6/5/6 *v/v/v/v*) (Berthod et al., 2005) using the ascending mode to give eight fractions [FD1 (28 mg), FD2 (277.5 mg), FD3 (137.1 mg), FD4 (147.9 mg), FD5 (368.1 mg), FD6 (72.3 mg), FD7 (34.5 mg) and FD8 (96.3 mg)]. Compounds of some fractions of interest from the DCM fraction were purified by preparative HPLC. The fraction FD4 (67 mg) was fractionated by preparative HPLC with the following gradient with B being acetonitrile [0-5 min (10-20% B), 5-30 min (20-60% B), 30-40 min (60-100% B), 40-50 min (100% B)] and a flow rate of 15 mL/min to yield compounds **7** (7.66 mg), **8** (2.69 mg) and **9** (3.68 mg). The compounds **7** (4.6 mg), **3** (229.17 mg), **4** (2.64 mg), **8** (3.8 mg), **10** (7.58 mg), **1** (17.64 mg) and **2** (2.34 mg) were purified from the fraction FD5 (368.1 mg) by preparative HPLC with the following gradient with B being acetonitrile [0-5 min (10-30% B), 5-20 min (30-50% B), 20-40 min (50-100% B), 40-50 min (100% B)] and a flow rate of 15 mL/min. The compound **1** was covered by the compound **5** in the

chromatograms (UV and TIC) of the DCM fraction (Supplementary data, Fig. S4-S6) and their separation was made possible by CPC. Fractionation of the fraction FD8 was performed by preparative HPLC with the following gradient with acetonitrile as solvent B [0-5 min (10-30% B), 5-25 min (30-40% B), 25-35 min (40-100% B), 35-45 min (100% B)] at a flow rate of 15 mL/min and let to the isolation of the compounds **7** (3.24 mg), **11** (1.53 mg), **12** (3.11 mg), **13** (4.21 mg), **14** (3.14 mg) and **2** (1.5 mg). The separations in preparative HPLC were monitored at 254 nm. The different chromatograms are shown in figures S1-S20, Supplementary data.

*Zanthoxyloithrine (**1**)*: brown powder; m.p: 215-216°C; $[\alpha]_D^{25}$ 0 (*c* 0.01, CH_2Cl_2); UHPLC-UV: λ_{max} (AU) 231 (0.69), 260 (0.88), 282 (0.62), 325 (0.31) nm; IR υ_{max} 3400, 3000, 2944, 2893, 2838, 2810, 1634, 1573, 1522, 1492, 1460, 1415, 1361, 1265, 1238, 1072, 1039 cm^{-1}; ^1H and ^{13}C NMR data, see Table 2; ESIMS: *m/z* (rel. int.) 593.1907 $[M+H]^+$ (100), 563 (12), 521 (6), 360 (3), 349 (7), 348 (28), 325 (12), 304 (1), 291(8); HRESIMS *m*/z $[M+H]^+$ calcd for $C_{34}H_{28}N_2O_8$, 593.1895; found 593.1907.

4.4. Experimental conditions of fractionation by centrifugal partition chromatography (CPC)

The fractionation of ZZD was carried out on a CPC-250 Armen instrument® system (250 mL CPC column). The Arizona M system (heptane/EtOAc/MeOH/H_2O 5/6/5/6 v/v/v/v) was chosen for the fractionation of ZZD. The two phases are previously prepared in a separating funnel in sufficient quantity and then separated. The lower phase being chosen as the stationary phase, the elution took place in ascending mode with an isocratic elution. The sample was solubilized in a volume of 8 mL of a stationary phase/mobile phase mixture (4: 4, v/v) and then filtered on a PTFE membrane (0.45 µm). The stationary and mobile phases were pumped by Shimadzu® LC-20AP pumps. The device was equipped with a 250 mL rotor. The cells composing the rotor were, initially, filled with the stationary phase at 30 mL/min and 500 rpm. The mobile phase was then added at 8 mL/min and 1600 rpm, until the stationary

started eluting. Once the system reached equilibrium, the sample (8 mL) was injected. The elution lasted 60 minutes. It was followed by extrusion (recovery of the stationary phase) during 15 minutes at 30 mL/min and 1600 rpm for the recovery of products that had not yet been eluted. Rinsing was carried out at 500 rpm and 30 mL/min with a MeOH/H_2O mixture (5: 5, v/v). At the end of the chain is a Shimadzu® SPD-M20A diode array detector. A controller CBM-20A was used to link the chain to the computer. Finally, a volume of 8 mL/tube was collected for each fraction during elution and 15 mL/tube during extrusion using a Gilson® FC204 automatic collector. The fractions were evaporated using a Speedvac system (miVAC QUATTRO concentrator, Genevac, England) and then analyzed in TLC, as well as by UHPLC-PDAMS between 200 and 790 nm. Fractions with the same chromatographic profile were grouped together.

4.5. UHPLC-UV-MS analyses

Extraction and purification process was followed by UHPLC-UV-MS analysis. The stationary phase was an Interchim Uptisphere C18-AQ column (2.1 x 100 mm, 2.6 µm) connected to a 0.2 µm in-line filter. The mobile phase was composed of two solvents: (A) ultrapure water + 0.1% formic acid and (B) Acetonitrile + 0.1% formic acid. Different methods were adopted depending on the sample for UHPLC-UV-MS analyses. The method adapted for the analysis of MeOH extract and EtOAc and aqueous extracts was performed following the elution program: 10% (B) (0-0.5 min), 10%-25% (B) (0.5-8.5 min), 25-100% (B) (8.5-9 min), 100% (B) (9-11 min), before returning to equilibrium for 3 min. The method adapted for the analysis of cyclohexane and DCM extracts, their fractions and isolated compounds followed a gradient mode with solvent B: 10-40% ((0-1.5 min), 40-100 % (1.5-11.5 min), 100-10% (11.5-14 min). Flow rate and column temperature were set at 0.3 $mL.min^{-1}$ and 30 °C respectively. The extracts were prepared at 1 $mg.mL^{-1}$ in analytical grade methanol and filtered through a PTFE 0.4 µm membrane before injection. The pure

compounds and DCM extract were prepared in acetonitrile. The injection volume was 2 µL (or 4 µL in some cases). Parameters for mass spectrometry analysis were as follows: negative and positive ionization mode, nitrogen as carrier gas, cone voltage at 15 V, capillary voltage at 0.8 kV, ionization energy at 15 eV, probe temperature at 600°C, MS-Scan mode from 100 to 950 Da.

4.6. HRMS/MS conditions for dereplication and molecular networking

HRMS/MS analyses were performed using the same column, the same solvents and the same methods described previously for UHPLC-UV-MS. The mass spectrometer was a LTQ Orbitrap XL operated with an electrospray ionization source in positive mode. HRMS spectra were acquired in full-scan mode with a mass range of 50-1000 *m/z*. All experimental data were acquired using daily external calibration prior to data acquisition. Appropriate tuning of the electrospray ion source was done, and the following electrospray inlet conditions were applied: flow rate 300 µL/min with a split of 50/50 before reaching mass detector; with spray voltage, 5 kV; sheath gas (N2) flow rate, 20 a.u.; auxiliary gas (N2) flow rate, 20 a.u.; discharge current of 5 µA; capillary temperature of 250 °C; capillary voltage of 21 V and tube lens voltage of 75 V. The data-dependent MS/MS events were performed on the most intense ion detected in full scan MS with a collision energy of 35 eV. Data acquisition and processing were performed with Xcalibur software.

4.7. MZmine 3 data preprocessing and GNPS platform analysis

The raw mass data acquired by UPLC-LTQ Orbitrap XL was converted to .mzML file format using the MSConvert software (Chambers et al., 2012). All files were imported to the open-source software package MZmine 3 (v3.3.0) for data processing (Pluskal et al., 2010). Mass detection was realized with a noise level set to 1.0E4 for MS^1 and 0 for MS^2. The ADAP Chromatogram builder was achieved using a minimum group size of scan of five, a group intensity threshold of 1.0E4, a minimum highest intensity of 1.0E4, and an *m/z*

tolerance of 0.01 (or 10 ppm). The smoothing parameters were set to 5. The ADAP wavelet was used for chromatogram deconvolution with the following settings: S/N threshold of 10, minimum feature height of 1.0E4, coefficient/area threshold of 10, peak duration range of 0.01-0.7 min, RT wavelet range of 0.01-0.10 min. The *m/z* and RT range for MS/MS scan pairing were set to 0.2 Da and 0.2 min, respectively. Isotopes were detected using the isotope peak grouper with a *m/z* tolerance of 10 ppm, a RT tolerance of 0.03 min (absolute), the maximum charge set at 1, and the representative isotope used was the most intense. Then, the aligned list peak was gap-filled with RT range of 0.7 min and *m*/z tolerance of 10 ppm. The resulting list was filtered using the peak list rows filter option to remove all the duplicates and all the features without MS^2 spectrum associated. Then, the processed output MS/MS data (.mgf) and (.csv) were exported by MZmine 3.3.0 and uploaded to the GNPS (Global Natural Product Social Molecular Networking, https://gnps.ucsd.edu) online platform to generate Feature Based Molecular Networks (FBMN). The precursor ion mass tolerance and the fragment ion tolerance were set as 0.03 Da. A molecular network was then created where edges were filtered to have a cosine score above 0.3 and more than 3 matched peaks. Further, edges between two nodes were kept in the network if and only if each of the nodes appeared in each other's respective top 10 most similar nodes. All matches kept between network spectra and library spectra were required to have a score of 0.7 and at least 6 matched peaks. The DEREPLICATOR was used to annotate MS/MS spectra. Peak area data from the .csv file obtained from MZmine was added to the network. Node size was set proportionally to the total area of each peak detected in both cyclohexane and DCM extracts. Edge widths were set corresponding to the cosine score. Finally, for a more advanced retreatment of the network, the molecular network created in GNPS was also exported to Cytoscape v3.10.1. The GNPS analyses results could be viewed at https://gnps.ucsd.edu/ProteoSAFe/status.jsp?task=e7fa20167f3d4d0b877003e534b6e173.

The prediction of molecular formulas of ions in positive mode is performed with MZmine with isotope *m/z* tolerance 5 ppm and a minimum score of 0.7. Additional putative identification of unmatched peaks was carried out comparing available MS/MS fragmentation patterns with the literature and using the databases integrated into the MZmine software (KEGG and PubChem).

4.8. Antitrypanosomal and antileishmanial assays

The antiparasitic activity of the various extracts and isolated compounds was evaluated *in vitro* against *Trypanosoma brucei brucei* (strain 427) and against promastigotes of *Leishmania mexicana mexicana* (MHOM/BZ/84/BEL46) according to the protocol described by Bero et *al.* (Bero et al., 2011) with some modifications. All extracts and compounds to be tested were solubilized in DMSO (Sigma-Aldrich, Germany) to obtain a stock solution of 20 mg/mL (or 2 mg/mL for some pure compounds).

The *T. brucei brucei* cells were grown in HMI9 medium (Sigma-Aldrich, Bornem, Belgium) containing 10% heat-inactivated foetal bovine serum (FBS) (Sigma-Aldrich, Bornem, Belgium), 150 mM L-cysteine and 20 mM beta-mercaptoethanol and incubated at 37 °C in a humid atmosphere with 5% CO_2. The cells of *L. mexicana mexicana* were grown in HOMEM medium (Sigma-Aldrich, Bornem, Belgium) with the addition of 15% heat-inactivated FBS and 5 mg/mL hemin and incubated at 28 °C in an atmosphere moistened with 5% CO_2. Suramin and pentamidine (or amphotericin B) (Sigma-Aldrich, Steinheim, Germany) were used as positive controls for antitrypanosomal and antileishmanial activities, respectively. In 96-well plates, parasites at a final concentration of 5×10^4 cells/mL were added to samples prepared at eight-fold dilutions between 100-0.046 µg/mL (or eight-fold dilutions between 10-0.0046 µg/mL for positive controls), final concentrations. After 72 hours of incubation, the wells were treated with 10 µL of a revealing solution; AlamarBlue® (BIO-RAD, UK) (diluted in 1:1 PBS solution, v/v). After four hours of incubation, the fluorescence (excitation at 530

nm and emission at 590 nm) was measured with a spectrophotometer (SpectraMax M2e, Molecular Devices, UK). The tests were performed in triplicate and repeated three times. The results were expressed in IC_{50} (concentration of a product that can inhibit 50% of the growth of parasites).

4.9. Antiviral and cytotoxic assays

Stock solutions of extracts and compounds were prepared in DMSO (Sigma-Aldrich, USA) respectively at 25 mg/mL and 100 mM. Human hepatoma cell line Huh-7 and the stable Huh-7 transduced with a lentivirus encoding for TMPRSS2 (Huh-7/TMPRSS2), a cellular protease that allows fusion of the virus at the host cell surface, were grown in Dulbecco's modified Eagle medium (DMEM) with glutaMAX-I (from Life Technologies) and 10% foetal bovine serum (FBS) (from Eurobio) in an incubator at 37 °C with 5% CO_2. Huh-7 cells, as well as Huh-7/TMPRSS2, were used for all HCoV-229E-Luc infection assays. The viral recombinant HCoV-229E-Luc was used (Ba et al., 2024). The cell toxicity assay was performed as follows: 6×10^4 Huh-7 cells were seeded in 96-well plates and incubated for 16 h at 37 °C in a 5% CO_2 incubator. The cells were then treated with increasing concentrations of each extract or compound and incubated for 24 h. Then, an MTS-[3-(4,5-dimethylthiazol-2-yl)-5-(3-carboxymethoxyphenyl)-2-(4-sulfophenyl)-2*H*-tetrazolium]-based viability assay (Cell Titer 96 Aqueous nonradioactive cell proliferation assay, Promega, Madison, WI, USA) was performed (Ba et al., 2024). The absorbance of formazan at 490 nm was measured using a plate reader (ELX 808 Bio-Tek Instruments Inc., Charlotte, VT, USA). For antiviral assays, Huh-7 and Huh-7/TMPRSS2 cells were inoculated with HCoV-229E-Luc at a MOI of 0.5 in a final volume of 50 µL for 1h at 37 °C in the presence of each extract or compound at increasing concentrations. The virus was removed and replaced with culture medium containing the different extract or compounds for 6 h at 37 °C. Cells were lysed in 20 µL of Renilla Lysis Buffer (Promega, Madison, USA), and luciferase activity was quantified in a

Tristar LB 941 luminometer (Berthold Technologies, Bad Wildbad, Germany) using the Renilla Luciferase Assay System (Promega, Madison, WI, USA). All measures were performed in triplicate, and each experiment was repeated three times.

4.10. Cytotoxicity Assay Against WI-38 cells

The cytotoxic activity of the different extracts was evaluated according to the protocol described by Bero et *al*. (Bero et al., 2009) on human cells, non-cancerous lung fibroblasts WI-38 (ATCC CCL-75, from LGC standards, Molsheim, France), using the tetrazolium salt colorimetric method MTT-[3-(4,5-dimethylthiazol-2-yl)-5-(3-carboxymethoxyphenyl)-2-(4-sulfophenyl)-2*H*-tetrazolium]-based on cleavage of the reagent by mitochondrial dehydrogenase in viable cells (Gonzalez and Tarloff, 2001). The cells were seeded in 96-well microplate wells in Dulbecco's modified Eagle medium (DMEM) (Gibco™, UK) containing 4 mM L-glutamine, 1 mM sodium pyruvate and enriched with 10% heat-inactivated FBS (Life Technologies Europe B.V, Bleiswijk, The Netherlands) and some antibiotics (penicillin/streptomycin mixture 100 IU/mL, Sigma-Aldrich, Germany). All extracts and compounds to be tested were solubilized in DMSO to have a stock solution of 20 mg/mL (or 2 mg/mL for some compounds). Camptothecin (2 mg/mL) (Sigma-Aldrich, Germany) was used as a positive control. From the stock solutions, a series of dilutions was prepared in DMEM culture medium.

After 24 hours of incubation at 37 °C in an atmosphere humidified with 5% CO_2, 20 µL of each dilution of extract, compound, or positive control, were added to wells containing 180 µL of cells seeded the day before (5000 cells/well) to obtain a range of eight-fold dilutions between 100-0.046 µg/mL (or 10-0.0046 µg/mL). A 0.2% DMSO control in the culture medium (negative control) was performed. After 72 hours of incubation at 37 °C in an atmosphere moistened with 5% CO_2, the culture medium of each well was completely emptied and replaced by 100 µL of MTT (ThermoFisher Scientific®, Illkirch, France) and the

plates were incubated for 50 minutes. The MTT solution has been emptied and 100 µL of DMSO were added to each well. The absorbance measurement was made directly using a spectrophotometer (SpectraMax M2e, Molecular Devices, UK) at wavelengths 570 and 620 nm. The tests were performed in triplicate and repeated three times. The CC_{50} of each extract or compound was determined using Microsoft Excel and GraphPad Prism software (v8.4.2).

4.11. Statistical analysis

Data were analyzed and processed using GraphPad Prism 8.4.2 and by comparing each treated group and untreated group (DMSO control). Data were analyzed by one-way ANOVA and were expressed as mean ± SEM from three independent experiments, performed in triplicates. Statistical significance was set at $p < 0.05$.

CRediT authorship contribution statement

AB: Conceptualization, Data Curation, Formal analysis, Funding Acquisition, Investigation, Methodology, Resources, Visualization, Writing - original draft; **VR:** Investigation, Methodology, Supervision, Validation, Writing - review & editing; **MAI:** Formal analysis, Investigation, Methodology, Visualization; **KH:** Formal analysis, Investigation, Methodology, Writing - review & editing; **TH:** Validation; **JS:** Investigation, Methodology; **SS:** Project administration; **MAB:** Investigation, Validation, Writing - review & editing; **MFH:** Investigation, Validation; **KS:** Methodology, Validation**,** Writing – review & editing; **JQL:** Methodology, Project administration, Validation, Writing - review & editing; **MS:** Conceptualization, Funding acquisition, Methodology, Project administration, Resources, Supervision, Validation, Writing - review & editing; **CR:** Conceptualization, Data Curation, Funding acquisition, Investigation, Methodology, Project administration, Supervision, Validation, Writing - review & editing;

Declaration of competing interest

The authors declare no competing financial interest.

Data availability

Data will be made available on request.

Acknowledgments

The authors are grateful to the French Government through the Embassy of France in Senegal (SCAC Scholarship), the Senegalese Government through the Ministry of Higher Education, Research and Innovation (PhD Foreign Scholarship), as well as the Haut-de-France Doctoral College (Mobility Scholarship to Belgium) and the University of Lille (Moblilex Scholarship) for the various funding granted. The authors are grateful to the members of the various research teams implicated in this study. UHPLC-HR-MS analysis were realized in the MASSMET platform of LDRI. We would like to thank Prof Nathalie Azaroual for the access to the UFR3S NMR technical platform located at the Faculty of Pharmacy of Lille, as well as Alexandre Rech and Vincent Ultré for their help in optimizing some parameters for NMR analyses (1D & 2D). We also thank Prof Pascal Marchand at Nantes University for the access to their electrothermal digital melting point apparatus.

Appendix A. Supplementary data

UHPLC or HPLC chromatograms of cyclohexane and DCM extracts, as well as fractions (FD1-FD8); Total ion chromatograms of cyclohexane and DCM extracts obtained by HR-ESI-MS; UV, IR, and 1D (^{1}H, ^{13}C), 2D-NMR (COSY, HSQC-DEPT and HMBC) spectra, MS spectra; Cytotoxicity evaluation of compounds **1**, **2**, **3**, **7**, **10**, **11**, **12**, and **13** on Huh-7 cells.; MS/MS fragmentation analysis and putative identification of chemical constituents in cyclohexane and dichloromethane extracts by using the MS^2 data obtained by HR-ESI-MS/MS.

Supplementary data to this article can be found online at https://doi.org/...

Dear author, please, make sure that you can answer YES to all these questions before submission:

1. Does your work deal with natural products? YES
2. Does your manuscript fit with the molecular trait of the Journal? YES
3. Are the results of your investigation original and not predictable based on the literature? YES
4. Has the organism investigated in your manuscript been properly identified? YES
5. If you report the study of the bioactivity of an extract, has this been phytochemically characterized, and have its active constituents identified and biologically assayed ? YES
6. Has a positive (or a negative) reference compound be used in the bioassays you report? YES
7. If your manuscript present docking experiments, have they been validated by biological assays. NOT CONCERNED
8. Have isolation and bioactivity evaluation been described in full details? YES
9. Have you included original NMR spectra in the SI for all novel compounds, making the discussion of structure elucidation easier to follow for readers? YES
10. Have all structural formulas been prepared according to the Journal's instructions (ChemDraw, ACS Style)? YES
11. Has configuration at all stereocenters been clearly indicated with the wedge/broken line notation? YES

References

Adesina, S.K., Reisch, J., 1988. Arnottianamide and Other Constituents of Zanthoxylum gillettii Root. J. Nat. Prod. 51, 601–602. https://doi.org/10.1021/np50057a031

Alotaibi, A., Ebiloma, G.U., Williams, R., Alfayez, I.A., Natto, M.J., Alenezi, S., Siheri, W., AlQarni, M., Igoli, J.O., Fearnley, J., De Koning, H.P., Watson, D.G., 2021. Activity of Compounds from Temperate Propolis against Trypanosoma brucei and Leishmania mexicana. Molecules 26, 3912. https://doi.org/10.3390/molecules26133912

Ba, A., Roumy, V., Al Ibrahim, M., Raczkiewicz, I., Samaillie, J., Hakem, A., Sahpaz, S., Belouzard, S., Diatta, W., Sidybé, M., Neut, C., Séron, K., Seck, M., Rivière, C., 2024. Antibacterial and anti-coronavirus investigation of selected Senegalese plant

species according to an ethnobotanical survey. J. Ethnopharmacol. 118070. https://doi.org/10.1016/j.jep.2024.118070

Bafandeh, S., Khodadadi, E., Ganbarov, K., Asgharzadeh, M., Köse, Ş., Samadi Kafil, H., 2023. Natural Products as a Potential Source of Promising Therapeutics for COVID-19 and Viral Diseases. Evid.-Based Complement. Altern. Med. ECAM 2023, 5525165. https://doi.org/10.1155/2023/5525165

Bero, J., Ganfon, H., Jonville, M.-C., Frédérich, M., Gbaguidi, F., DeMol, P., Moudachirou, M., Quetin-Leclercq, J., 2009. In vitro antiplasmodial activity of plants used in Benin in traditional medicine to treat malaria. J. Ethnopharmacol. 122, 439–444. https://doi.org/10.1016/j.jep.2009.02.004

Bero, J., Hannaert, V., Chataigné, G., Hérent, M.-F., Quetin-Leclercq, J., 2011. In vitro antitrypanosomal and antileishmanial activity of plants used in Benin in traditional medicine and bio-guided fractionation of the most active extract. J. Ethnopharmacol. 137, 998–1002. https://doi.org/10.1016/j.jep.2011.07.022

Berthod, A., Hassoun, M., Ruiz-Angel, M.J., 2005. Alkane effect in the Arizona liquid systems used in countercurrent chromatography. Anal. Bioanal. Chem. 383, 327–340. https://doi.org/10.1007/s00216-005-0016-7

Castillo, D., Sauvain, M., Rivaud, M., Jullian, V., 2014. In vitro and in vivo activity of benzo[c]phenanthridines against Leishmania amazonensis. Planta Med. 80, 902–906. https://doi.org/10.1055/s-0034-1382826

Chakraborty, S., Mallick, D., Goswami, M., Guengerich, F.P., Chakrabarty, A., Chowdhury, G., 2022. The Natural Products Withaferin A and Withanone from the Medicinal Herb Withania somnifera Are Covalent Inhibitors of the SARS-CoV-2 Main Protease. J. Nat. Prod. 85, 2340–2350. https://doi.org/10.1021/acs.jnatprod.2c00521

Chakravarty, A.K., Sarkar, T., Masuda, K., Shiojima, K., 1999. Carbazole alkaloids from roots of Glycosmis arborea. Phytochemistry 50, 1263–1266. https://doi.org/10.1016/S0031-9422(98)00666-9

Chambers, M.C., Maclean, B., Burke, R., Amodei, D., Ruderman, D.L., Neumann, S., Gatto, L., Fischer, B., Pratt, B., Egertson, J., Hoff, K., Kessner, D., Tasman, N., Shulman, N., Frewen, B., Baker, T.A., Brusniak, M.-Y., Paulse, C., Creasy, D., Flashner, L., Kani, K., Moulding, C., Seymour, S.L., Nuwaysir, L.M., Lefebvre, B., Kuhlmann, F., Roark, J., Rainer, P., Detlev, S., Hemenway, T., Huhmer, A., Langridge, J., Connolly, B., Chadick, T., Holly, K., Eckels, J., Deutsch, E.W., Moritz, R.L., Katz, J.E., Agus, D.B., MacCoss, M., Tabb, D.L., Mallick, P., 2012. A cross-platform toolkit for mass spectrometry and proteomics. Nat. Biotechnol. 30, 918–920. https://doi.org/10.1038/nbt.2377

Chappuis, F., Sundar, S., Hailu, A., Ghalib, H., Rijal, S., Peeling, R.W., Alvar, J., Boelaert, M., 2007. Visceral leishmaniasis: what are the needs for diagnosis, treatment and control? Nat. Rev. Microbiol. 5, 873–882. https://doi.org/10.1038/nrmicro1748

Couillerot, E., Caron, C., Comoe, L., Audran, J.-C., Molinatti, P., Zeches, M., Le Men-Olivier, L., Jardillier, J.-C., Chenieux, J.-C., 1994. Benzophenanthridine and furoquinoline accumulation in cell suspension cultures of Fagara zanthoxyloides. Phytochemistry, The International Journal of Plant Biochemistry 37, 425–428. https://doi.org/10.1016/0031-9422(94)85072-0

Danielewski, M., Zielińska, S., Matuszewska, A., Słupski, W., Włodarczyk, M., Jęśkowiak, I., Wiatrak, B., Kowalski, K., Jezierska-Domaradzka, A., Ziółkowski, P., Szeląg, A., Nowak, B., 2022. Sanguinarine-Chelerythrine Fraction of Coptis chinensis Exerts Anti-inflammatory Activity in Carrageenan Paw Oedema Test in Rats and Reveals

Reduced Gastrotoxicity. Oxid. Med. Cell. Longev. 2022, 1504929. https://doi.org/10.1155/2022/1504929

Dofuor, A.K., Djameh, G.I., Ayertey, F., Bolah, P., Amoa-Bosompem, M., Kyeremeh, K., Okine, L.K., Gwira, T.M., Ohashi, M., 2019a. Antitrypanosomal Effects of Zanthoxylum zanthoxyloides (Lam.) Zepern. & Timler Extracts on African Trypanosomes. Evid.-Based Complement. Altern. Med. ECAM 2019, 1730452. https://doi.org/10.1155/2019/1730452

Dofuor, A.K., Kwain, S., Osei, E., Mawuli Tetevi, G., Okine, L.K., Ohashi, M., Gwira, T.M., Kyeremeh, K., 2019b. N-(Isobutyl)-3,4-methylenedioxy Cinnamoyl Amide. Molbank 2019, M1070. https://doi.org/10.3390/M1070

Fotie, J., Bohle, D.S., Olivier, M., Adelaida Gomez, M., Nzimiro, S., 2007. Trypanocidal and antileishmanial dihydrochelerythrine derivatives from Garcinia lucida. J. Nat. Prod. 70, 1650–1653. https://doi.org/10.1021/np0702281

Fuchino, H., Kawano, M., Mori-Yasumoto, K., Sekita, S., Satake, M., Ishikawa, T., Kiuchi, F., Kawahara, N., 2010. In vitro leishmanicidal activity of benzophenanthridine alkaloids from Bocconia pearcei and related compounds. Chem. Pharm. Bull. (Tokyo) 58, 1047–1050. https://doi.org/10.1248/cpb.58.1047

Gonzalez, R.J., Tarloff, J.B., 2001. Evaluation of hepatic subcellular fractions for Alamar blue and MTT reductase activity. Toxicol. Vitro Int. J. Publ. Assoc. BIBRA 15, 257–259. https://doi.org/10.1016/s0887-2333(01)00014-5

Guetchueng, S.T., Nahar, L., Ritchie, K.J., Ismail, F.M.D., Evans, A.R., Sarker, S.D., 2018. Zanthoamides G-I: Three new alkamides from Zanthoxylum zanthoxyloides. Phytochem. Lett. 26, 125–129. https://doi.org/10.1016/j.phytol.2018.05.031

He, N., Wang, Peiqing, Wang, Pengyu, Ma, C., Kang, W., 2018. Antibacterial mechanism of chelerythrine isolated from root of Toddalia asiatica (Linn) Lam. BMC Complement. Altern. Med. 18, 261. https://doi.org/10.1186/s12906-018-2317-3

Houeze, E.A., Wang, Y., Zhou, Q., Zhang, H., Wang, X., 2023. Comparison study of Beninese and Chinese herbal medicines in treating COVID-19. J. Ethnopharmacol. 308, 116172. https://doi.org/10.1016/j.jep.2023.116172

Hu, Y.-Q., Gao, C., Zhang, S., Xu, L., Xu, Z., Feng, L.-S., Wu, X., Zhao, F., 2017. Quinoline hybrids and their antiplasmodial and antimalarial activities. Eur. J. Med. Chem. 139, 22–47. https://doi.org/10.1016/j.ejmech.2017.07.061

Ishii, H., Ishikawa, T., Lu, S.-T., Chen, I.-S., 1976. Arnottianamide and isoarnottianamide : The structural establishment due to chemical conversion from the known benzo[C]phenanthridine alkaloids by the novel baeyer-villiger like oxidation of an immonium group. Tetrahedron Lett. 17, 1203–1206. https://doi.org/10.1016/S0040-4039(00)78018-X

Kanehisa, M., Furumichi, M., Sato, Y., Kawashima, M., Ishiguro-Watanabe, M., 2023. KEGG for taxonomy-based analysis of pathways and genomes. Nucleic Acids Res. 51, D587–D592. https://doi.org/10.1093/nar/gkac963

Ke, Q., Duan, K., Cheng, Y., Xu, S., Xiao, S., Fang, L., 2023. Sanguinarine Exhibits Antiviral Activity against Porcine Reproductive and Respiratory Syndrome Virus via Multisite Inhibition Mechanisms. Viruses 15, 688. https://doi.org/10.3390/v15030688

Kerharo, 1971. L'aromathérapie et la gemmothérapie dans la pharmacopée sénégalaise traditionnelle. J. Agric. Tradit. Bot. Appliquée 18, 109–141. https://doi.org/10.3406/jatba.1971.6847

Kim, S., Chen, J., Cheng, T., Gindulyte, A., He, J., He, S., Li, Q., Shoemaker, B.A., Thiessen, P.A., Yu, B., Zaslavsky, L., Zhang, J., Bolton, E.E., 2023. PubChem 2023 update. Nucleic Acids Res. 51, D1373–D1380. https://doi.org/10.1093/nar/gkac956

Klejdus, B., Lojková, L., Kosina, P., Ulrichová, J., Šimánek, V., Kubáň, V., 2007. Liquid chromatographic/electrospray mass spectrometric determination (LC/ESI-MS) of chelerythrine and dihydrochelerythrine in near-critical CO2 extracts from real and spiked plasma samples. Talanta 72, 1348–1356. https://doi.org/10.1016/j.talanta.2007.01.055

Kodra, D., Pousinis, P., Vorkas, P.A., Kademoglou, K., Liapikos, T., Pechlivanis, A., Virgiliou, C., Wilson, I.D., Gika, H., Theodoridis, G., 2022. Is Current Practice Adhering to Guidelines Proposed for Metabolite Identification in LC-MS Untargeted Metabolomics? A Meta-Analysis of the Literature. J. Proteome Res. 21, 590–598. https://doi.org/10.1021/acs.jproteome.1c00841

Latarissa, I.R., Barliana, M.I., Meiliana, A., Lestari, K., 2021. Potential of Quinine Sulfate for COVID-19 Treatment and Its Safety Profile: Review. Clin. Pharmacol. Adv. Appl. 13, 225–234. https://doi.org/10.2147/CPAA.S331660

Lin, Q., Ma, C., Guan, H., Chen, L., Xie, Q., Cheng, X., Wang, C., 2020. Metabolites identification and reversible interconversion of chelerythrine and dihydrochelerythrine in vitro/in vivo in rats using ultra-performance liquid chromatography combined with electrospray ionization quadrupole time-of-flight tandem mass spectrometry. J. Pharm. Biomed. Anal. 189, 113462. https://doi.org/10.1016/j.jpba.2020.113462

Liu, L., Huang, Y., Zhang, K., Song, S., Li, S., Li, Y., Lan, Y., 2018. Hepatitis B core antigen regulates dendritic cell proliferation and apoptosis through regulation of PKC/NF-κB signaling pathway. Mol. Med. Rep. 18, 5726–5732. https://doi.org/10.3892/mmr.2018.9604

Loe, M.W.C., Lee, R.C.H., Chin, W.-X., Min, N., Teo, Z.Y., Ho, S.X., Yi, B., Chu, J.J.H., 2023. Chelerythrine chloride inhibits Zika virus infection by targeting the viral NS4B protein. Antiviral Res. 219, 105732. https://doi.org/10.1016/j.antiviral.2023.105732

Ma, C.H., Ke, W., Sun, Z.L., Peng, J.Y., Li, Z.X., Zhou, X., Fan, G.R., Huang, C.G., 2006. Large-Scale Isolation and Purification of Scoparone from Herba artemisiae scopariae by High-Speed Counter-Current Chromatography. Chromatographia 64, 83–87. https://doi.org/10.1365/s10337-006-0789-7

Malhotra, R., Rarhi, C., Diveshkumar, K.V., Barik, R., D'cunha, R., Dhar, P., Kundu, M., Chattopadhyay, S., Roy, S., Basu, S., Pradeepkumar, P.I., Hajra, S., 2016. Dihydrochelerythrine and its derivatives: Synthesis and their application as potential G-quadruplex DNA stabilizing agents. Bioorg. Med. Chem. 24, 2887–2896. https://doi.org/10.1016/j.bmc.2016.04.059

Mbaze, L.M., Lado, J.A., Wansi, J.D., Shiao, T.C., Chiozem, D.D., Mesaik, M.A., Choudhary, M.I., Lacaille-Dubois, M.-A., Wandji, J., Roy, R., Sewald, N., 2009. Oxidative burst inhibitory and cytotoxic amides and lignans from the stem bark of Fagara heitzii (Rutaceae). Phytochemistry 70, 1442–1447. https://doi.org/10.1016/j.phytochem.2009.08.007

Miao, F., Yang, X.-J., Zhou, L., Hu, H.-J., Zheng, F., Ding, X.-D., Sun, D.-M., Zhou, C.-D., Sun, W., 2011. Structural modification of sanguinarine and chelerythrine and their antibacterial activity. Nat. Prod. Res. 25, 863–875. https://doi.org/10.1080/14786419.2010.482055

Min, Y.D., Kwon, H.C., Yang, M.C., Lee, K.H., Choi, S.U., Lee, K.R., 2007. Isolation of limonoids and alkaloids from Phellodendron amurense and their multidrug resistance (MDR) reversal activity. Arch. Pharm. Res. 30, 58–63. https://doi.org/10.1007/BF02977779

Misra, L.N., Wouatsa, N.A.V., Kumar, S., Venkatesh Kumar, R., Tchoumbougnang, F., 2013. Antibacterial, cytotoxic activities and chemical composition of fruits of two Cameroonian Zanthoxylum species. J. Ethnopharmacol. 148, 74–80. https://doi.org/10.1016/j.jep.2013.03.069

Nayar, M.N.S., Sutar, C.V., Bhan, M.K., 1971. Alkaloids of the stem bark of Hesperethusa crenulata. Phytochemistry 10, 2843–2844. https://doi.org/10.1016/S0031-9422(00)97306-0

Oechslin, S.M., König, G.M., Oechslin-Merkel, K., Wright, A.D., Kinghorn, A.D., Sticher, O., Miyagawa, M., 1991. An Nmr Study of Four Benzophenanthridine Alkaloids. J. Nat. Prod. 54, 519–524. https://doi.org/10.1021/np50074a026

Okagu, I., Ndefo, J., Aham, E., Udenigwe, C.C., 2021. Zanthoxylum Species: A Comprehensive Review of Traditional Uses, Phytochemistry, Pharmacological and Nutraceutical Applications. Molecules 26, 4023. https://doi.org/10.3390/molecules26134023

Papi, F., Ferraroni, M., Rigo, R., Da Ros, S., Bazzicalupi, C., Sissi, C., Gratteri, P., 2017. Role of the Benzodioxole Group in the Interactions between the Natural Alkaloids Chelerythrine and Coptisine and the Human Telomeric G-Quadruplex DNA. A Multiapproach Investigation. J. Nat. Prod. 80, 3128–3135. https://doi.org/10.1021/acs.jnatprod.7b00350

Peng, L., Wen, L., Shi, Q., Gao, F., Huang, B., Wang, C., 2021. Chelerythrine Ameliorates Pulmonary Fibrosis via Activating the Nrf2/ARE Signaling Pathway. Cell Biochem. Biophys. 79, 337–347. https://doi.org/10.1007/s12013-021-00967-0

Plants of the World Online, n.d. Zanthoxylum L. | Plants of the World Online | Kew Science [WWW Document]. Plants World Online. URL

http://powo.science.kew.org/taxon/urn:lsid:ipni.org:names:329404-2 (accessed 4.13.24).

Pluskal, T., Castillo, S., Villar-Briones, A., Orešič, M., 2010. MZmine 2: Modular framework for processing, visualizing, and analyzing mass spectrometry-based molecular profile data. BMC Bioinformatics 11, 395. https://doi.org/10.1186/1471-2105-11-395

Pousset, 2004. Plantes médicinales d'Afrique: comment les reconnaître et les utiliser, Je choisis le naturel ! SECUM Édisud, [S.l.] Aix-en-Provence.

Queiroz, E., Hay, A.-E., Chaaib, F., van Diemen, D., Diallo, D., Hostettmann, K., 2006. New and Bioactive Aromatic Compounds from *Zanthoxylum zanthoxyloides*. Planta Med. 72, 746–750. https://doi.org/10.1055/s-2006-941504

Rinaldi, F., Giachè, S., Spinicci, M., Corsi, P., Ambu, S., Gianfaldoni, G., Rigacci, L., Arena, U., Bartoloni, A., Zammarchi, L., 2019. Focal spleen lesions in visceral leishmaniasis, a neglected manifestation of a neglected disease: report of three cases and systematic review of literature. Infection 47, 507–518. https://doi.org/10.1007/s15010-019-01279-5

Shoji, N., Umeyama, A., Iuchi, A., Saito, N., Takemoto, T., Nomoto, K., Ohizumi, Y., 1988. Isolation of a New Alkaloid from Evodia rutaecarpa. J. Nat. Prod. 51, 791–792. https://doi.org/10.1021/np50058a026

Valipour, M., Zarghi, A., Ebrahimzadeh, M.A., Irannejad, H., 2021. Therapeutic potential of chelerythrine as a multi-purpose adjuvant for the treatment of COVID-19. Cell Cycle Georget. Tex 20, 2321–2336. https://doi.org/10.1080/15384101.2021.1982509

Vila-Nova, N.S., de Morais, S.M., Falcão, M.J.C., Alcantara, T.T.N., Ferreira, P.A.T., Cavalcanti, E.S.B., Vieira, I.G.P., Campello, C.C., Wilson, M., 2013. Different susceptibilities of Leishmania spp. promastigotes to the Annona muricata acetogenins annonacinone and corossolone, and the Platymiscium floribundum coumarin

scoparone. Exp. Parasitol. 133, 334–338. https://doi.org/10.1016/j.exppara.2012.11.025

Wang, M., Carver, J.J., Phelan, V.V., Sanchez, L.M., Garg, N., Peng, Y., Nguyen, D.D., Watrous, J., Kapono, C.A., Luzzatto-Knaan, T., Porto, C., Bouslimani, A., Melnik, A.V., Meehan, M.J., Liu, W.-T., Crüsemann, M., Boudreau, P.D., Esquenazi, E., Sandoval-Calderón, M., Kersten, R.D., Pace, L.A., Quinn, R.A., Duncan, K.R., Hsu, C.-C., Floros, D.J., Gavilan, R.G., Kleigrewe, K., Northen, T., Dutton, R.J., Parrot, D., Carlson, E.E., Aigle, B., Michelsen, C.F., Jelsbak, L., Sohlenkamp, C., Pevzner, P., Edlund, A., McLean, J., Piel, J., Murphy, B.T., Gerwick, L., Liaw, C.-C., Yang, Y.-L., Humpf, H.-U., Maansson, M., Keyzers, R.A., Sims, A.C., Johnson, A.R., Sidebottom, A.M., Sedio, B.E., Klitgaard, A., Larson, C.B., Boya P, C.A., Torres-Mendoza, D., Gonzalez, D.J., Silva, D.B., Marques, L.M., Demarque, D.P., Pociute, E., O'Neill, E.C., Briand, E., Helfrich, E.J.N., Granatosky, E.A., Glukhov, E., Ryffel, F., Houson, H., Mohimani, H., Kharbush, J.J., Zeng, Y., Vorholt, J.A., Kurita, K.L., Charusanti, P., McPhail, K.L., Nielsen, K.F., Vuong, L., Elfeki, M., Traxler, M.F., Engene, N., Koyama, N., Vining, O.B., Baric, R., Silva, R.R., Mascuch, S.J., Tomasi, S., Jenkins, S., Macherla, V., Hoffman, T., Agarwal, V., Williams, P.G., Dai, J., Neupane, R., Gurr, J., Rodríguez, A.M.C., Lamsa, A., Zhang, C., Dorrestein, K., Duggan, B.M., Almaliti, J., Allard, P.-M., Phapale, P., Nothias, L.-F., Alexandrov, T., Litaudon, M., Wolfender, J.-L., Kyle, J.E., Metz, T.O., Peryea, T., Nguyen, D.-T., VanLeer, D., Shinn, P., Jadhav, A., Müller, R., Waters, K.M., Shi, W., Liu, X., Zhang, L., Knight, R., Jensen, P.R., Palsson, B.Ø., Pogliano, K., Linington, R.G., Gutiérrez, M., Lopes, N.P., Gerwick, W.H., Moore, B.S., Dorrestein, P.C., Bandeira, N., 2016. Sharing and community curation of mass spectrometry data with Global Natural Products Social

Molecular Networking. Nat. Biotechnol. 34, 828–837. https://doi.org/10.1038/nbt.3597

Wasilewicz, A., Bojkova, D., Beniddir, M.A., Cinatl, J., Rabenau, H.F., Grienke, U., Rollinger, J.M., Kirchweger, B., 2024. Molecular networking unveils anti-SARS-CoV-2 constituents from traditionally used remedies. J. Ethnopharmacol. 319, 117206. https://doi.org/10.1016/j.jep.2023.117206

Wei, Q., Cui, D., Liu, X., Chai, Y., Zhao, N., Wang, J., Zhao, M., 2020. In vitro antifungal activity and possible mechanisms of action of chelerythrine. Pestic. Biochem. Physiol. 164, 140–148. https://doi.org/10.1016/j.pestbp.2020.01.007

Wu, Y.-R., Ma, Y.-B., Zhao, Y.-X., Yao, S.-Y., Zhou, J., Zhou, Y., Chen, J.-J., 2007. Two New Quaternary Alkaloids and Anti-Hepatitis B Virus Active Constituents from Corydalis saxicola. Planta Med. 73, 787–791. https://doi.org/10.1055/s-2007-981549

Xia, X., Toy, P.H., 2014. Synthesis of γ-Sanshool and Hydroxy-γ-sanshool. Synlett 25, 2787–2790. https://doi.org/10.1055/s-0034-1379215

Yang, S., Tian, M., Yuan, L., Deng, H., Wang, L., Li, A., Hou, Z., Li, Y., Zhang, Y., 2016. Analysis of E. rutaecarpa Alkaloids Constituents In Vitro and In Vivo by UPLC-Q-TOF-MS Combined with Diagnostic Fragment. J. Anal. Methods Chem. 2016, e4218967. https://doi.org/10.1155/2016/4218967

Yang, T., Xu, R., Su, Q., Wang, H., Liu, F., Dai, B., Wang, B., Zhang, Y., 2020. Chelerythrine hydrochloride inhibits proliferation and induces mitochondrial apoptosis in cervical cancer cells via PI3K/BAD signaling pathway. Toxicol. Vitro Int. J. Publ. Assoc. BIBRA 68, 104965. https://doi.org/10.1016/j.tiv.2020.104965

Yang, Z., Zhang, D., Ren, J., Yang, M., 2012. Skimmianine, a furoquinoline alkaloid from Zanthoxylum nitidum as a potential acetylcholinesterase inhibitor. Med. Chem. Res. 21, 722–725. https://doi.org/10.1007/s00044-011-9581-9

Zeng, Q., Wang, Z.-J., Chen, S., Wang, H., Xie, T.-Z., Xu, X.-J., Xiang, M.-L., Chen, Y.-C., Luo, X.-D., 2022. Phytochemical and anti-MRSA constituents of Zanthoxylum nitidum. Biomed. Pharmacother. 148, 112758. https://doi.org/10.1016/j.biopha.2022.112758

Zepernick, B., Timler, F.K., 1981. Zanthoxylum zanthoxyloides (Lam.) Zepernick & Timler comb. nova (Rutaceae). Willdenowia 11, 361–362.

Table 1.

Antileishmanial, antitrypanosomal and cytotoxic activities of the crude extract ZZM and its partitions (ZZC, ZZD, ZZE, and ZZA) as well as isolated pure compounds (1-14).

Extract/Partitions/ Compounds	Parasitic strains		WI-38 cells	Selectivity Index (CC_{50}/ IC_{50})	
	IC_{50} ± SD (µg/mL or µM)[a]		**CC_{50} ± SD (µg/mL or µM)[a]**		
	L. mexicana mexicana	*T. brucei brucei*	WI-38	SI (Lmm)	SI (Tbb)
ZZM	0.61 ± 0.03	2.15 ± 0.20	41.42 ± 14.12	67.0	19.3
ZZE	1.37 ± 0.46	5.69 ± 0.39	>100	>72.8	>17.6
ZZA	0.17 ± 0.04	7.37 ± 0.50	53.07 ± 8.97	299.9	7.2
ZZC	0.66 ± 0.08	5.17 ± 2.03	41.44 ± 8.39	62.8	8.0
ZZD	0.07 ± 0.00	0.22 ± 0.01	18.22 ± 3.58	252.4	81.5
1	0.14 ± 0.03	0.36 ± 0.06	7.49 ± 0.24	52.0	20.8
2	0.03 ± 0.01	0.18 ± 0.02	5.81 ± 0.26	168.7	32.0
3	31.24 ± 4.08	68.19 ± 3.15	208.56 ± 23.96	6.7	3.1
4	34.77 ± 0.23	n.d	53.40 ± 0.30	1.5	-
5	92.87 ± 26.01	59.12 ± 11.18	147.29 ± 53.37	1.6	2.5
6	7.92 ± 0.40	18.21 ± 1.13	49.35 ± 10.93	6.2	2.7
7	0.06 ± 0.00	0.49 ± 0.05	17.40 ± 0.91	271.7	35.3
8	8.73 ± 3.49	36.35 ± 3.77	67.68 ± 5.72	7.8	1.9
9	5.90 ± 0.35	14.13 ± 1.57	13.62 ± 4.77	2.3	1.0
10	15.39 ± 0.95	n.d	22.98 ± 3.06	1.5	-
11	2.56 ± 0.16	9.54 ± 0.21	95.42 ± 1.79	37.2	10.0
12	56.14 ± 5.85	60.04 ± 52.33	63.67 ± 31.86	1.1	1.1
13	48.61 ± 8.45	56.41 ± 4.62	77.52 ± 7.59	1.6	1.4
14	48.12 ± 0.68	n.d	93.74 ± 3.32	1.9	-
Pentamidine	0.23 ± 0.03				
Amphotericin B	0.09 ± 0.01				
Suramin		0.04 ± 0.01			
Camptothecin			0.07 ± 0.01		

[a]: IC_{50} or CC_{50} in µg/mL for extracts, and in µM for pure compounds

n.d: not determined (viability always above 50%)

Crude methanolic extract (ZZM) and partitions: cyclohexane (ZZC), DCM (ZZD), EtOAc (ZZE) and aqueous (ZZA) of *Z. zanthoxyloides*

Selectivity indexes were specified. Parasitic strains and WI-38 cells were treated with increasing concentrations (in DMSO) for 72 h. Alamar Blue™ (on parasites) and MTT (on cells) assays were performed. Pentamidine, amphotericin B, suramin and camptothecin were used as positive controls. Data are expressed as mean ± SEM from three independent experiments performed in triplicates ($P < 0.001$ for all results).

Table 2.
^{1}H (500 MHz) and ^{13}C NMR (125 MHz) Assignments for Compound **1** in $CDCl_3$ (δ in ppm).

Position	δ_C, type	δ_H, mult. (J in Hz)	HMBC ($^{1}H \rightarrow ^{13}C$)
1	104.4, CH	7.07, s	3, 4, 12a
2	147.5, C		
3	148.1, C		
4	100.6, CH	7.76, s	1, 2, 4b, 12a
4a	126.8, C		
4b	139.6, C		
5-NMe	42.2, CH_3	2.80, s	4b, 6
6	55.3, CH	5.83, d (1.4)	2', 3', 4b, 6a, 7
6a	124.5, C		
7	146.4, C		
8	152.1, C		
9	112.3, CH	7.08, d (8.6)	
10	119.1, CH	7.61, d (8.6)	
10a	125.5, C		
10b	123.3, C		
11	119.8, CH	7.69, d (8.6)	
12	124.0, CH	7.43, d (8.6)	
12a	131.0, C		
2'	150.2, C		
3'	104.9, CH	6.26, d (1.4)	2', 3'a, 4', 6, 9'a
3'a	106.2, C		
4'	173.6, C=O		
4'a	118.8, C		
5'	122.2, CH	8.02, d (9.1)	
6'	107.9, CH	6.90, d (9.1)	
7'	153.1, C		
8'	134.7, C		
8'a	131.1, C		
9'-NH		9.06, s	3'a, 4'a, 8'
9'a	154.7, C		
2-O-CH_2-O-3	101.0, CH_2	6.06, dd (10.3, 1.2)	2, 3
7-OMe	61.2, CH_3	3.91, s	7
8-OMe	55.8, CH_3	3.99, s	8
7'-OMe	56.1, CH_3	3.95, s	7'
8'-OMe	61.0, CH_3	3.97, s	8'

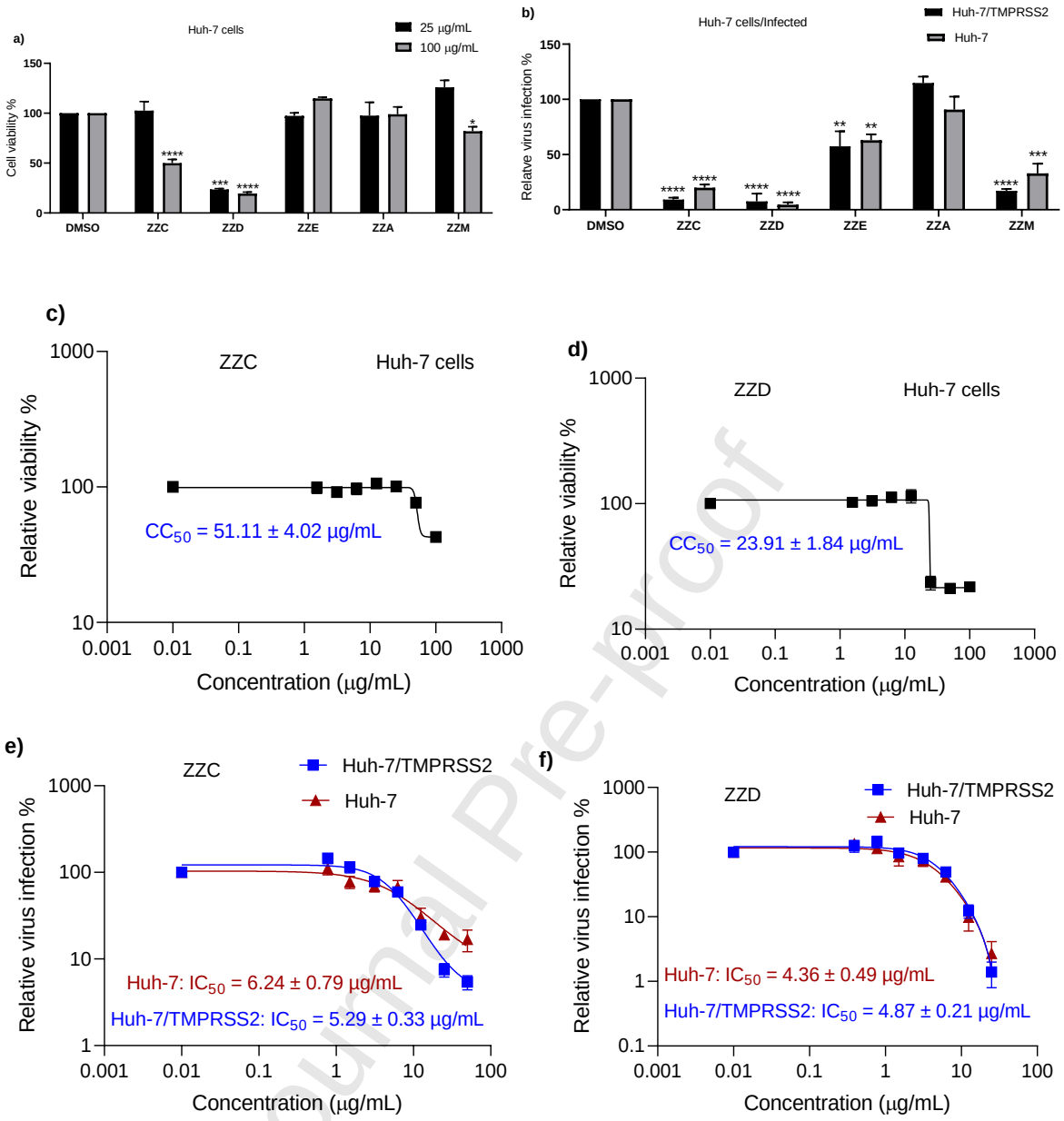

Fig. 1. Effects of the crude extract (ZZM) and the extracts (ZZC, ZZD, ZZE and ZZA) on (**a**) the Huh-7 cell proliferation by using the MTS assay at 25 µg/mL and 100 µg/mL, and (**b**) their antiviral activity at 25 µg/mL on HCoV-229E-Luc in Huh-7 and Huh-7/TMPRSS2 cells. Toxicity and antiviral evaluation in dose-response of ZZC ((**c**) and (**e**)) and ZZD ((**d**) and (**f**)). Data were analyzed by the One-way ANOVA and are expressed as mean ± SEM from three independent experiments, performed in triplicates. **** *P < 0.0001*, *** *P < 0.001*, ** *P < 0.01*, * *P < 0.05* (significantly different from DMSO control).

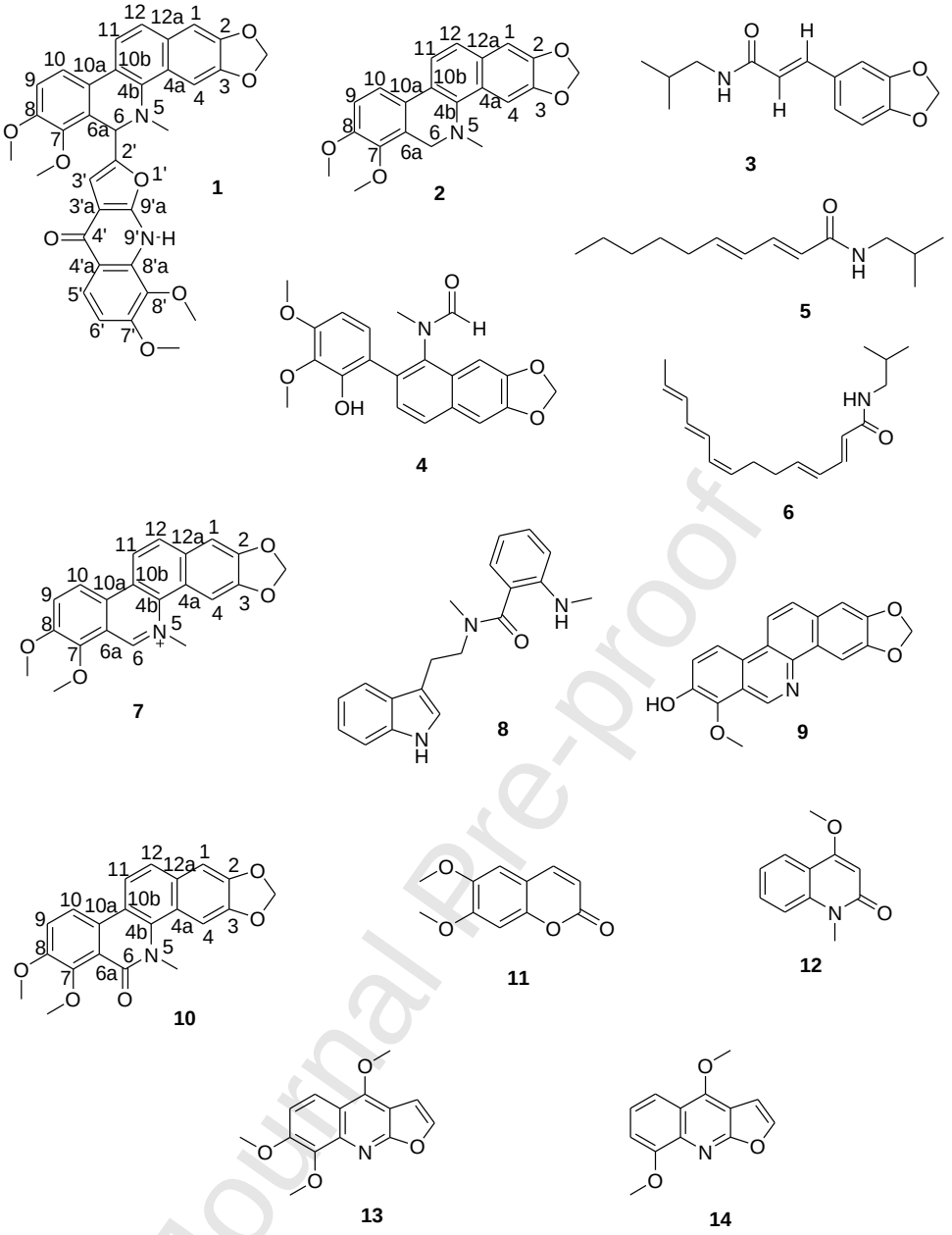

Fig. 2. The structures of compounds **1–14**.

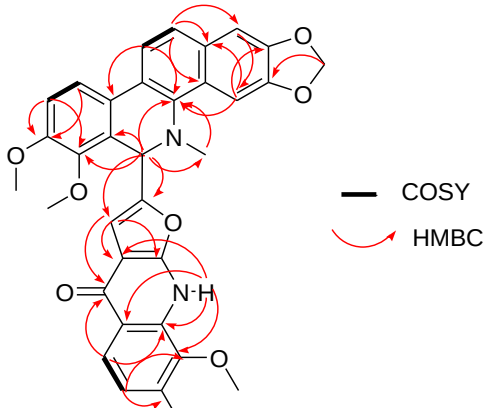

Fig. 3. Correlations observed in COSY and HMBC for compound **1.**

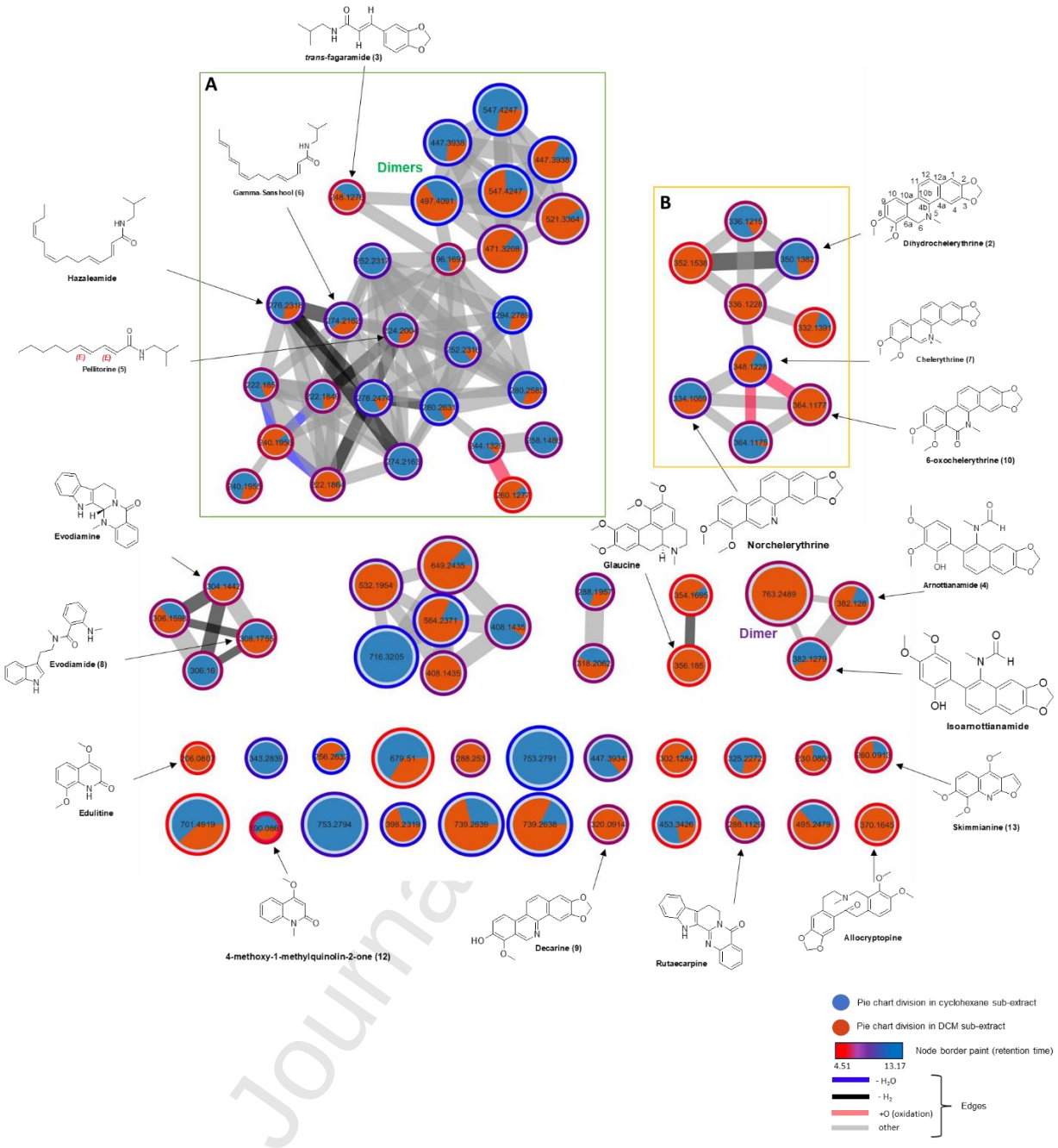

Fig. 4. Molecular network of cyclohexane (ZZC) and DCM (ZZD) extracts of *Z. zanthoxyloides*. A: Amides and B: Benzophenanthridines alkaloids clusters. Pie chart division of nodes are proportional to corresponding peak area in the extract. The size of the nodes is proportional to the *m/z* of the compounds. The size of the edges is proportional to the cosine score.

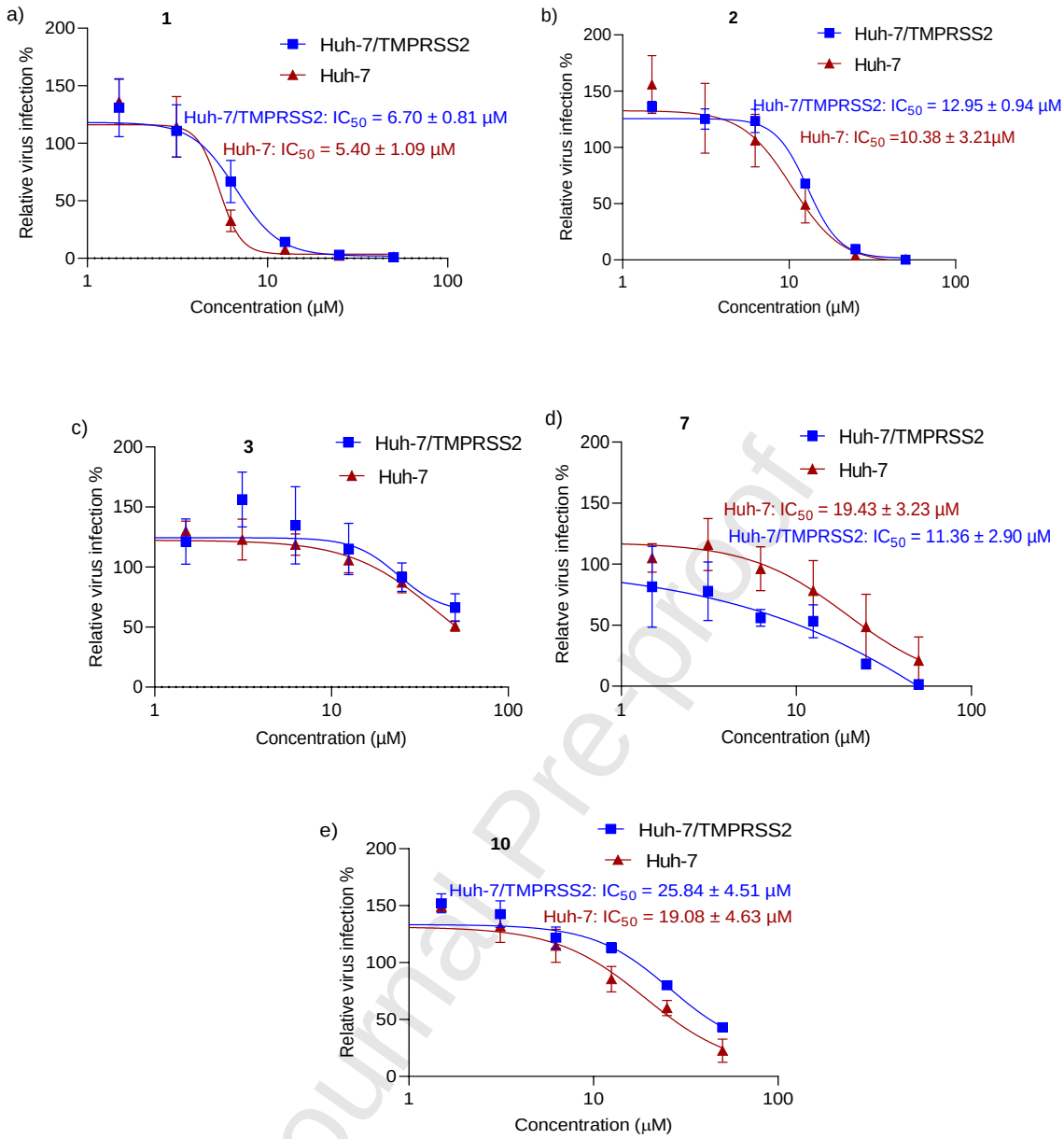

Fig. 5. Antiviral activity of compounds **1**, **2**, **3**, **7**, and **10** against HCoV-229E. For each compound, antiviral activity was determined with increasing concentrations. Huh-7 and Huh-7/TMPRSS2 cells seeded in 96-well plate were inoculated with HCoV-229E-Luc in the presence of the compound at the indicated concentrations. Cells were lysed after 7 h post inoculation, and luciferase activity was quantified. Data are expressed relative to the control DMSO ($P < 0.0001$, for all results). Results are expressed as mean ± SEM from three independent experiments, performed in triplicates.

Supplementary Material

Antileishmanial, antitrypanosomal and anti-coronavirus activities of benzophenanthridine alkaloids and other specialized metabolites isolated from the root bark of *Zanthoxylum zanthoxyloides* (Lam.) B.Zepernick & Timler

Abda Ba,[a,b] Vincent Roumy,[a] Malak Al Ibrahim,[a,c,†] Kristelle Hughes,[d,†] Thierry Hennebelle,[a] Jennifer Samaillie,[a] Sevser Sahpaz,[a] Mehdi A. Beniddir,[e] Marie-France Hérent,[d] Karin Séron,[c] Joëlle Quetin Leclercq,[d] Matar Seck,[b] and Céline Rivière[a,*]

[a] *Joint Research Unit 1158 BioEcoAgro, Univ. Lille, Junia, INRAE, Univ. Liège, UPJV, Univ. Artois, ULCO, F-59650 Villeneuve d'Ascq, France*

[b] *Laboratoire de Chimie Organique et Thérapeutique, Faculté de Médecine, de Pharmacie et d'Odontologie de l'Université Cheikh Anta Diop de Dakar, BP 5005, Dakar-Fann, Sénégal*

[c] *Univ. Lille, CNRS, Inserm, CHU Lille, Institut Pasteur de Lille, U1019 – UMR9017 – Center for Infection and Immunity of Lille (CIIL), F-59000 Lille, France*

[d] *Pharmacognosy Research Group, Louvain Drug Research Institute, Université catholique de Louvain (UCLouvain), Avenue E. Mounier, 72, B B01.72.03-1200 Brussels, Belgium*

[e] *Equipe Chimie des Substances Naturelles, BioCIS, CNRS, Université Paris-Saclay, 17 Avenue des Sciences, 91400, Orsay, France*

Corresponding Author

Céline Rivière - *Joint Research Unit 1158 BioEcoAgro, Laboratory of pharmacognosy, UFR3S Pharmacy, University of Lille, 3 rue du Professeur Laguesse, 59000 Lille; orcid.org/0000-0002-8618-5530; E-mail:* celine.riviere@univ-lille.fr

[†] These authors contributed equally to this work.

Contents

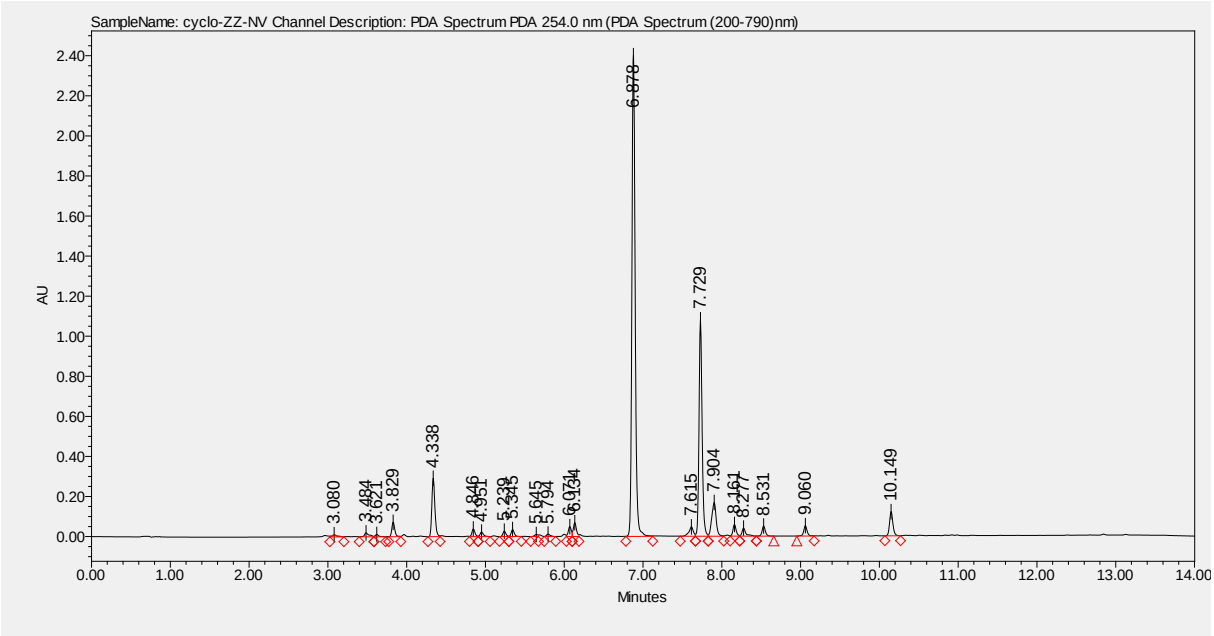

Fig. S1. Chromatographic profile of the cyclohexane extract at 254 nm obtained by UHPLC-UV-MS analysis.

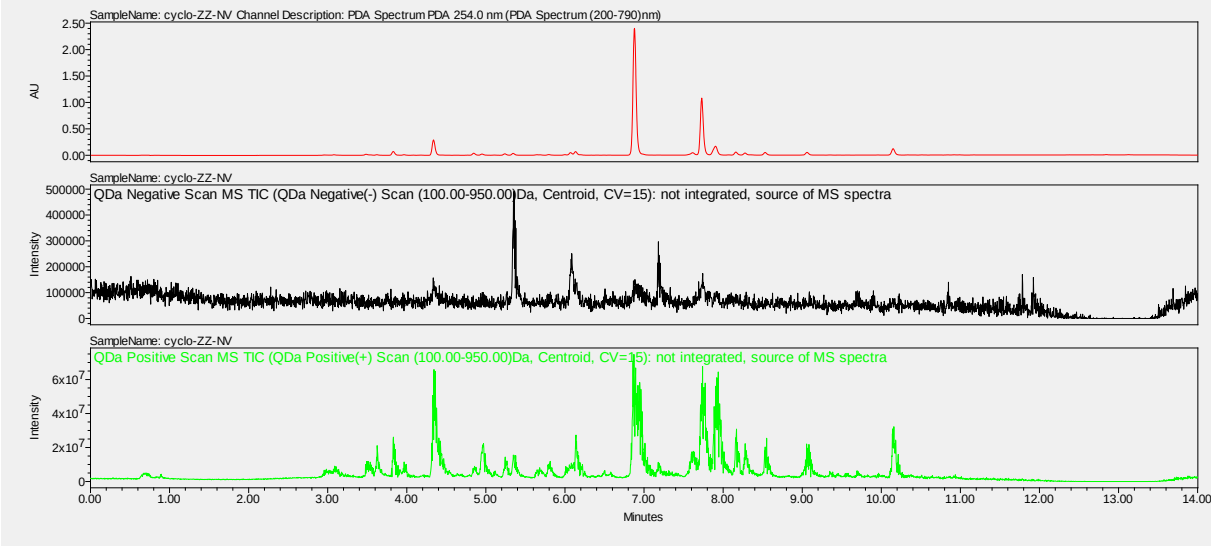

Fig. S2. Chromatographic profile of cyclohexane extract at 254 nm (top) and Total Ion Chromatograms in negative (middle) and positive (bottom) mode obtained by UHPLC-UV-MS analysis.

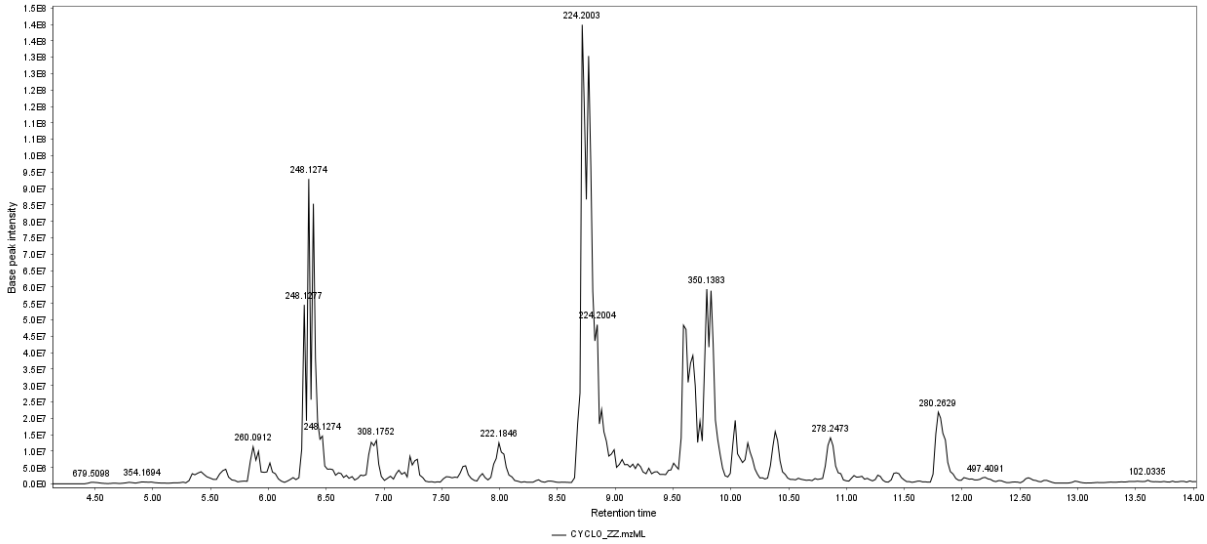

Fig. S3. Base peak chromatogram of the cyclohexane extract in positive ion mode obtained by UPLC-HRMS/MS analysis.

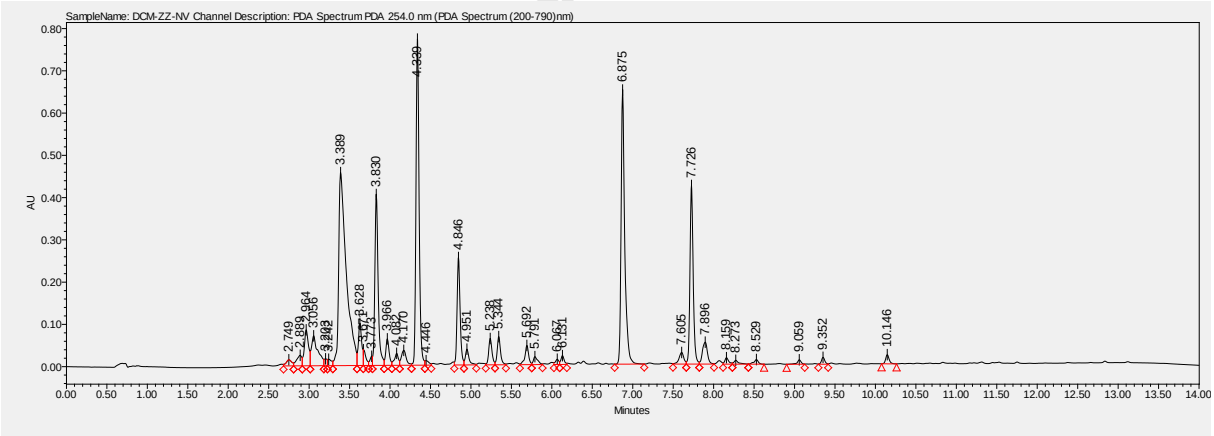

Fig. S4. Chromatographic profile of the dichloromethane extract at 254 nm obtained by UHPLC-UV-MS analysis.

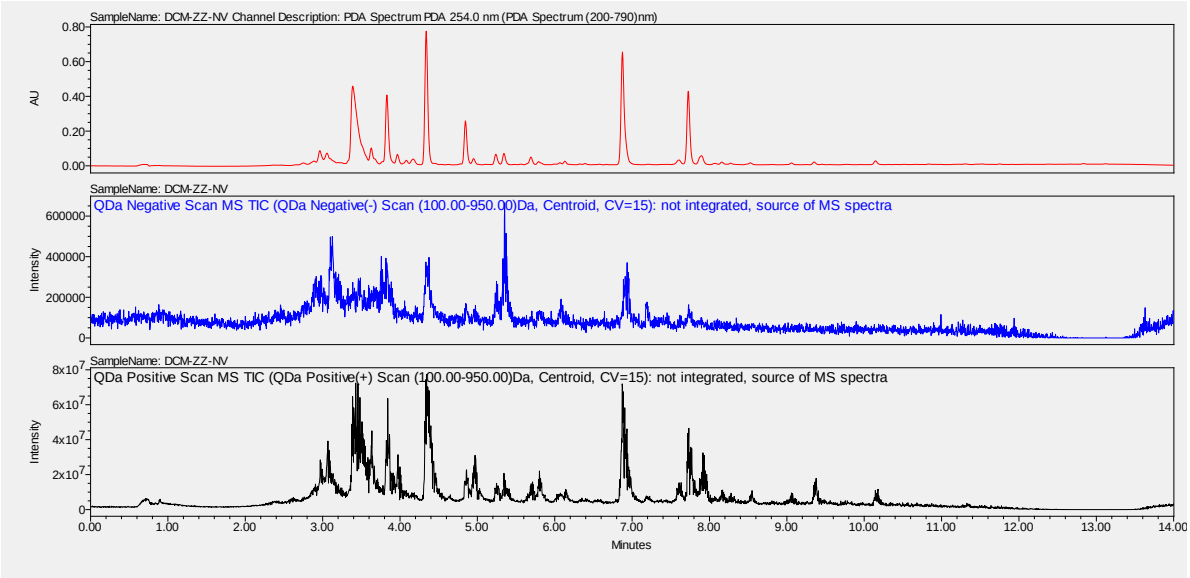

Fig. S5. Chromatographic profile of dichloromethane extract at 254 nm (top) and Total Ion Chromatograms in negative (middle) and positive (bottom) mode obtained by UHPLC-UV-MS analysis.

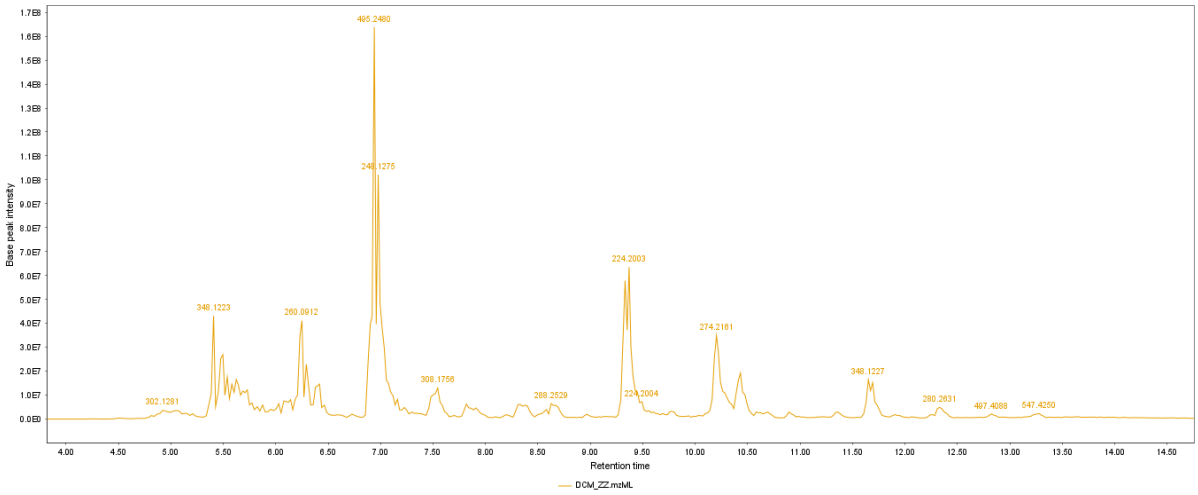

Fig. S6. Base peak chromatogram of the dichloromethane extract in positive ion mode obtained by UHPLC-HRMS/MS.

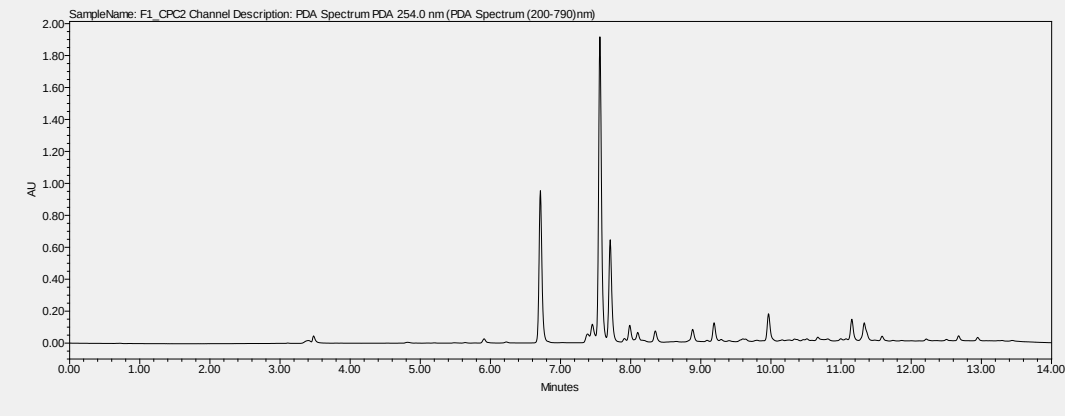

Fig. S7. Chromatographic profile of the FD1 fraction of dichloromethane extract at 254 nm obtained by UHPLC-UV-MS analysis.

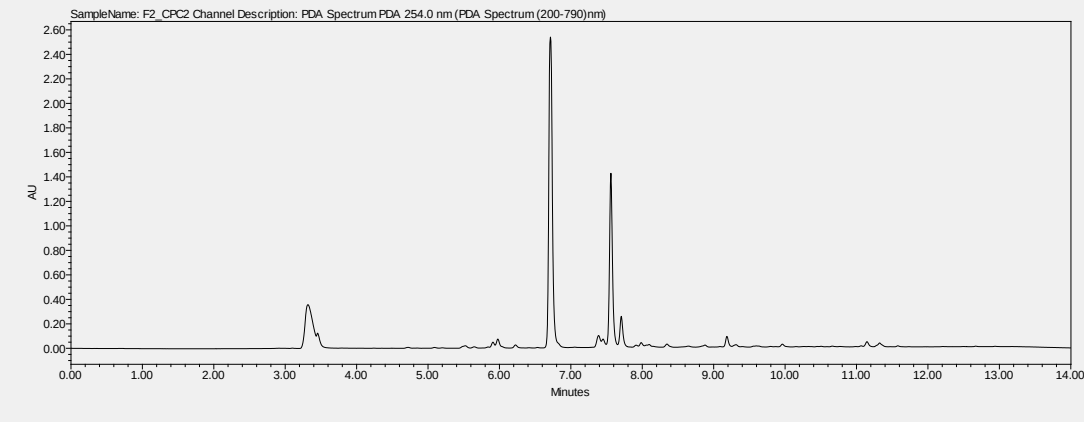

Fig. S8. Chromatographic profile of the FD2 fraction of dichloromethane extract at 254 nm obtained by UHPLC-UV-MS analysis.

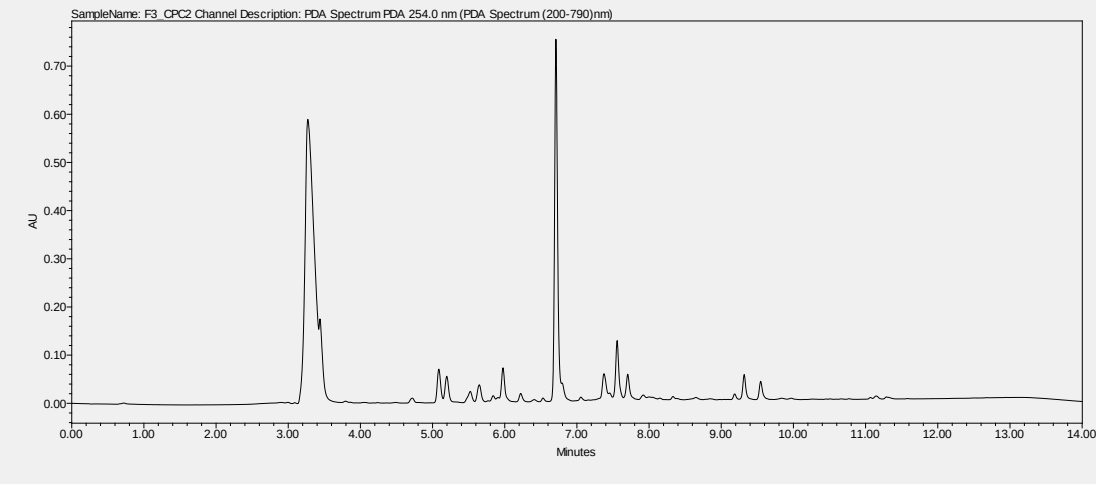

Fig. S9. Chromatographic profile of the FD3 fraction of dichloromethane extract at 254 nm obtained by UHPLC-UV-MS analysis.

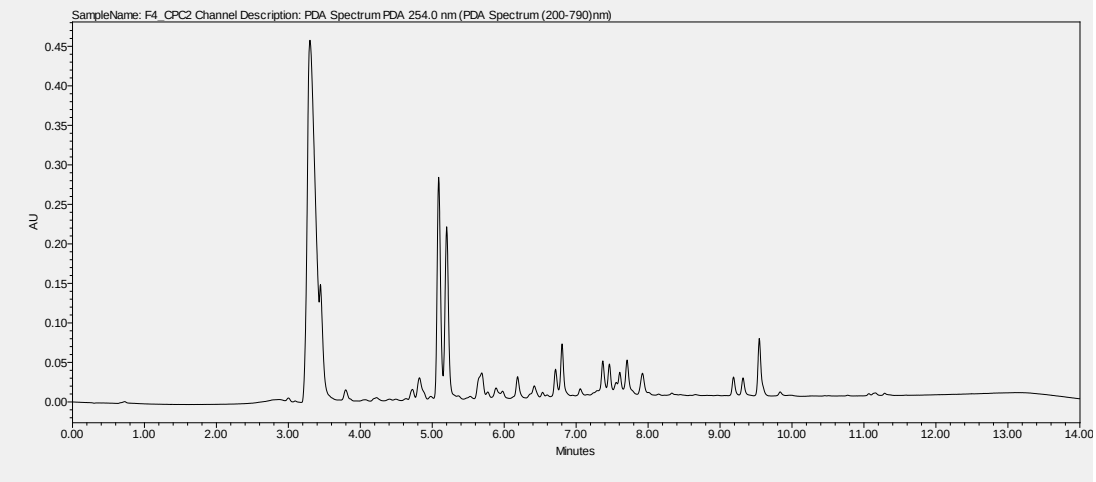

Fig. S10. Chromatographic profile of the FD4 fraction of dichloromethane extract at 254 nm obtained by UHPLC-UV-MS analysis.

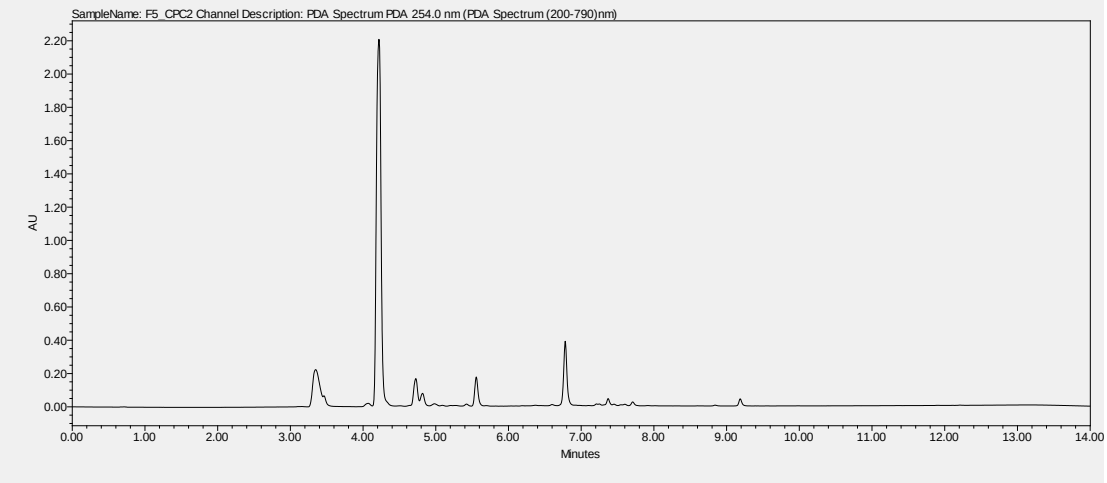

Fig. S11. Chromatographic profile of the FD5 fraction of dichloromethane extract at 254 nm obtained by UHPLC-UV-MS analysis.

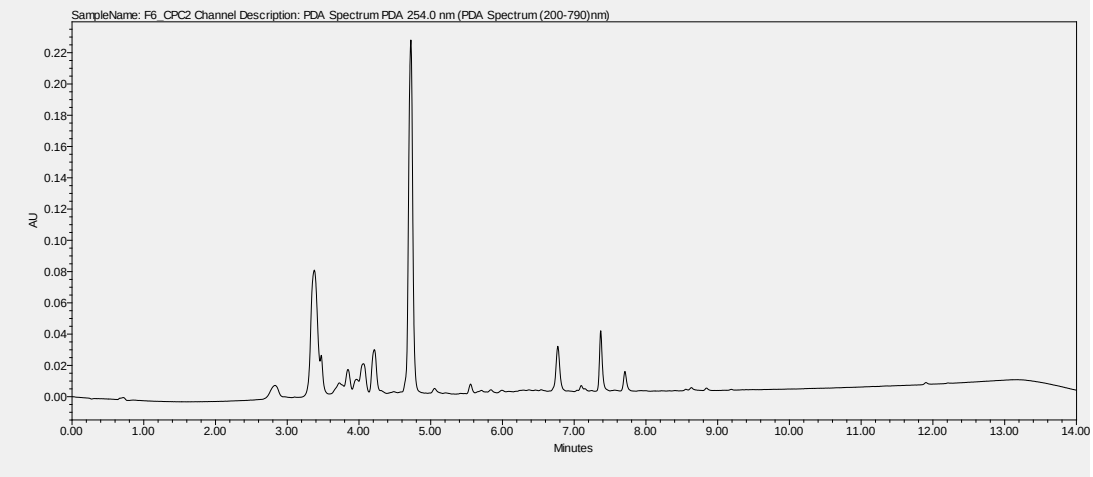

Fig. S12. Chromatographic profile of the FD6 fraction of dichloromethane extract at 254 nm obtained by UHPLC-UV-MS analysis.

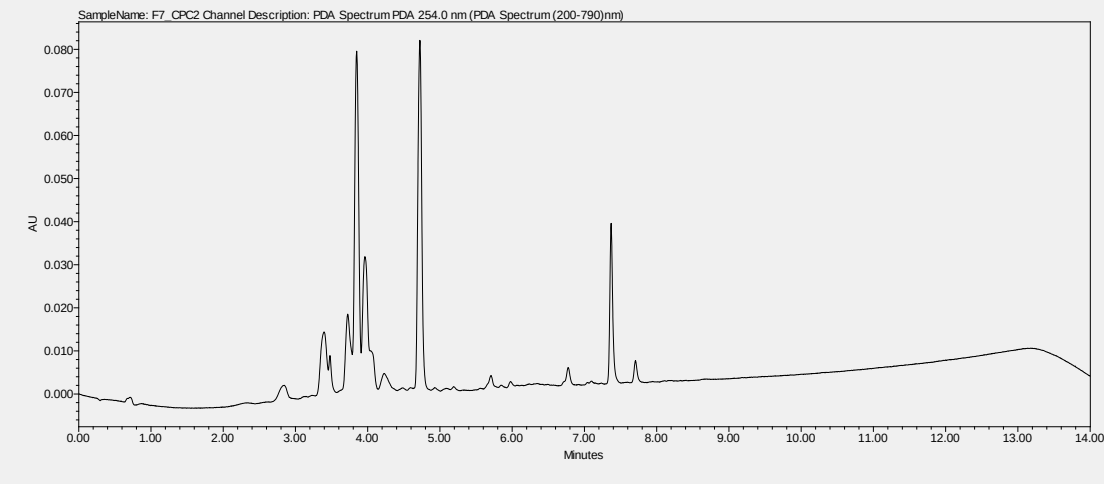

Fig. S13. Chromatographic profile of the FD7 fraction of dichloromethane extract at 254 nm obtained by UHPLC-UV-MS analysis.

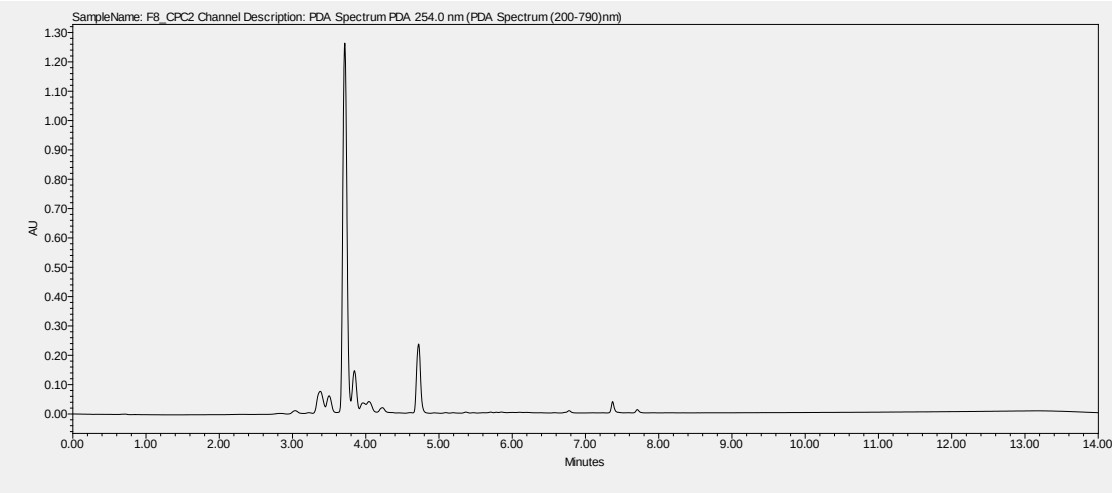

Fig. S14. Chromatographic profile of the FD8 fraction of dichloromethane extract at 254 nm obtained by UHPLC-UV-MS analysis.

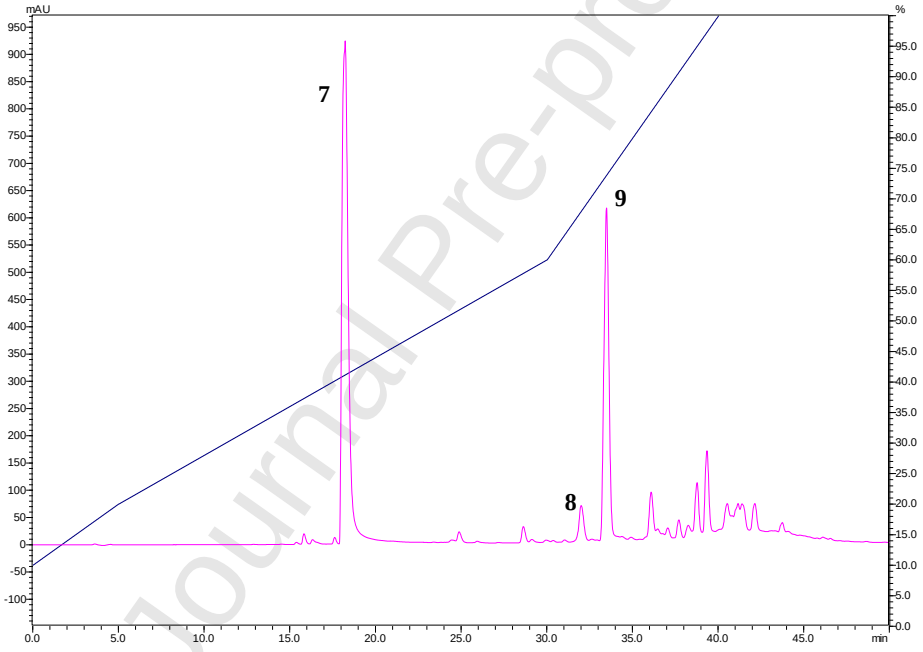

Fig. S15. Chromatographic profile of the FD4 fraction of dichloromethane extract at 254 nm obtained by HPLC-UV analysis.

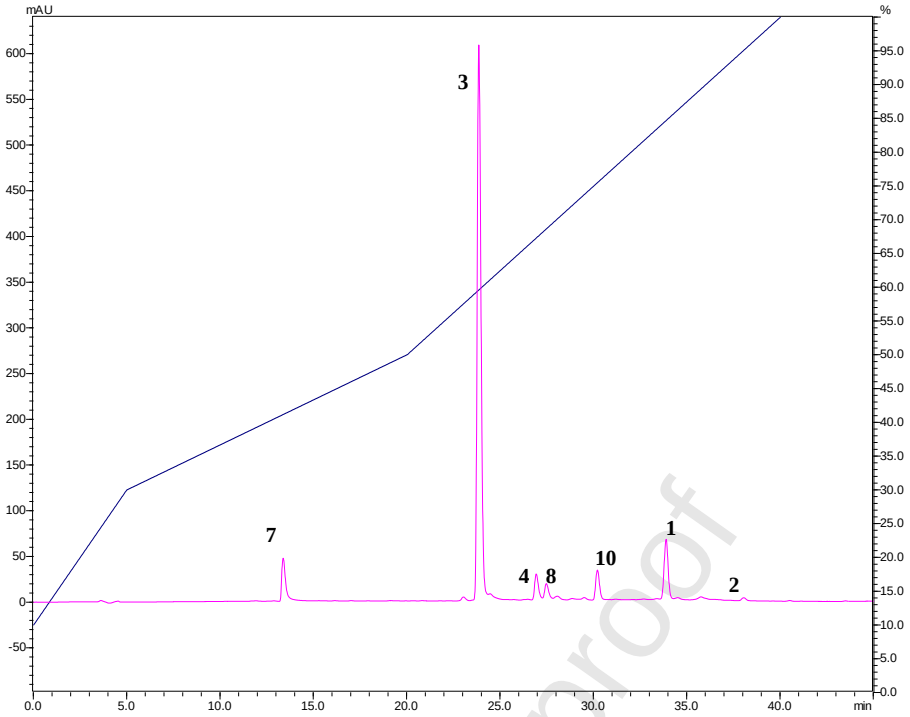

Fig. S16. Chromatographic profile of the FD5 fraction of dichloromethane extract at 254 nm obtained by HPLC-UV analysis.

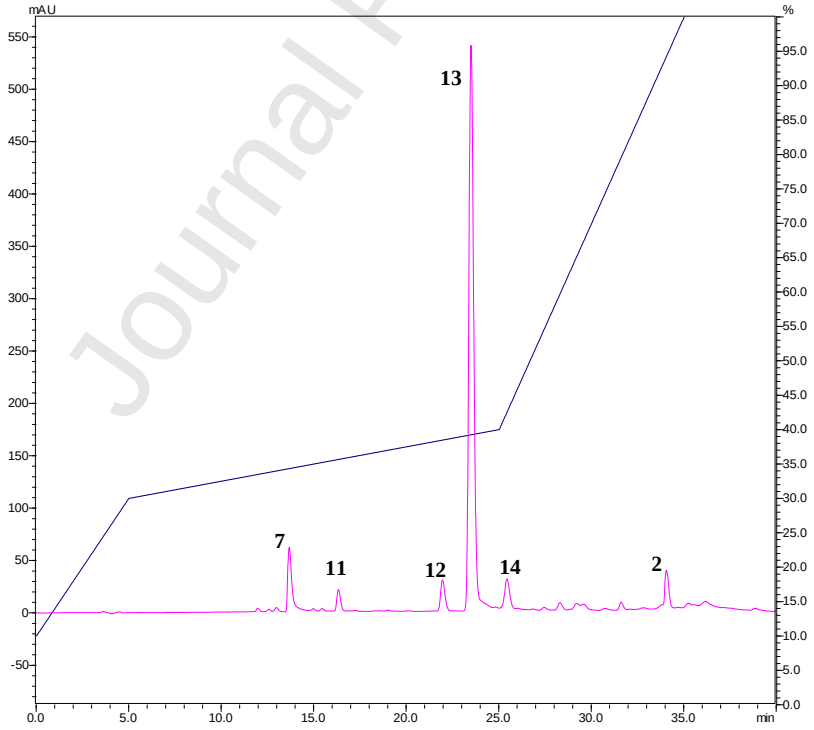

Fig. S17. Chromatographic profile of the FD8 fraction of dichloromethane extract at 254 nm obtained by HPLC-UV analysis.

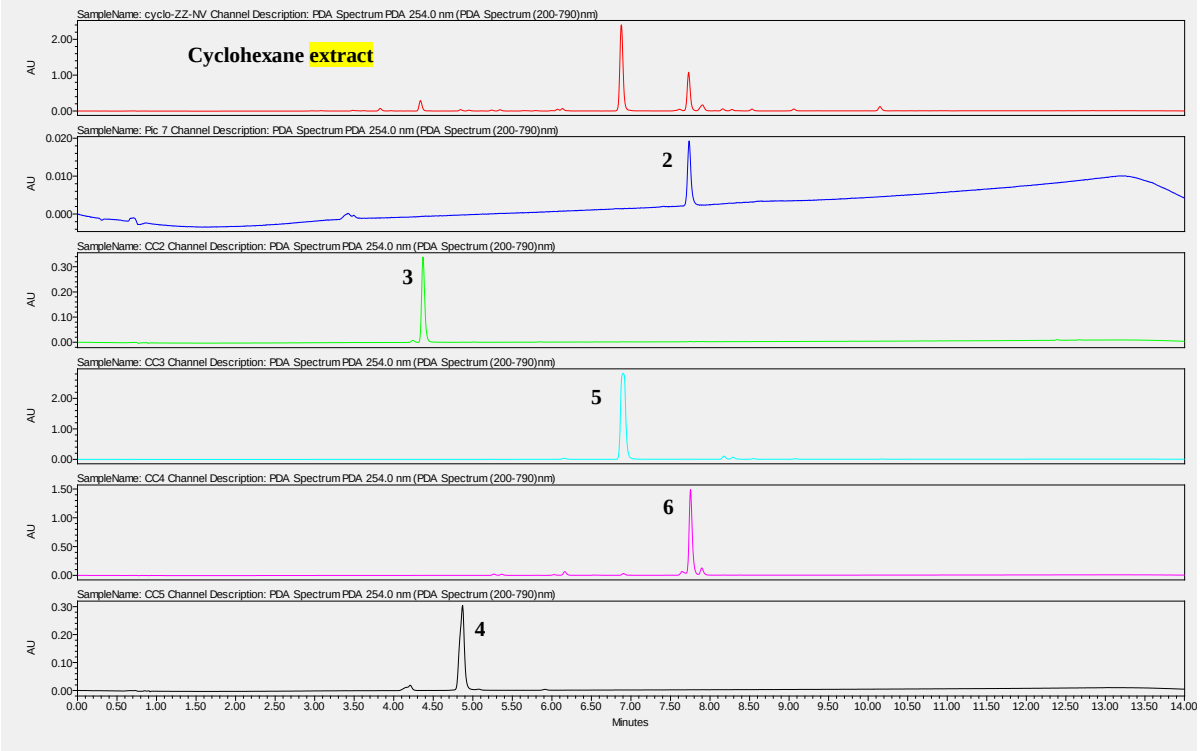

Fig. S18. Chromatographic profile of the cyclohexane extract with its isolated compounds at 254 nm obtained by UHPLC-UV-MS analysis.

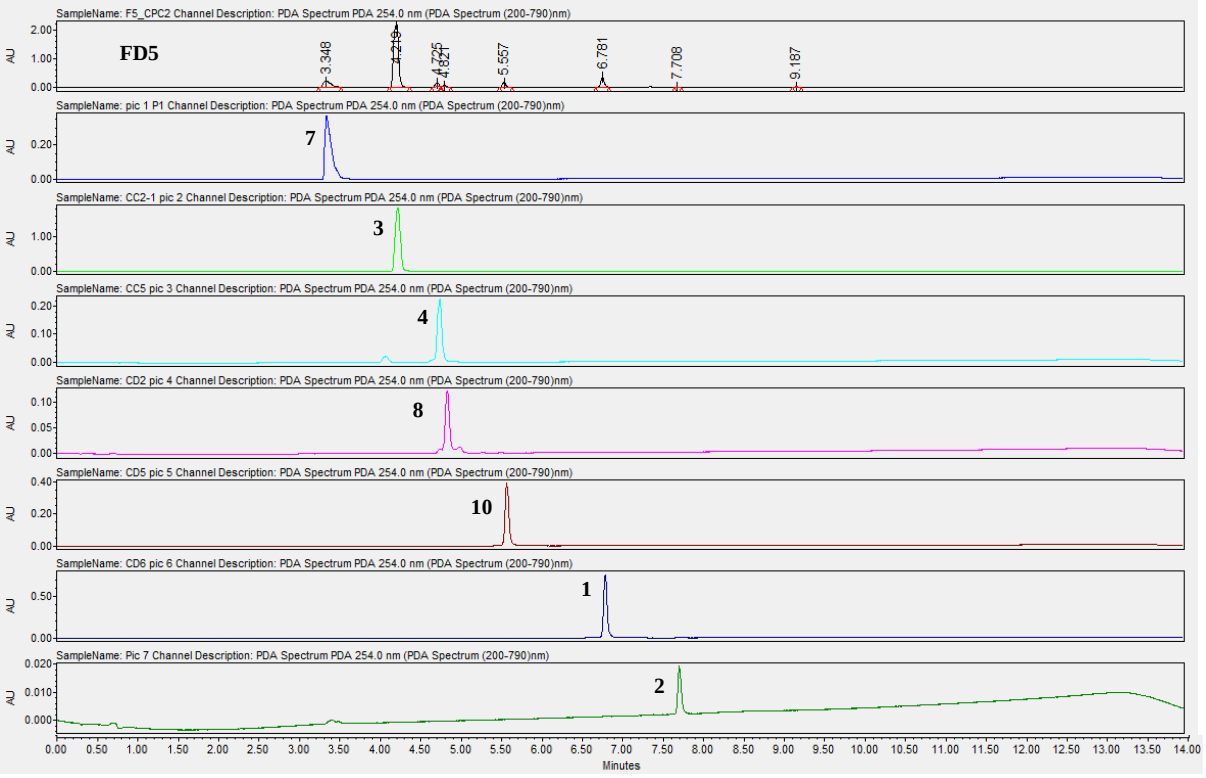

Fig. S19. Chromatographic profile of the FD5 fraction with its isolated compounds at 254 nm obtained by UHPLC-UV-MS analysis.

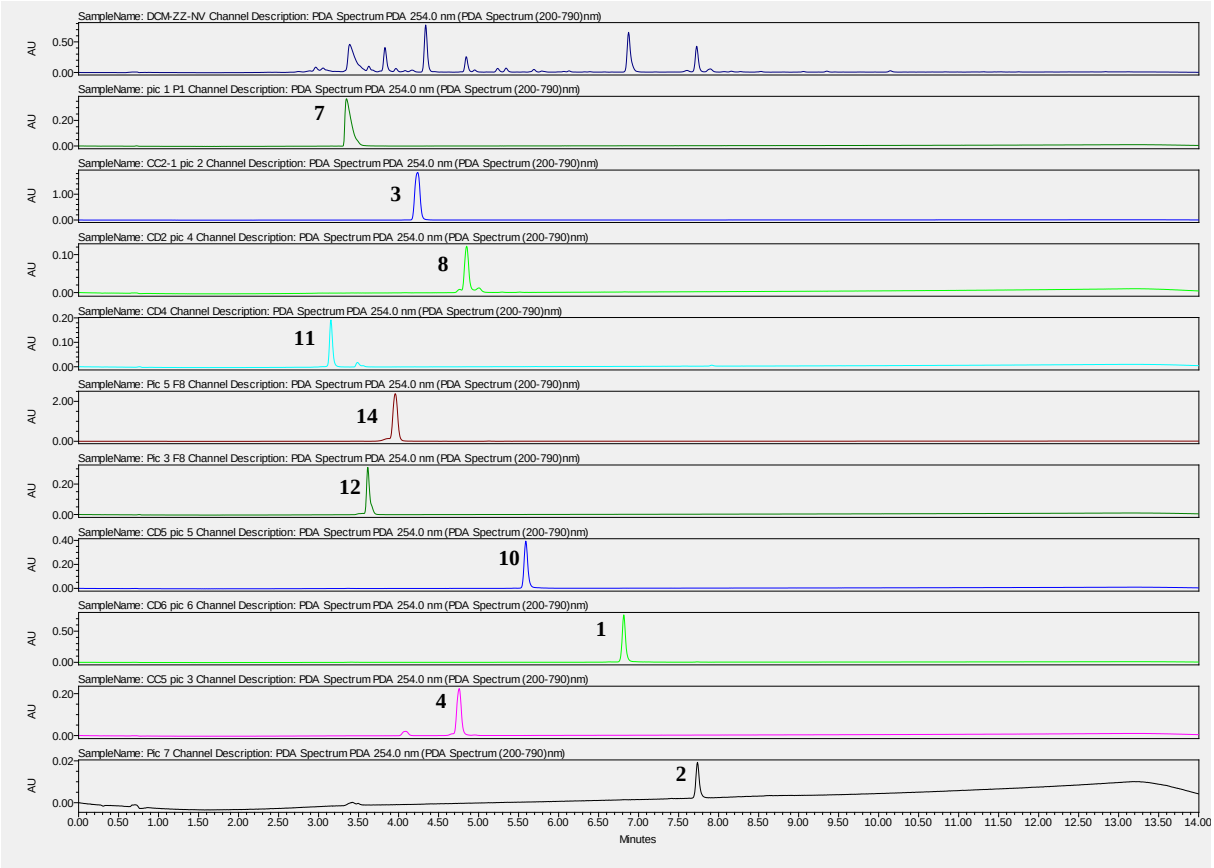

Fig. S20. Chromatographic profile of the dichloromethane extract with its isolated compounds at 254 nm obtained by UHPLC-UV-MS analysis.

Zanthoxyloithrine (1)

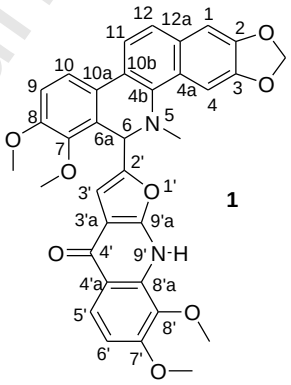

Brown powder; m.p: 215-216°C; $[\alpha]_D^{25}$ 0 (*c* 0.01, CH_2Cl_2); UHPLC-UV: λ_{max} (AU) 231 (0.69), 260 (0.88), 282 (0.62), 325 (0.31) nm; IR υ_{max} 3400, 3000, 2944, 2893, 2838, 2810, 1634, 1573, 1522, 1492, 1460, 1415, 1361, 1265, 1238, 1072, 1039 cm^{-1}; ^1H NMR ($CDCl_3$, 500 MHz) δ (ppm) 9.06 (1H, s, NH), 8.02 (1H, d, *J* = 9.1 Hz, H-5'), 7.76 (1H, s, H-4), 7.69 (1H, d, *J* = 8.6 Hz, H-11), 7.61 (1H, d, *J* = 8.6 Hz, H-10), 7.43 (1H, d, *J* = 8.6 Hz, H-12), 7.08

(1H, d, *J* = 8.6 Hz, H-9), 7.07 (1H, s, H-1), 6.90 (1H, d, *J* = 9.1 Hz, H-6'), 6.26 (1H, d, *J* = 1.4 Hz, H-3'), 6.06 (2H, dd, *J* = 10.3, 1.2 Hz, C-2-O-CH_2-O-C-3), 5.83 (1H, d, *J* = 1.4 Hz, H-6), 3.99 (3H, s, C-8-O-CH_3), 3.97 (3H, s, C-8'-O-CH_3), 3.95 (3H, s, C-7'-O-CH_3), 3.91 (3H, s, C-7-O-CH_3), 2.80 (3H, s, N-CH_3); ^{13}C NMR ($CDCl_3$, 125 MHz) δ (ppm) 173.6 (C=O, C-4'), 154.7 (C, C-9'a), 153.1 (C, C-7'), 152.1 (C, C-8), 150.2 (C, C-2'), 148.1 (C, C-3), 147.5 (C, C-2), 146.4 (C, C-7), 139.6 (C, C-4b), 134.7 (C, C-8'), 131.1 (C, C-8'a), 131.0 (C, C-12a), 126.8 (C, C-4a), 125.5 (C, C-10a), 124.5 (C, C-6a), 124.0 (CH, C-12), 123.3 (C, C-10b), 122.2 (CH, C-5'), 119.8 (CH, C-11), 119.1 (CH, C-10), 118.8 (C, C-4'a), 112.3 (CH, C-9), 107.9 (CH, C-6'), 106.2 (C, C-3'a), 104.9 (CH, C-3'), 104.4 (CH, C-1), 101.0 (CH_2, C-2-O-CH_2-O-C-3), 100.6 (CH, C-4), 61.2 (CH_3, C-7-O-CH_3), 61.0 (CH_3, C-8'-O-CH_3), 56.1 (CH_3, C-7'-O-CH_3), 55.8 (CH_3, C-8-O-CH_3), 55.3 (CH, C-6), 42.2 (CH_3, N-CH_3); ESIMS: *m/z* (rel. int.) 593.1907 $[M+H]^+$ (100), 563 (12), 521 (6), 360 (3), 349 (7), 348 (28), 325 (12), 304 (1), 291(8); HRESIMS *m/z* calcd for $C_{34}H_{28}N_2O_8$, 593.1895; found 593.1907.

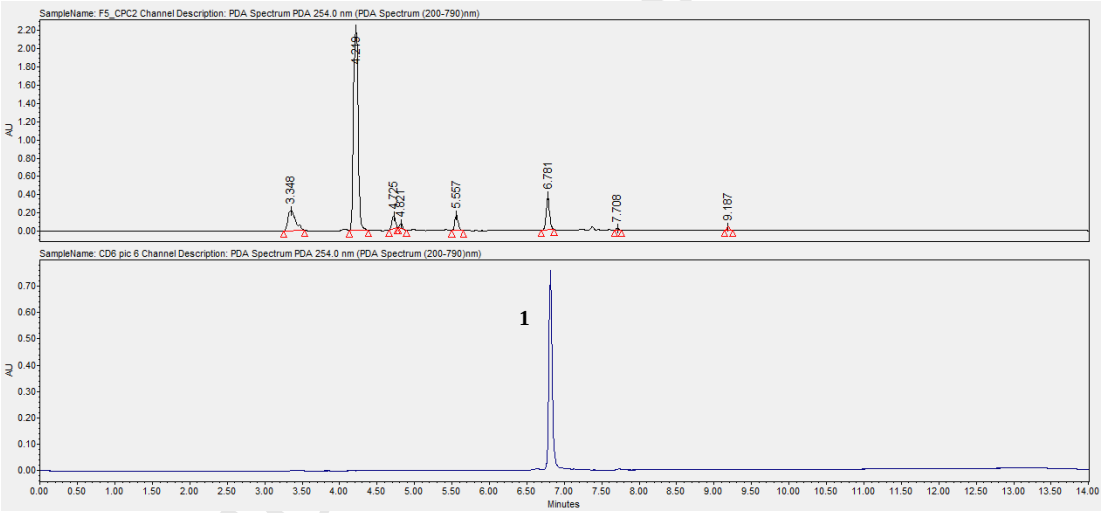

Fig. S21. Chromatographic profile of the FD5 fraction with the compound **1** at 254 nm obtained by UHPLC-UV-MS analysis.

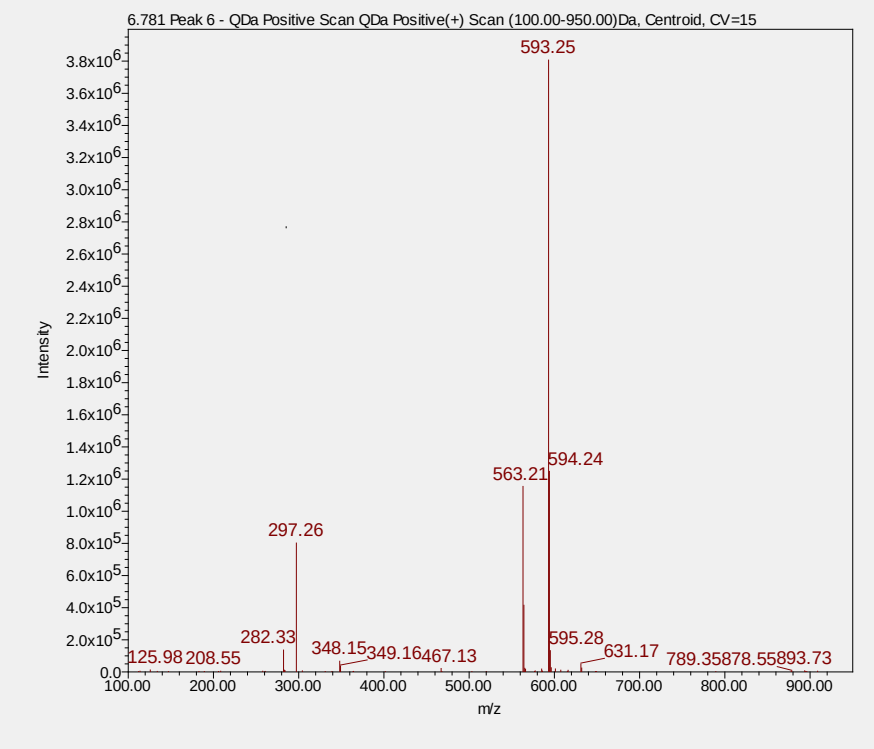

Fig. S22. MS spectrum of compound **1** in positive mode obtained by UHPLC-UV-MS.

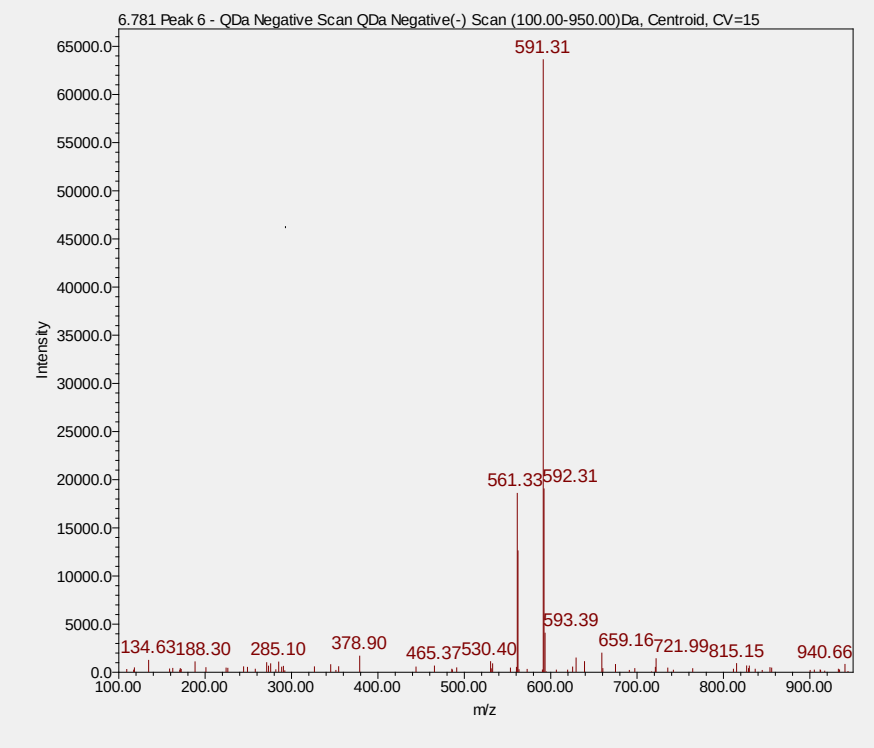

Fig. S23. MS spectrum of compound **1** in negative mode obtained by UHPLC-UV-MS.

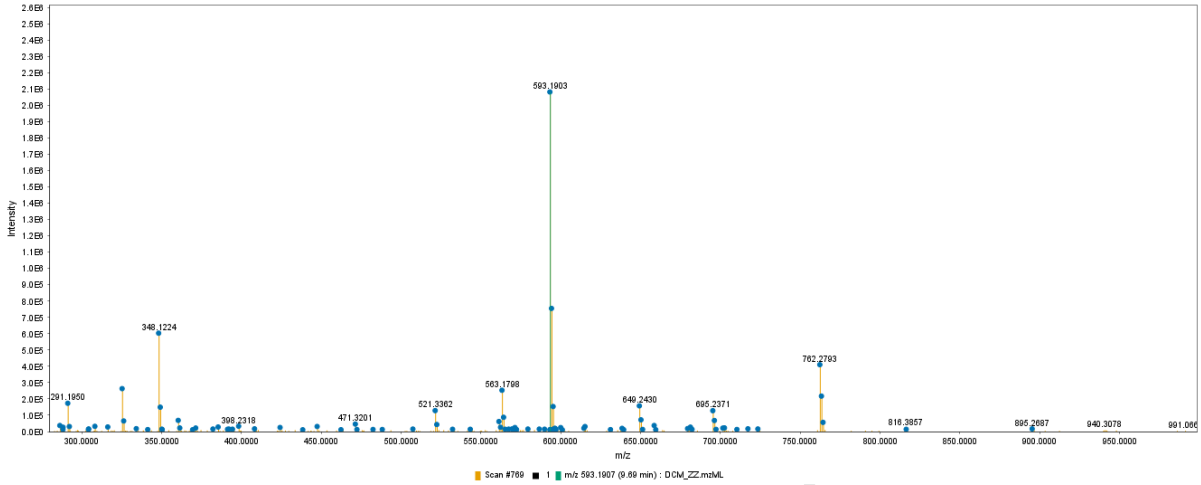

Fig. S24. HR-ESI-MS spectrum of the new compound **1.**

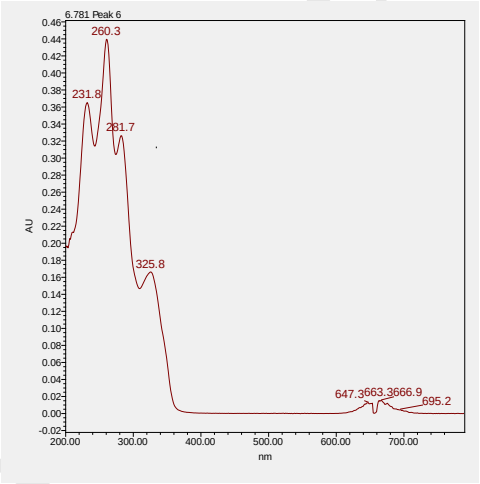

Fig. S25. UV spectrum of the new compound **1.**

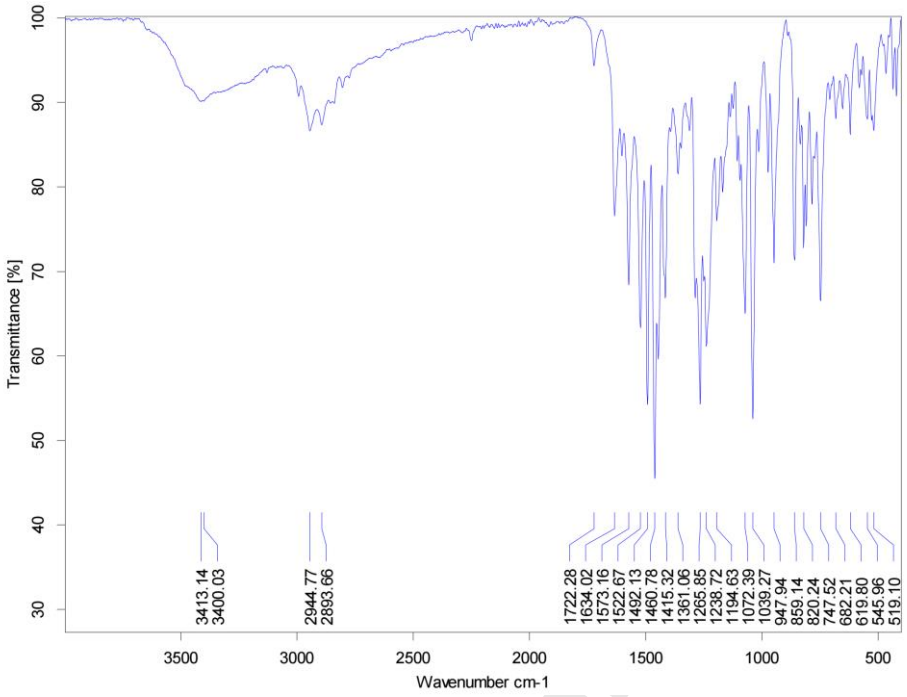

Fig. S26. IR spectrum of the new compound **1.**

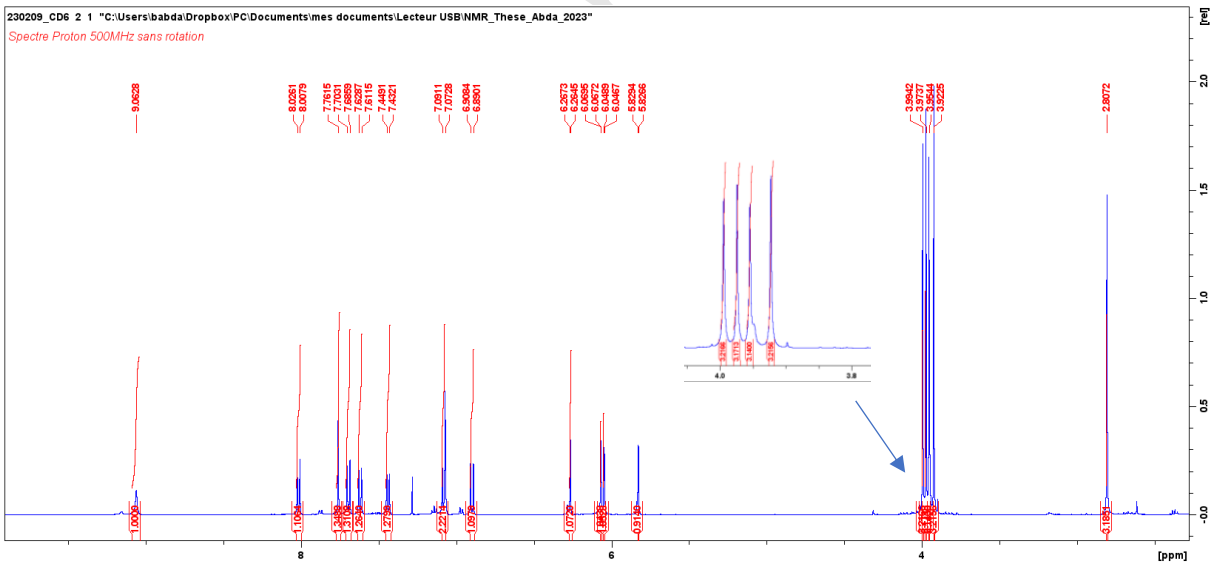

Fig. S27. ^{1}H-NMR (500 MHz, $CDCl_3$) spectrum of the new compound **1.**

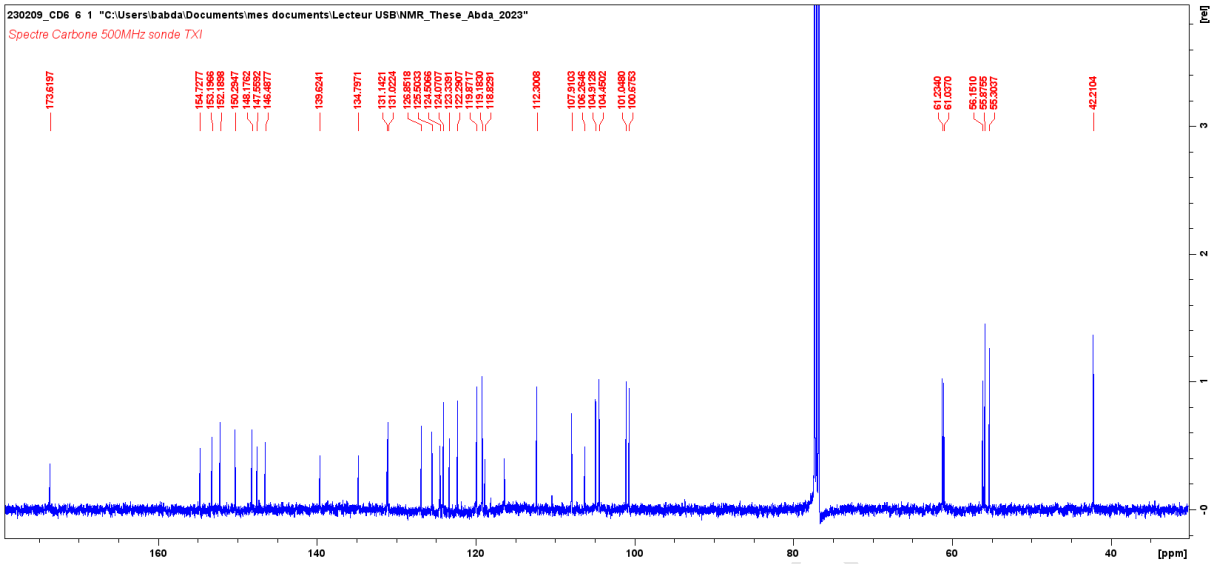

Fig. S28. ^{13}C-NMR (125 MHz, $CDCl_3$) spectrum of the new compound **1.**

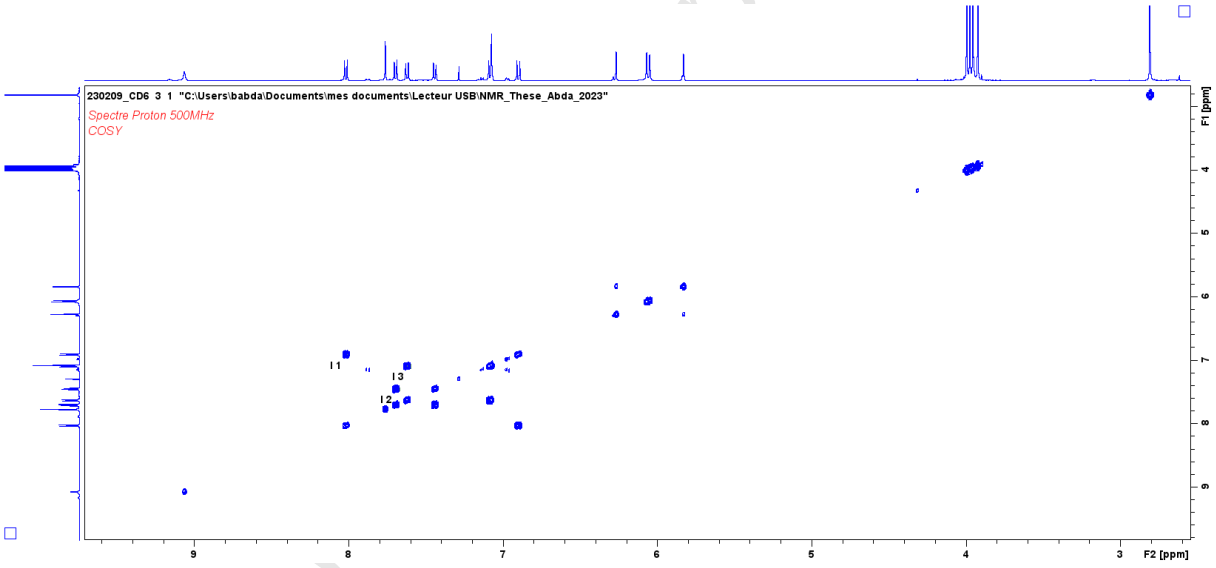

Fig. S29. ^{1}H-^{1}H COSY (500 MHz, $CDCl_3$) spectrum of the new compound **1.**

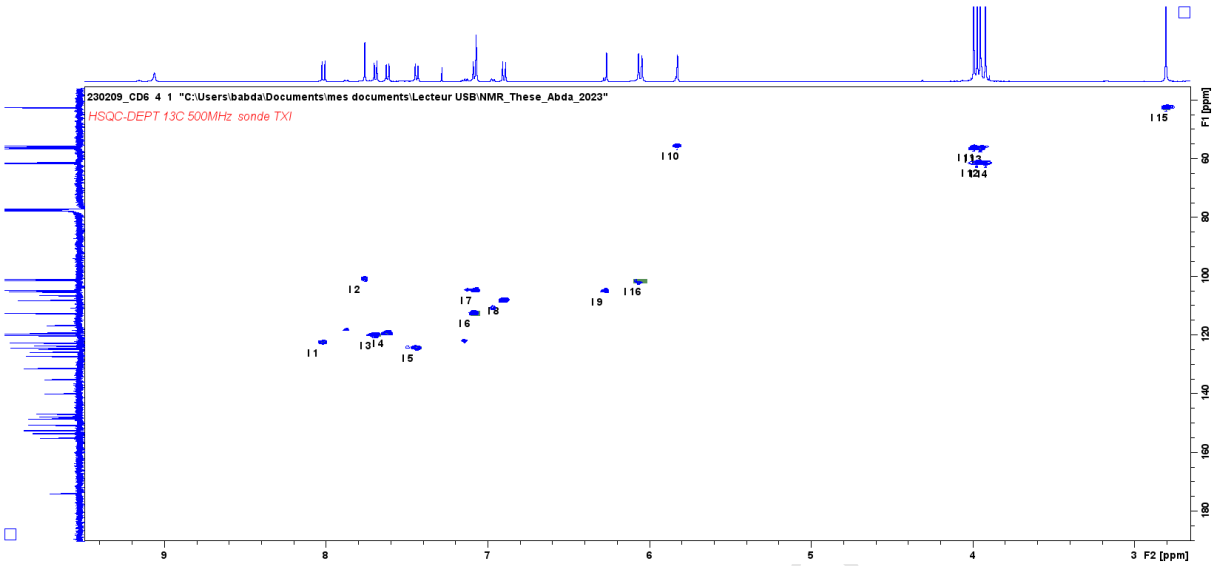

Fig. S30. HSQC-DEPT (500 MHz, $CDCl_3$) spectrum of the new compound **1.**

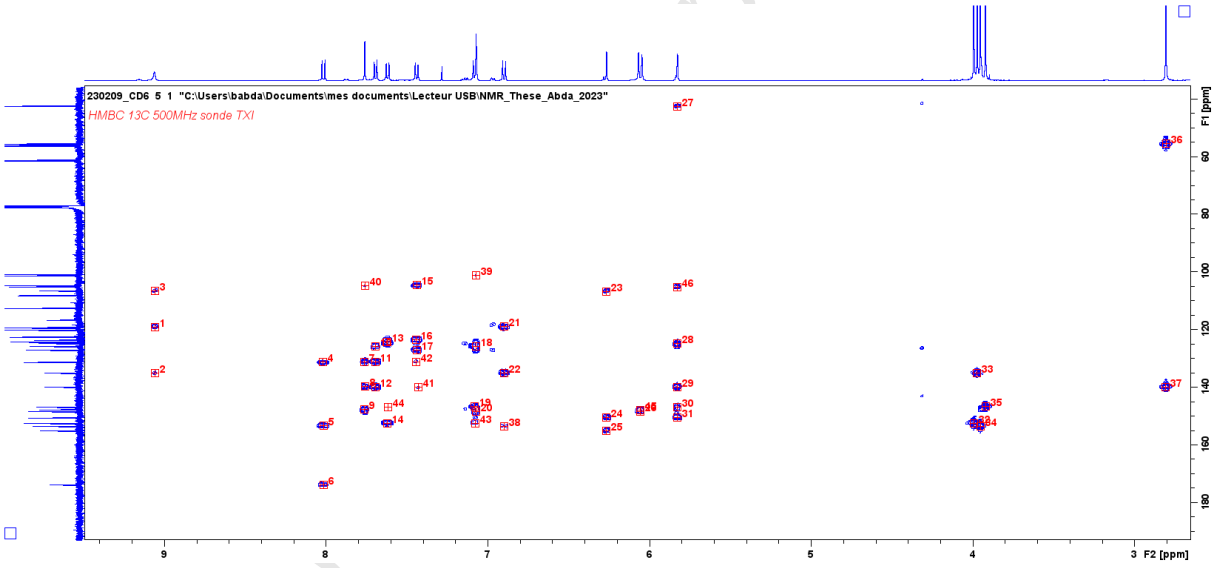

Fig. S31. HMBC (500 MHz, $CDCl_3$) spectrum of the new compound **1.**

Dihydrochelerythrine (2):

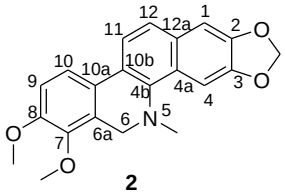

2

Yellow powder; UHPLC-UV: λ_{max} (AU) 230 (0.034), 279 (0.045), 317 (0.018), 350 (sh) nm; ^{1}H NMR ($CDCl_3$, 500 MHz) δ (ppm) 7.74 (1H, d, J = 8.6 Hz, H-11), 7.71 (1H, s, H-4), 7.55

(1H, d, *J* = 8.5 Hz, H-10), 7.52 (1H, d, *J* = 8.6 Hz, H-12), 7.16 (1H, s, H-1), 6.98 (1H, d, *J* = 8.5 Hz, H-9), 6.09 (2H, s, C-2-O-CH_2-O-C-3), 4.33 (2H, s, H-6), 3.97 (3H, s, C-7-O-CH_3), 3.91 (3H, s, C-8-O-CH_3), 2.64 (3H, s, N-CH_3); ^{13}C NMR ($CDCl_3$, 125.77 MHz) δ (ppm) 152.2 (C, C-7), 148.0 (C, C-2), 147.4 (C, C-3), 146.1 (C, C-8), 142.7 (C, C-4b), 130.8 (C, C-12a), 126.3 (C, C-10a), 126.2 (C, C-4a), 126.2 (C, C-6a), 124.2 (C, C-10b), 123.7 (CH, C-12), 120.1 (CH, C-11), 118.6 (CH, C-10), 110.9 (CH, C-9), 104.3 (CH, C-1), 101.0 (CH_2, C-2-O-CH_2-O-C-3), 100.7 (CH, C-4), 61.1 (CH_3, C-8-O-CH_3), 55.8 (CH_3, C-7-O-CH_3), 48.7 (CH_2, C-6), 41.3 (CH_3, N-CH_3); HR-ESI-MS: *m/z* 350.1385 $[M+H]^+$ (calcd for $C_{21}H_{20}NO_4$, 350.1386).

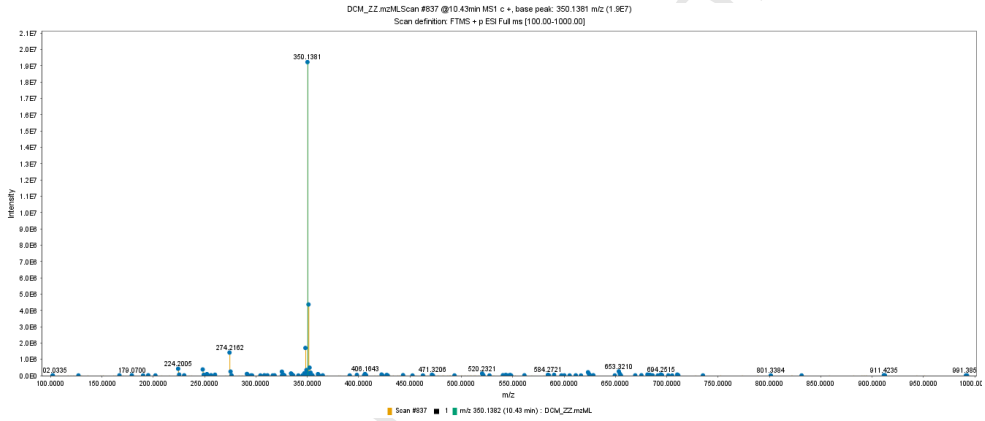

Fig. S32. HR-ESI-MS spectrum of compound **2.**

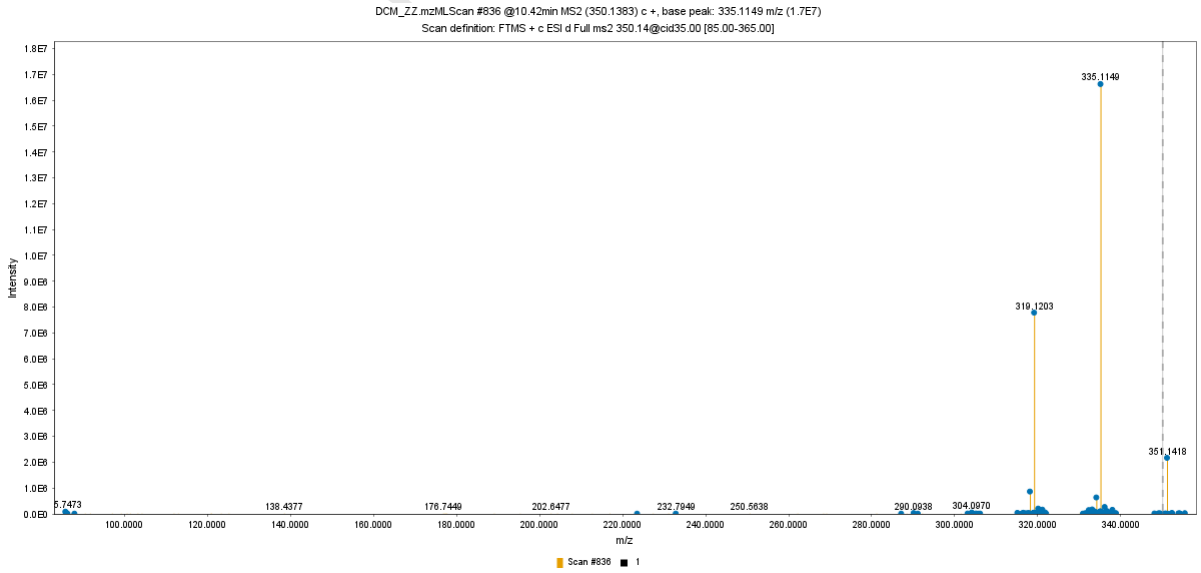

Fig. S33. HR-ESI-MS/MS spectrum of compound **2.**

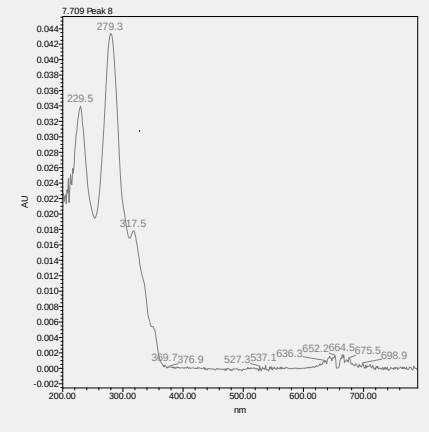

Fig. S34. UV spectrum of compound **2.**

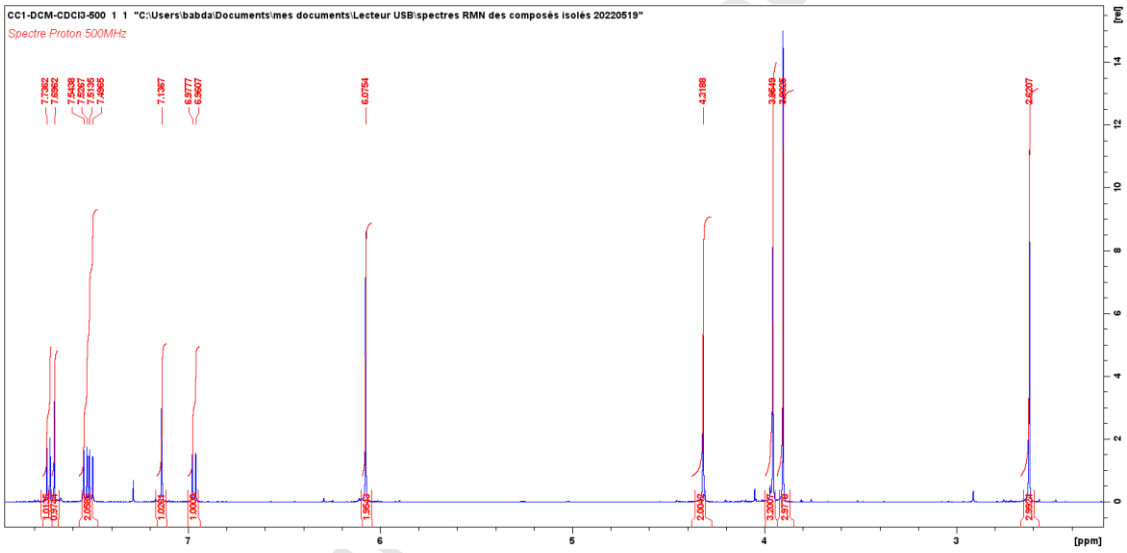

Fig. S35. ^{1}H-NMR (500 MHz, $CDCl_3$) spectrum of compound **2.**

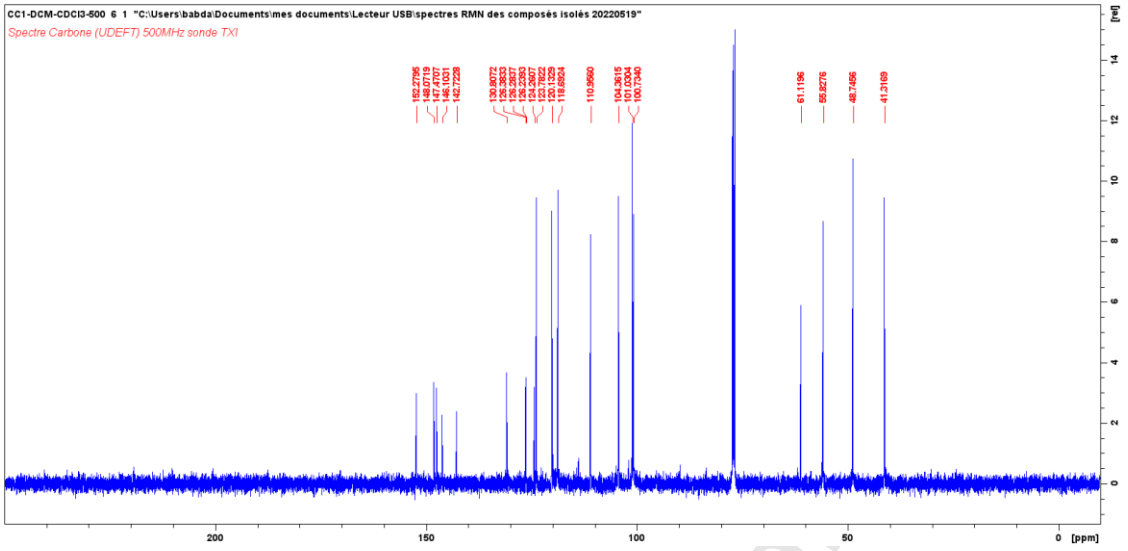

Fig. S36. ^{13}C-NMR (125 MHz, $CDCl_3$) spectrum of compound **2.**

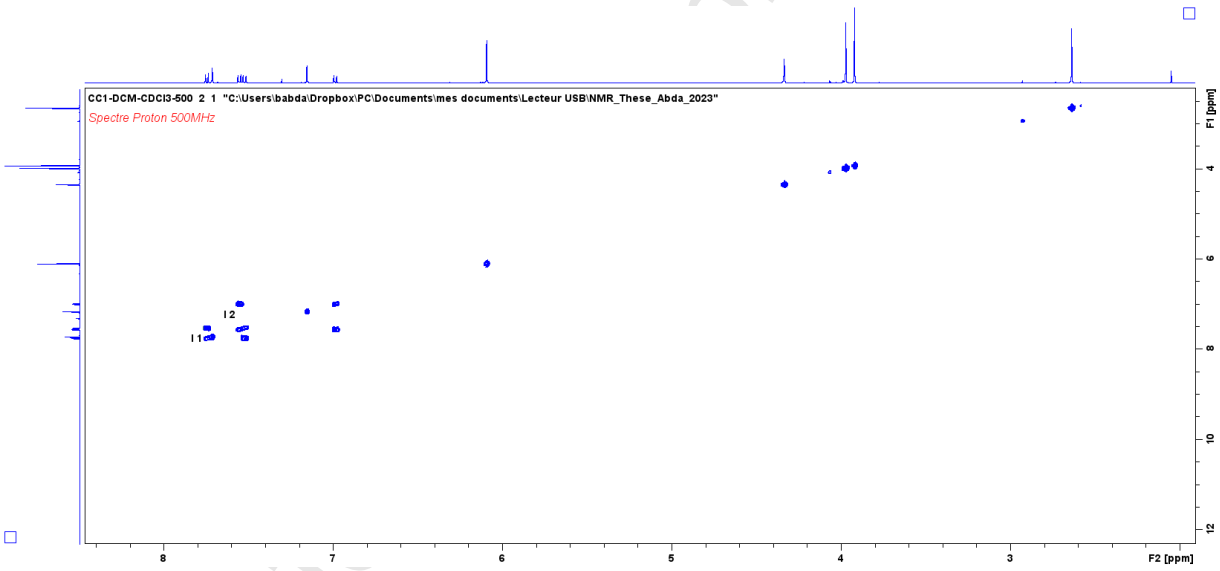

Fig. S37. ^{1}H-^{1}H COSY (500 MHz, $CDCl_3$) spectrum of compound **2.**

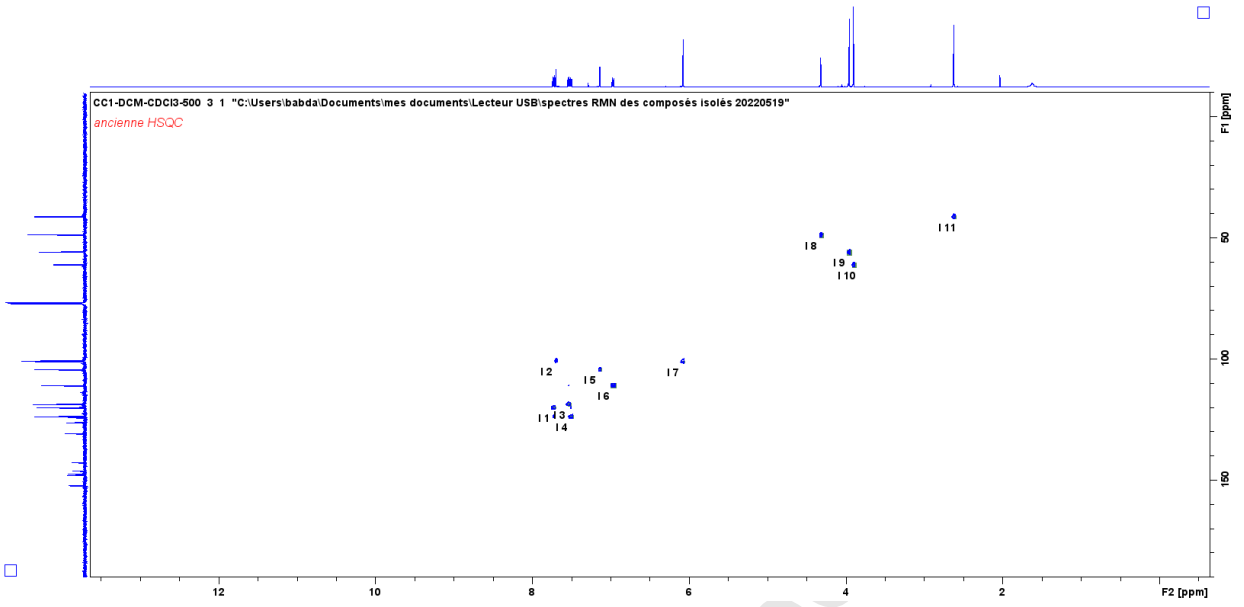

Fig. S38. HSQC-DEPT (500 MHz, $CDCl_3$) spectrum of compound **2.**

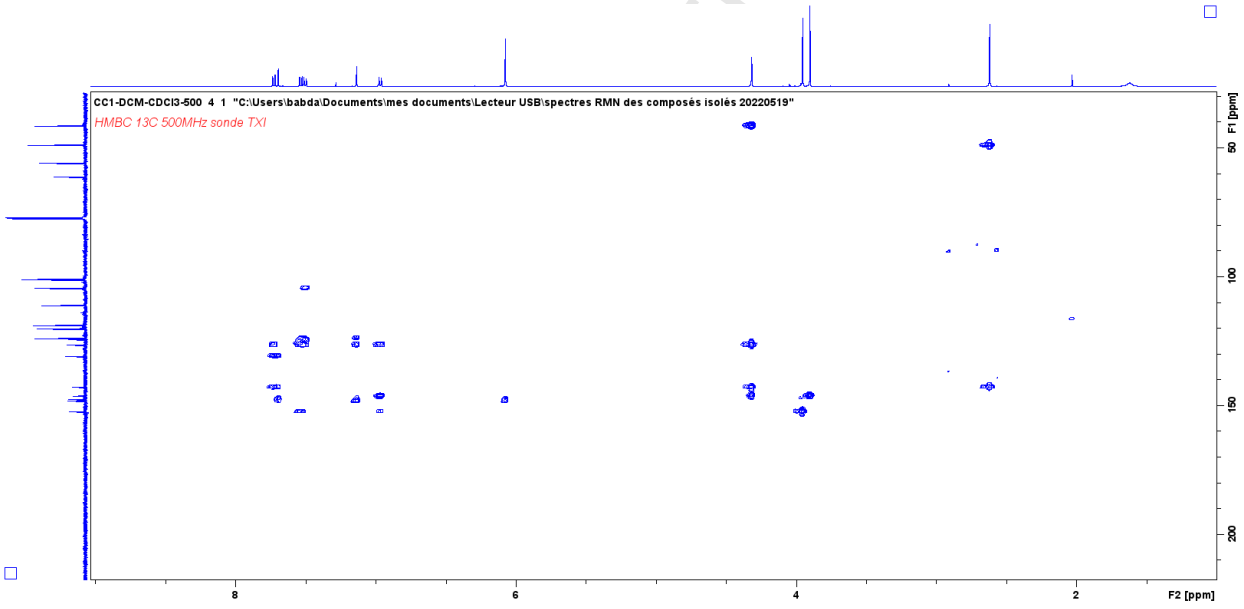

Fig. S39. HMBC (500 MHz, $CDCl_3$) spectrum of compound **2.**

***Trans*-fagaramide (3):**

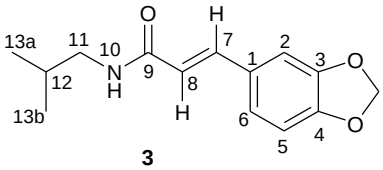

3

White needles; UHPLC-UV: λ_{max} (AU) 217 (0.69), 234 (0.57), 289 (0.58), 321 (0.70) nm; ^{1}H NMR ($CDCl_3$, 500 MHz) δ (ppm) 7.55 (1H, d, *J* = 15.4 Hz, H-7), 7.02 (1H, d, *J* = 1.6 Hz, H-2), 6.99 (1H, dd, *J* = 8.0, 1.6 Hz, H-6), 6.81 (1H, d, *J* = 8.0 Hz, H-5), 6.25 (1H, d, *J* = 15.4 Hz, H-8), 6.00 (2H, s, C-3-O-CH_2-O-C-4), 5.75 (1H, s, NH, *large*), 3.23 (2H, dd, *J* = 6.5, 0.6 Hz, H-11), 1.85 (1H, nonuplet, *J* = 6.7 Hz, H-12), 0.96 (6H, d, *J* = 6.7 Hz, H-13a, H-13b); ^{13}C NMR ($CDCl_3$, 125.77 MHz) δ (ppm) 166.1 (C=O, C-9), 148.9 (C, C-3), 148.2 (C, C-4), 140.5 (CH, C-7), 129.7 (C, C-1), 123.5 (CH, C-6), 118.2 (CH, C-8), 108.1 (CH, C-5), 105.9 (CH, C-2), 102.5 (CH_2, C-3-O-CH_2-O-C-4), 46.2 (CH_2, C-11), 28.9 (CH, C-12), 20.1 ($2CH_3$, C-13a, C-13b); HR-ESI-MS: *m/z* 248.1277 $[M+H]^+$ (calcd for $C_{14}H_{17}NO_3$, 248.1273).

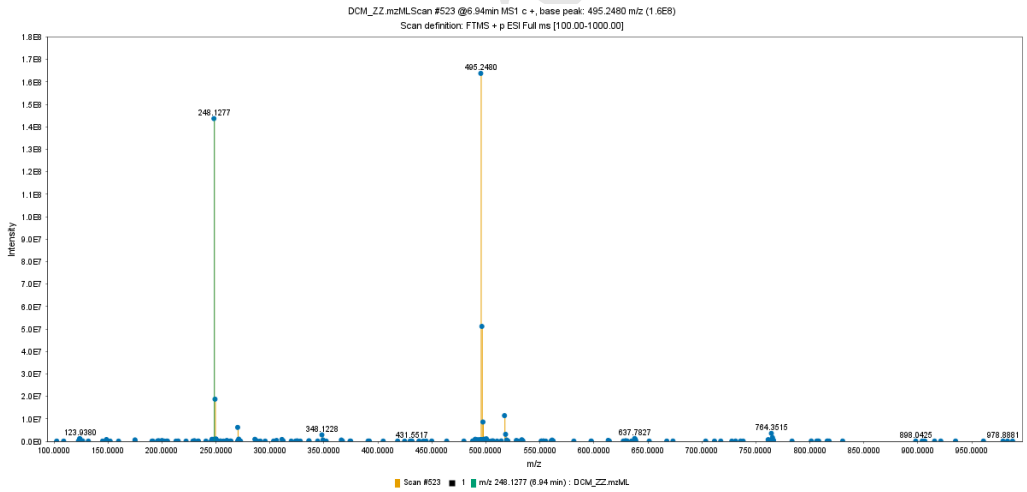

Fig. S40. HR-ESI-MS spectrum of compound **3.**

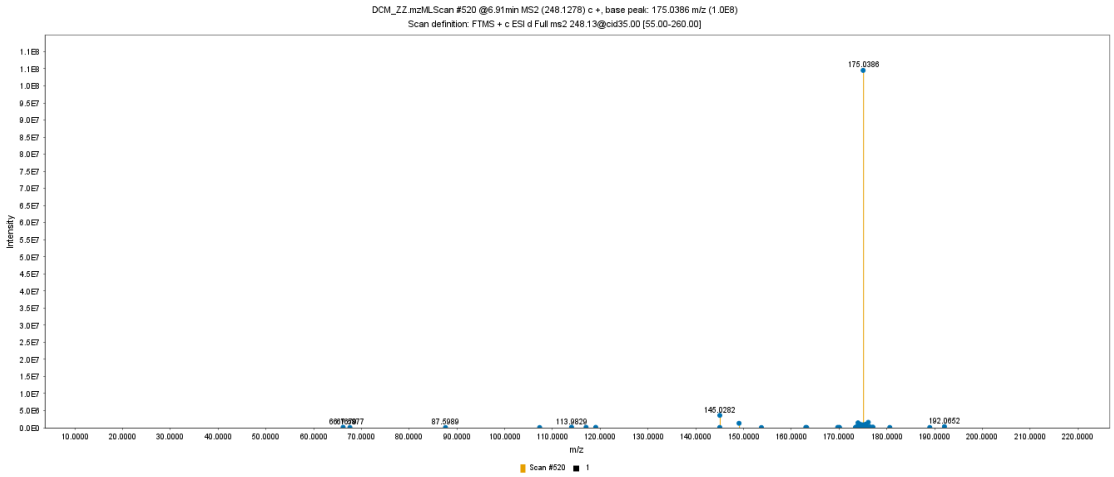

Fig. S41. HR-ESI-MS/MS spectrum of compound **3.**

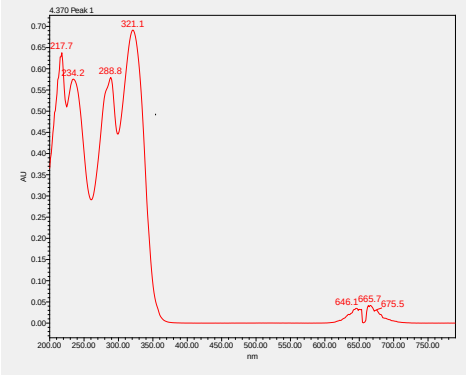

Fig. S42. UV spectrum of compound **3.**

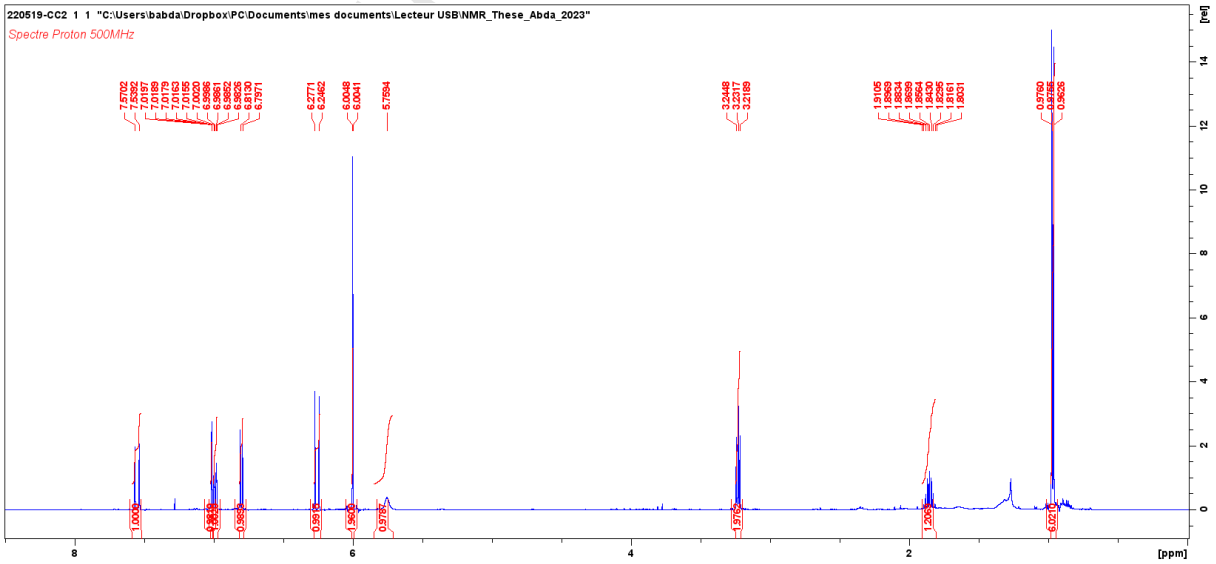

Fig. S43. ^{1}H-NMR (500 MHz, $CDCl_3$) spectrum of compound **3.**

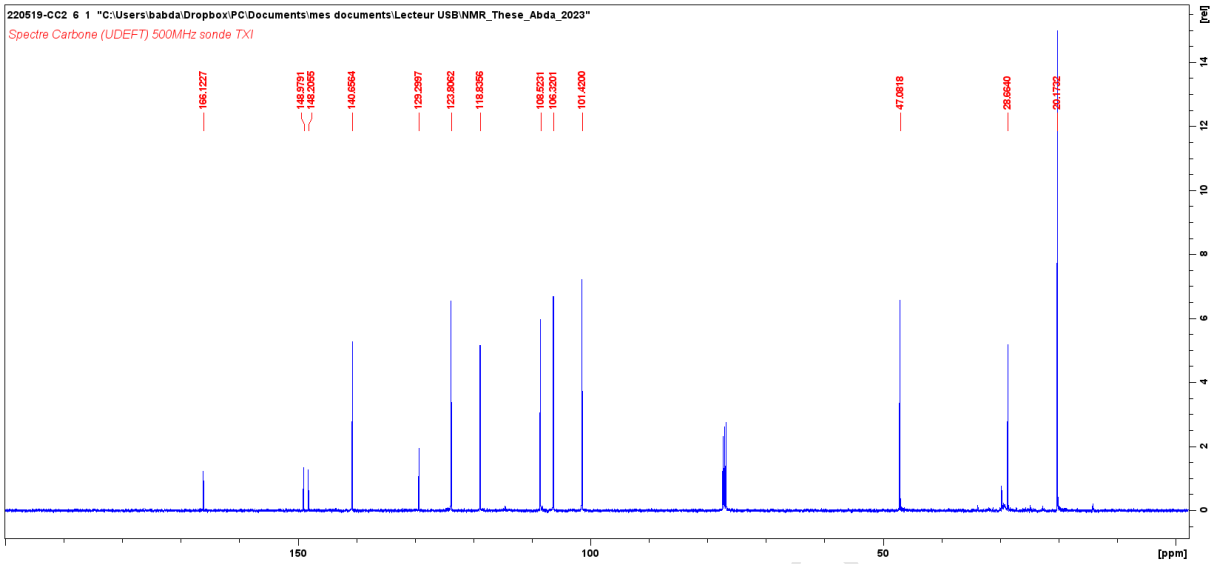

Fig. S44. ^{13}C-NMR (125 MHz, $CDCl_3$) spectrum of compound **3.**

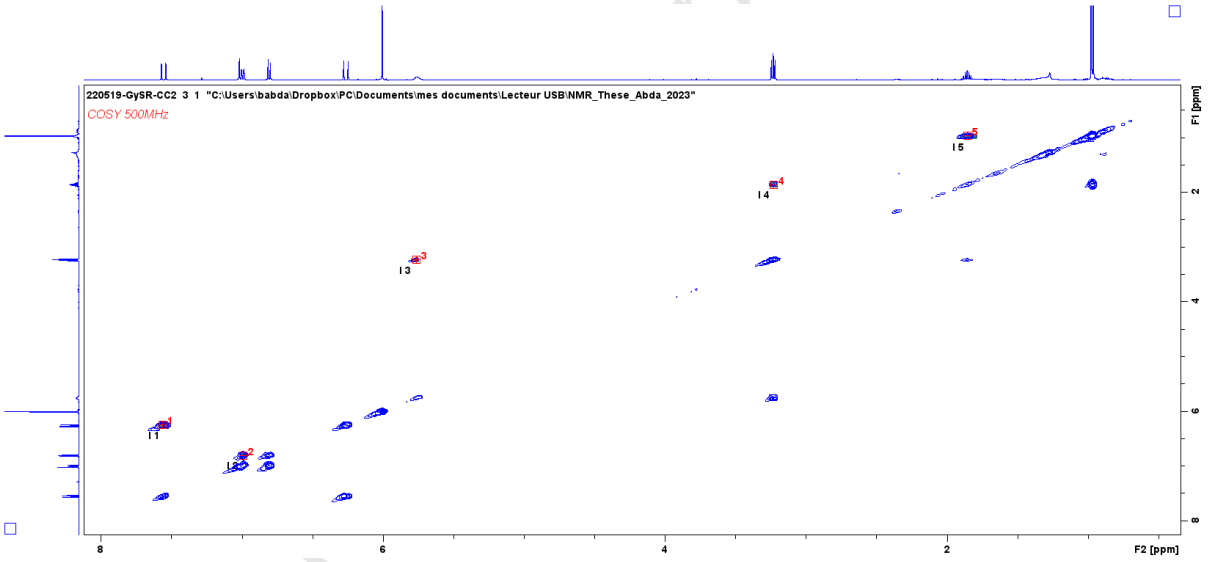

Fig. S45. ^{1}H-^{1}H COSY (500 MHz, $CDCl_3$) spectrum of compound **3.**

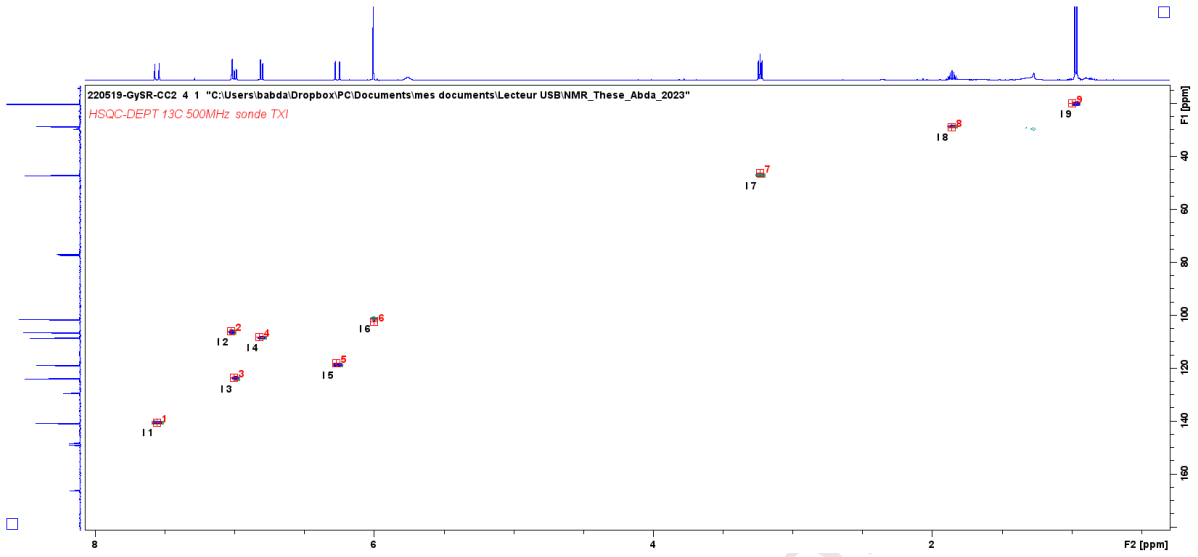

Fig. S46. HSQC-DEPT (500 MHz, $CDCl_3$) spectrum of compound **3.**

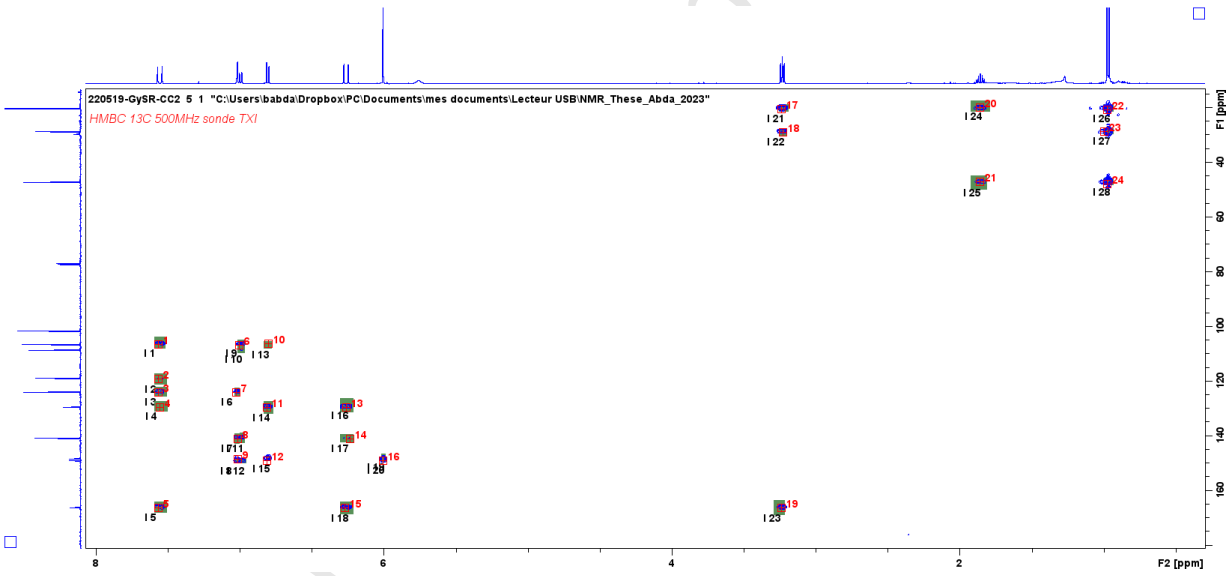

Fig. S47. HMBC (500 MHz, $CDCl_3$) spectrum of compound **3.**

Arnottianamide (4):

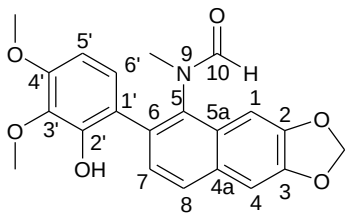

4

White powder; UHPLC-UV: λ_{max} (AU) 237 (0.44), 280(sh), 323 (sh), 331 (0.06) nm; ^{1}H NMR ($CDCl_3$, 500 MHz) δ (ppm) 8.18 (1H, s, H-10), 7.75 (1H, d, J = 8.3 Hz, H-8), 7.33 (1H,

d, *J* = 8.3 Hz, H-7), 7.22 (1H, s, H-4), 7.10 (1H, s, H-1), 6.82 (1H, d, *J* = 8.5 Hz, H-6'), 6.56 (1H, d, *J* = 8.6 Hz, H-5'), 6.10 (2H, s, C-2-O-CH_2-O-C-3), 5.98 (1H, s, OH), 3.95 (3H, s, C-3'-O-CH_3), 3.92 (3H, s, C-4'-O-CH_3), 3.02 (3H, s, N-CH_3); ^{13}C NMR ($CDCl_3$, 125.77 MHz) δ (ppm) 164.5 (CH, C-10); 151.9 (C, C-4'), 148.6 (C, C-3), 148.5 (C, C-2), 146.8 (C, C-2'), 135.7 (C, C-5), 135.5 (C, C-3'), 133.1 (C, C-4a), 131.3 (C, C-5a), 128.6 (C, C-6), 127.4 (CH, C-8), 127.3 (CH, C-7), 125.1 (CH, C-6'), 118.7 (C, C-1'), 104.3 (CH, C-4), 104.0 (CH, C-5'), 101.2 (CH_2, C-2-O-CH_2-O-C-3), 99.3 (CH, C-1), 61.1 (CH_3, C-3'-O-CH_3), 55.8 (CH_3, C-4'-O-CH_3), 33.1 (CH_3, N-CH_3); HR-ESI-MS: *m/z* 382.1281 $[M+H]^+$ (calcd for $C_{21}H_{19}NO_6$, 382.1277).

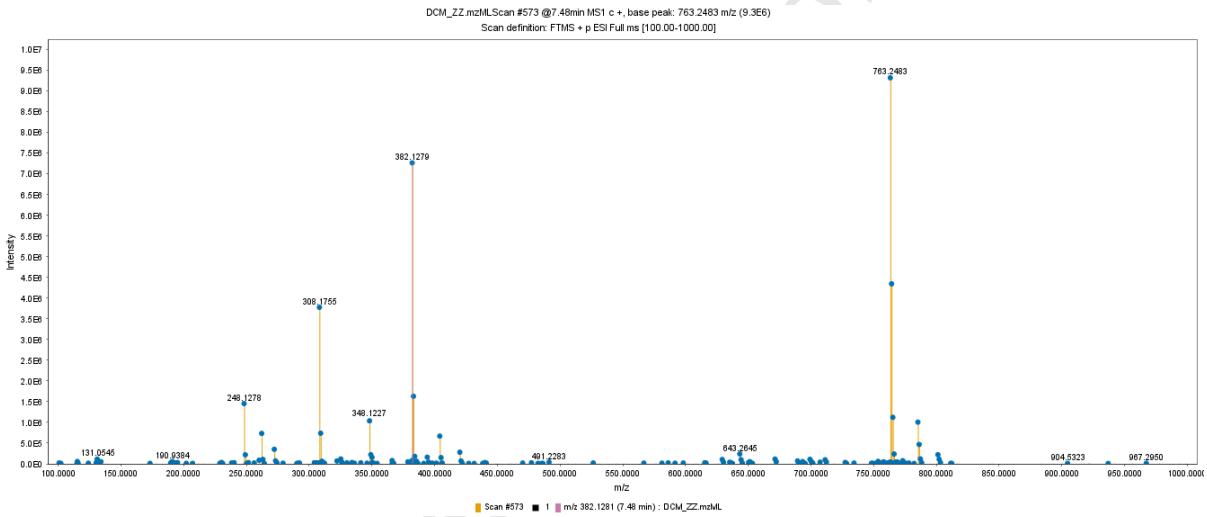

Fig. S48. HR-ESI-MS spectrum of compound **4.**

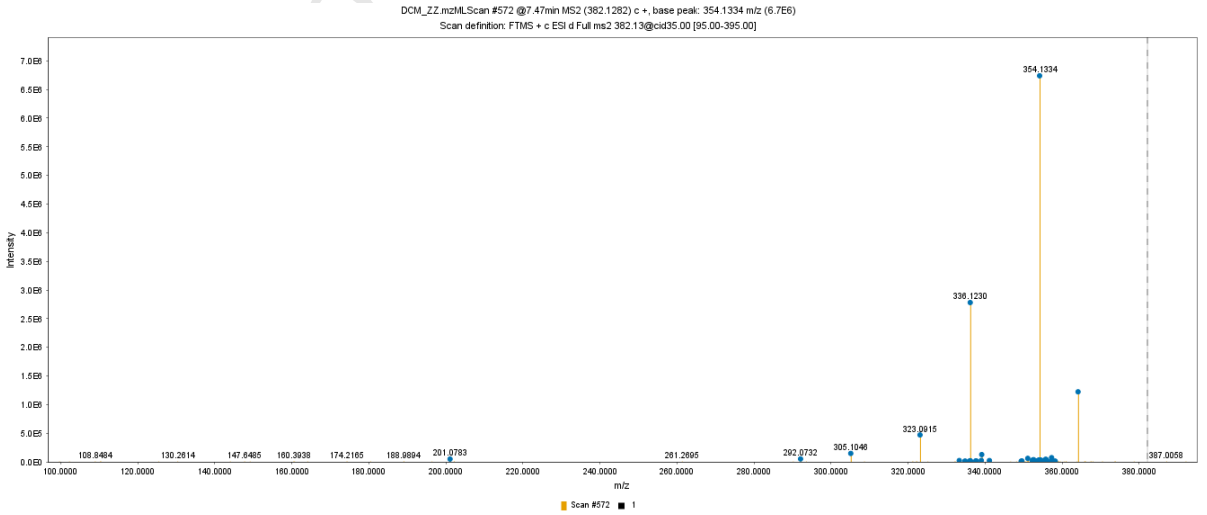

Fig. S49. HR-ESI-MS/MS spectrum of compound **4.**

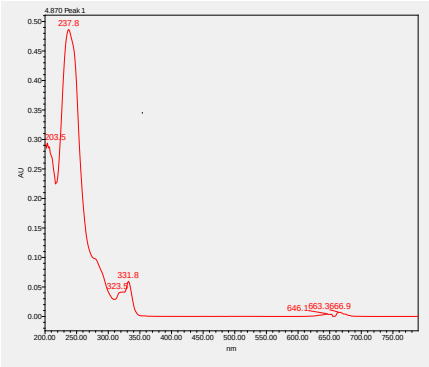

Fig. S50. UV spectrum of compound **4.**

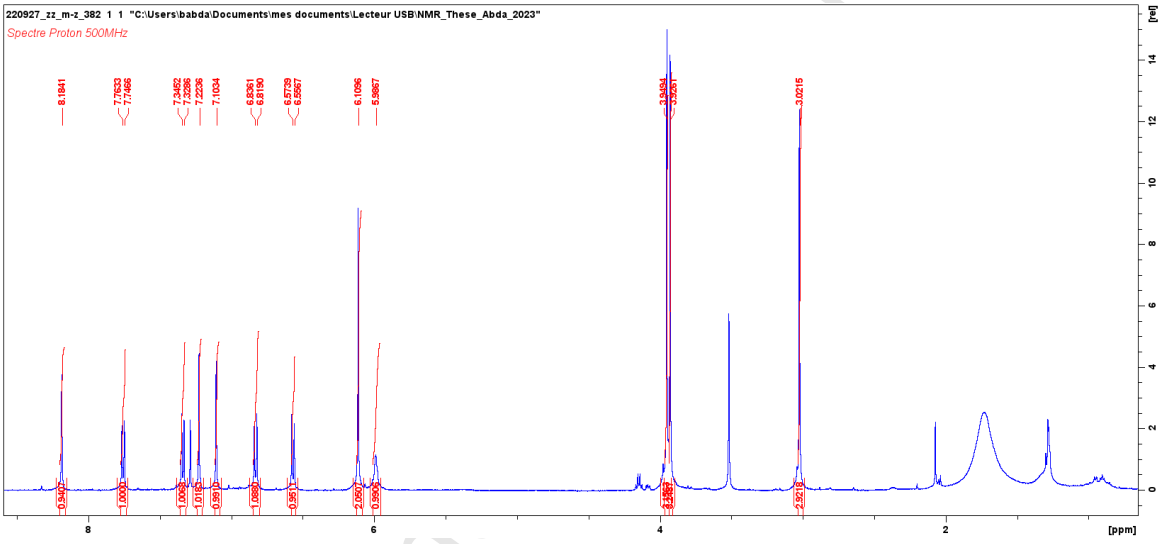

Fig. S51. ^{1}H-NMR (500 MHz, $CDCl_3$) spectrum of compound **4.**

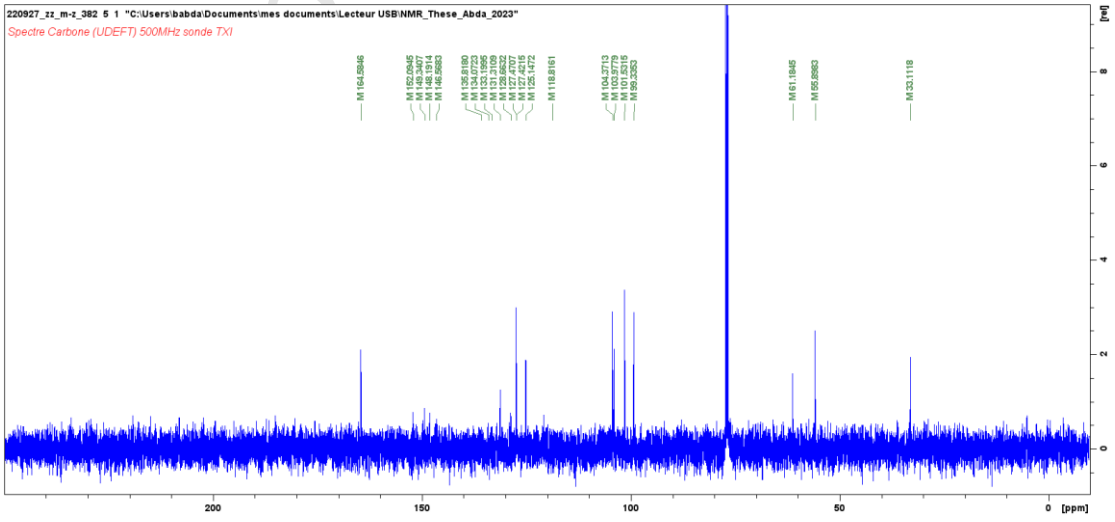

Fig. S52. ^{13}C-NMR (125 MHz, $CDCl_3$) spectrum of compound **4.**

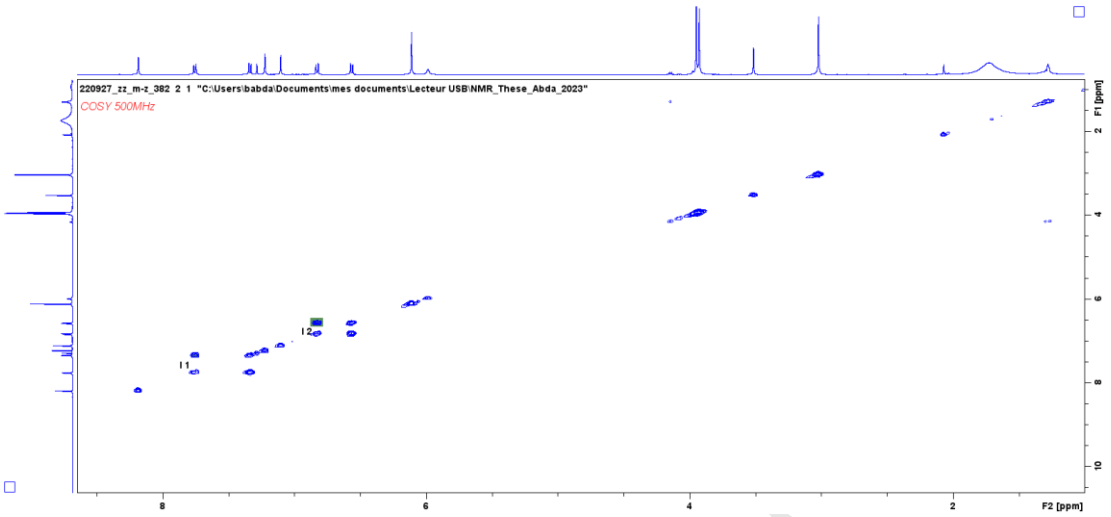

Fig. S53. ^{1}H-^{1}H COSY (500 MHz, $CDCl_3$) spectrum of compound **4.**

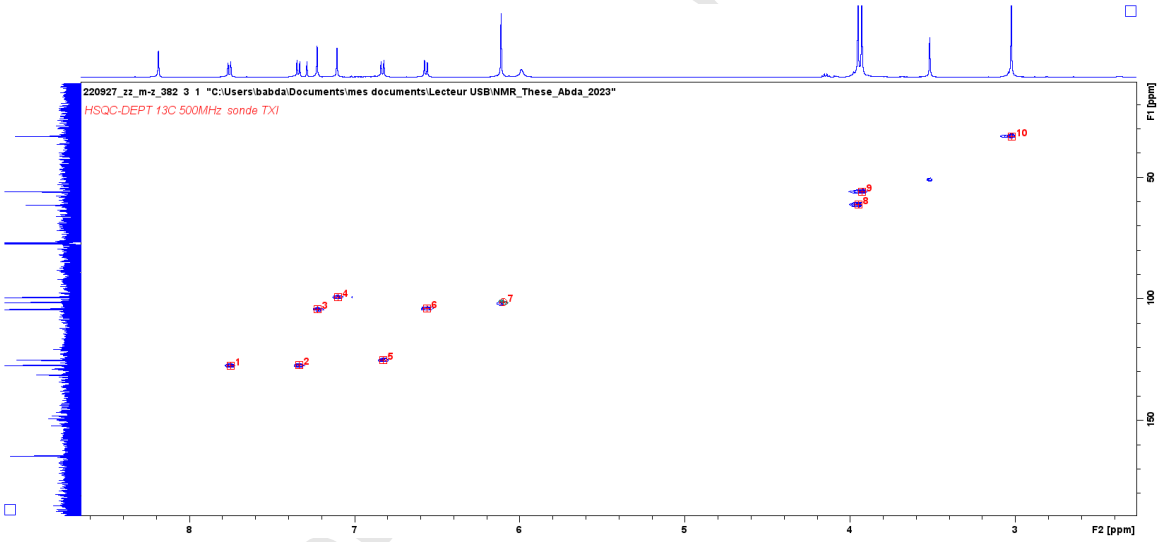

Fig. S54. HSQC-DEPT (500 MHz, $CDCl_3$) spectrum of compound **4.**

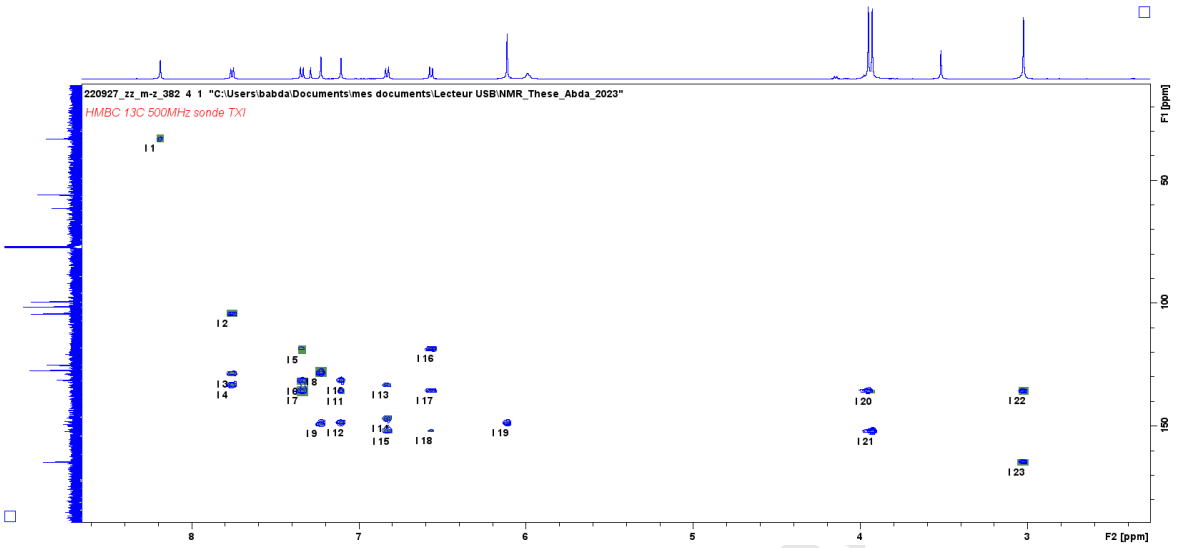

Fig. S55. HMBC (500 MHz, $CDCl_3$) spectrum of compound **4.**

Pellitorine (5):

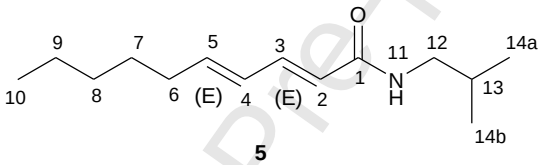

5

White needles; UHPLC-UV: λ_{max} (AU) 258 (2.82) nm; ^{1}H NMR ($CDCl_3$, 500 MHz) δ (ppm) 7.21 (1H, dd, *J* = 15.0 Hz, H-3), 6.14 (1H, dd, *J* = 15.1 Hz, H-4), 6.09 (1H, dt, *J* = 15.1, 6.70 Hz, H-5), 5.77 (1H, d, *J* = 15.0 Hz, H-2), 5.59 (1H, s, NH, *large*), 3.18 (2H, dd, *J* = 6.5, 0.6 Hz, H-12), 2.16 (2H, dt, *J* = 6.8 Hz, H-6), 1.81 (1H, nonuplet, *J* = 6.7 Hz, H-13), 1.44 (2H, m, H-7), 1.33 (2H, m, H-9), 1.29 (2H, m, H-8), 0.94 (6H, d, *J* = 6.7 Hz, H-14a, H-14b), 0.90 (3H, t, *J* = 7.0 Hz, H-10); ^{13}C NMR ($CDCl_3$, 125.77 MHz) δ (ppm) 166.4 (C=O, C-1), 143.3 (CH, C-5), 141.3 (CH, C-3), 128.1 (CH, C-4), 121.6 (CH, C-2), 46.9 (CH_2, C-12), 32.9 (CH_2, C-6), 31.3 (CH_2, C-8), 28.4 (CH_2, C-7), 28.6 (CH, C-13), 22.4 (CH_2, C-9), 20.1 ($2CH_3$, C-14a, C-14b), 14.0 (CH_3, C-10); HR-ESI-MS: *m/z* 224.2004 $[M+H]^+$ (calcd for $C_{14}H_{25}NO$, 224.1999).

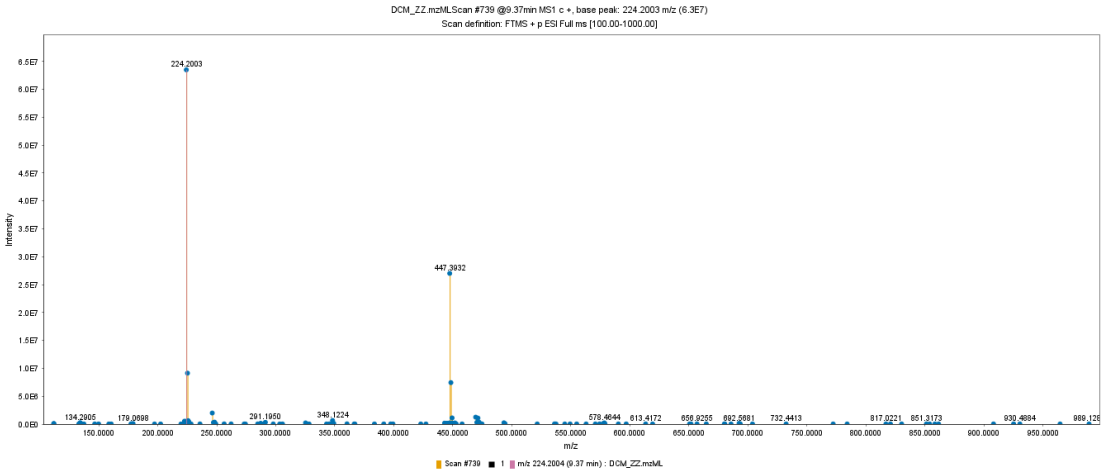

Fig. S56. HR-ESI-MS spectrum of compound **5.**

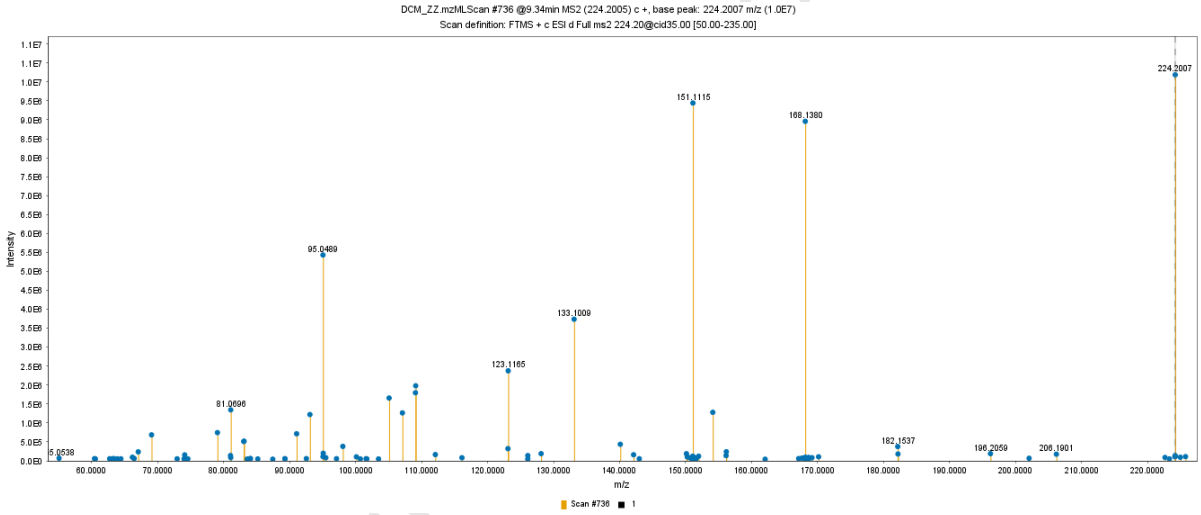

Fig. S57. HR-ESI-MS/MS spectrum of compound **5.**

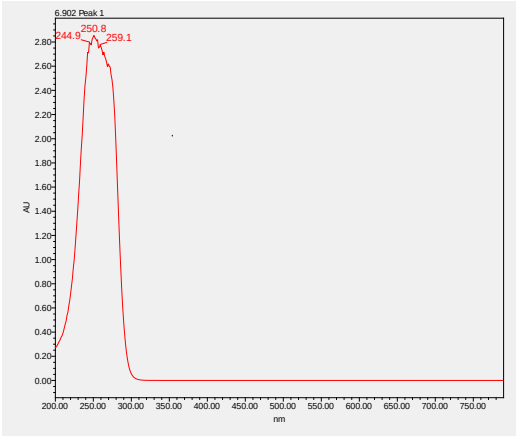

Fig. S58. UV spectrum of compound **5.**

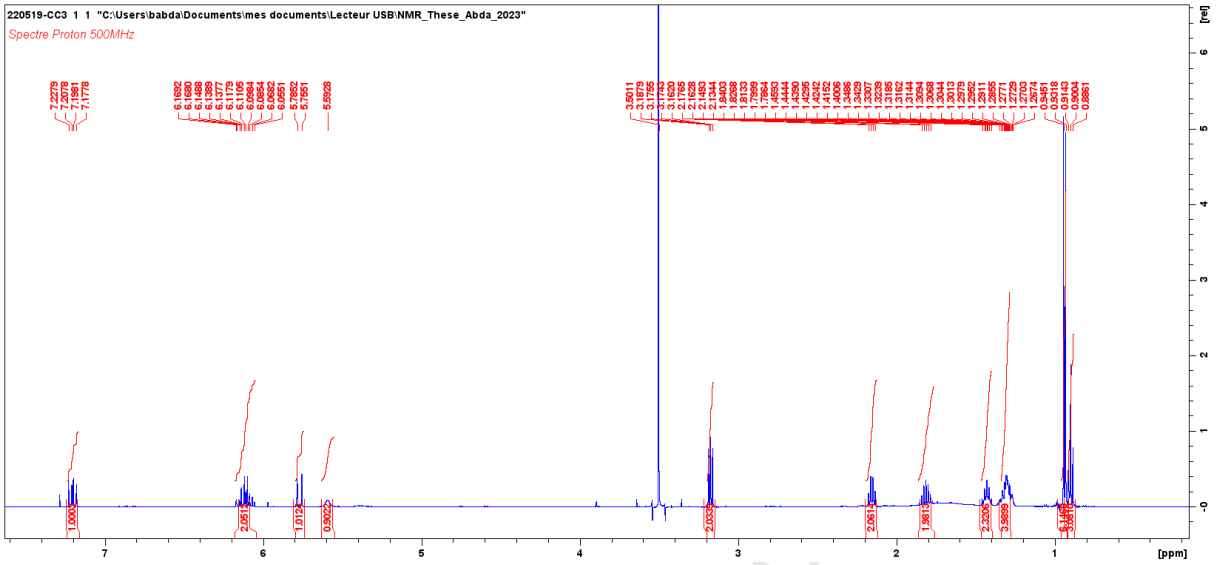

Fig. S59. ^{1}H-NMR (500 MHz, $CDCl_3$) spectrum of compound **5.**

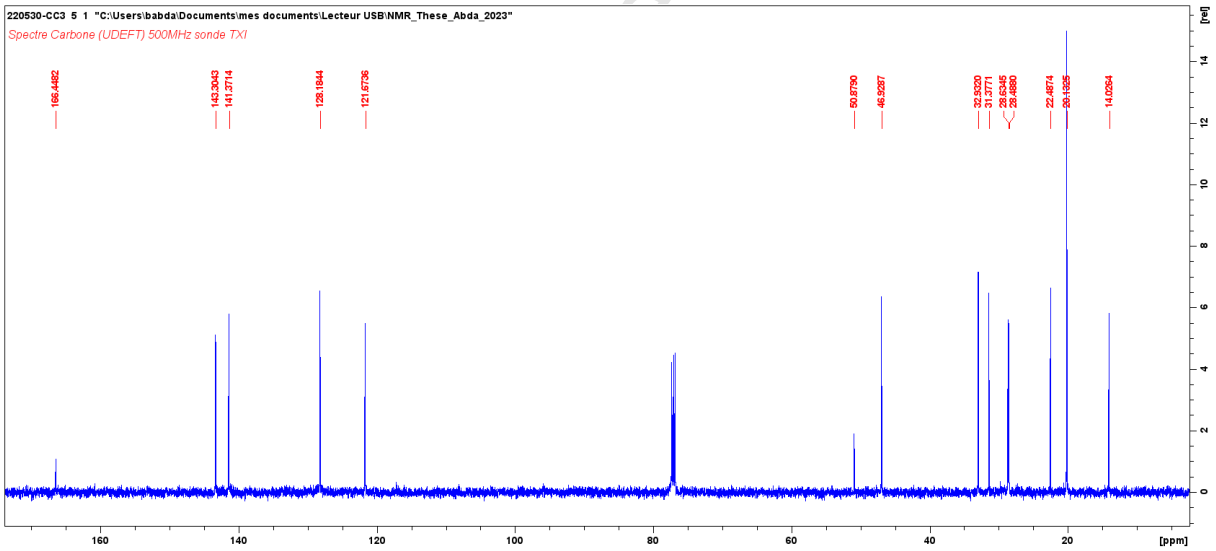

Fig. S60. ^{13}C-NMR (125 MHz, $CDCl_3$) spectrum of compound **5.**

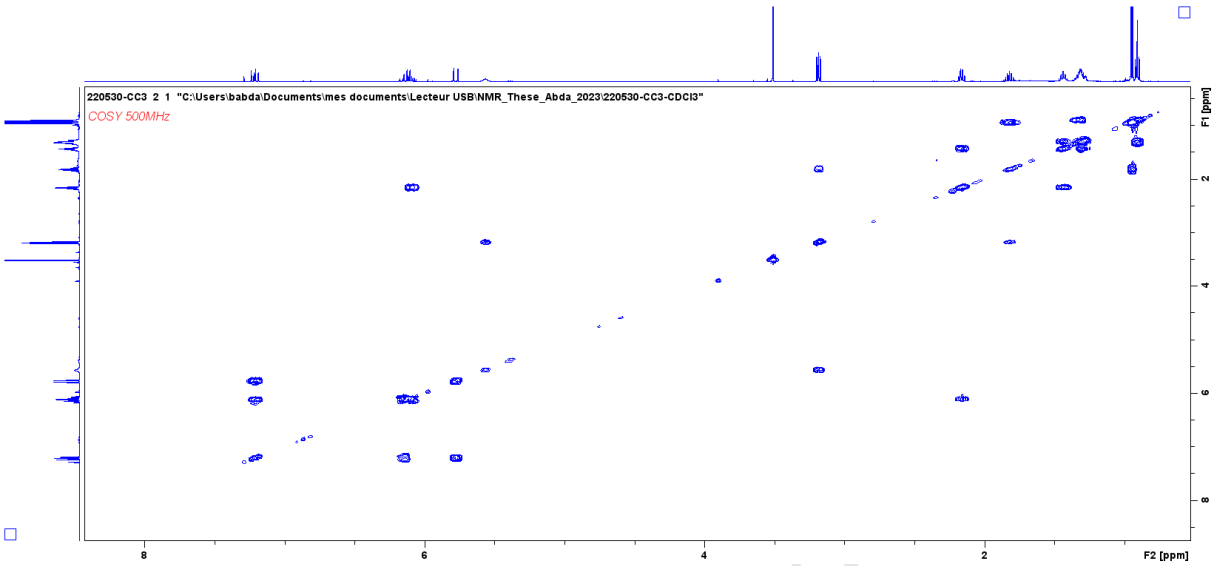

Fig. S61. ^{1}H-^{1}H COSY (500 MHz, $CDCl_3$) spectrum of compound **5.**

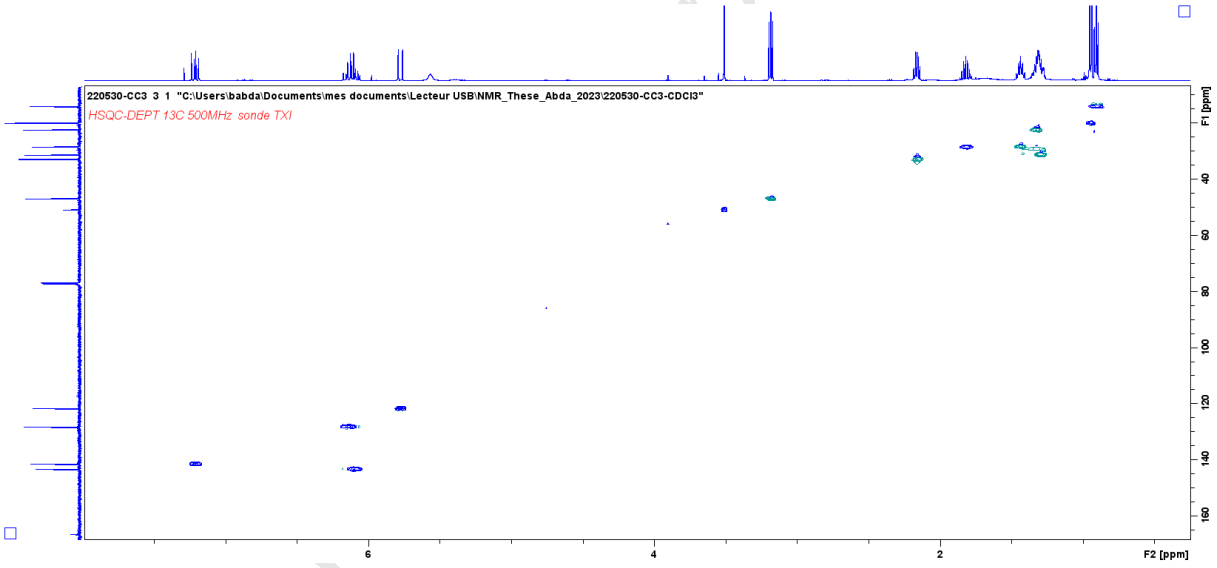

Fig. S62. HSQC-DEPT (500 MHz, $CDCl_3$) spectrum of compound **5.**

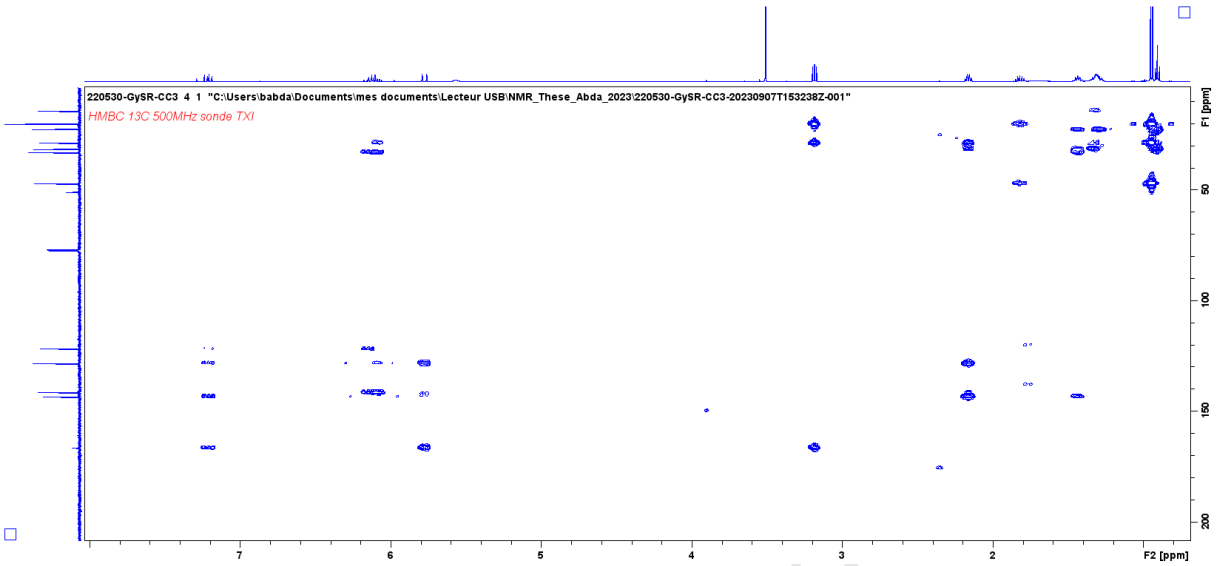

Fig. S63. HMBC (500 MHz, $CDCl_3$) spectrum of compound **5.**

γ-sanshool (6):

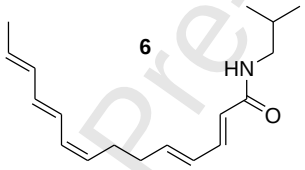

White needles; UHPLC-UV: λ_{max} (AU) 272 (1.81) nm; ^{1}H NMR ($CDCl_3$, 500 MHz) δ (ppm) 7.20 (1H, dd, *J* = 15.0, 10.5 Hz), 6.35 (1H, dd, *J* = 12.9, 2.4 Hz), 5.92-6.23 (5H, *J* = 15.2, 10.4 Hz, *J* = 15.4 Hz, *J* = 15.1, 10.4, 15.14, 7.0, 10.4), 5.70-5.80 (2H, *J* = 15.1, 7.2), 5.52 (1H, s, NH, large), 5.38 (1H, dt, *J* = 11.5, 7.4 Hz), 3.20 (2H, d, *J* = 6.4 Hz), 2.35 (2H, td, *J* = 7.4, 7.0 Hz), 2.25 (2H, *J* = 7.4 Hz), 1.75-1.88 (4H, *J* = 7.1, 6.8 Hz), 0.96 (6H, d, *J* = 6.7 Hz); HR-ESI-MS: *m/z* 274.2162 $[M+H]^+$ (calcd for $C_{18}H_{27}NO$, 274.2178).

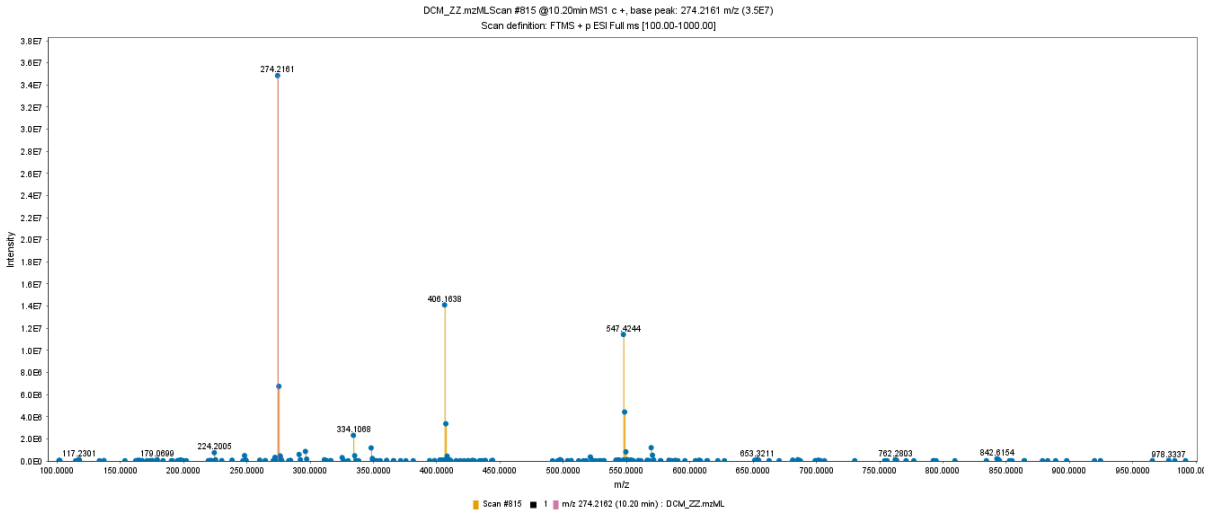

Fig. S64. HR-ESI-MS spectrum of compound **6.**

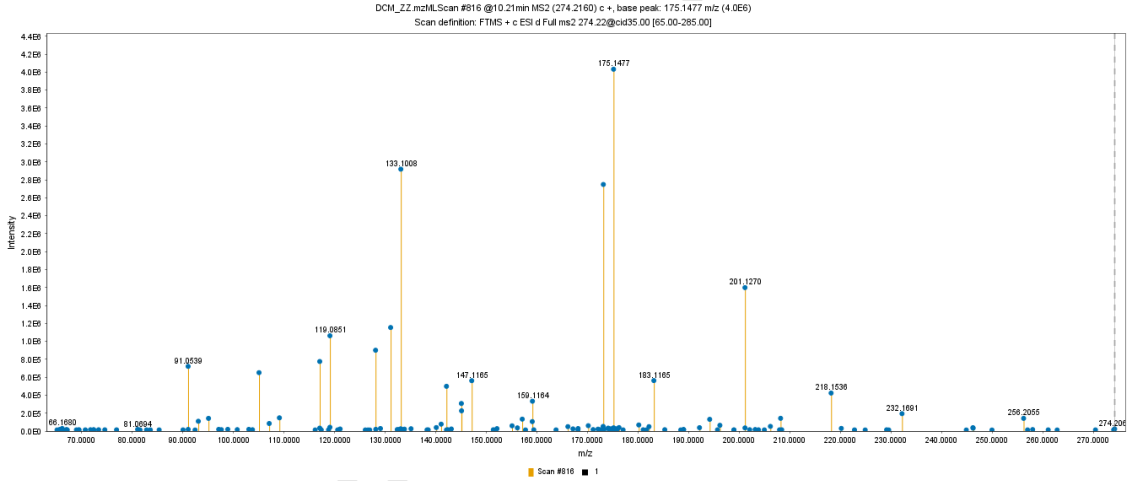

Fig. S65. HR-ESI-MS/MS spectrum of compound **6.**

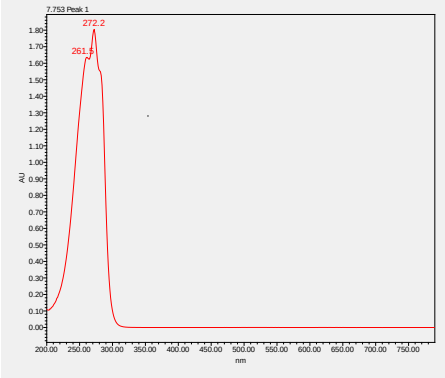

Fig. S66. UV spectrum of compound **6.**

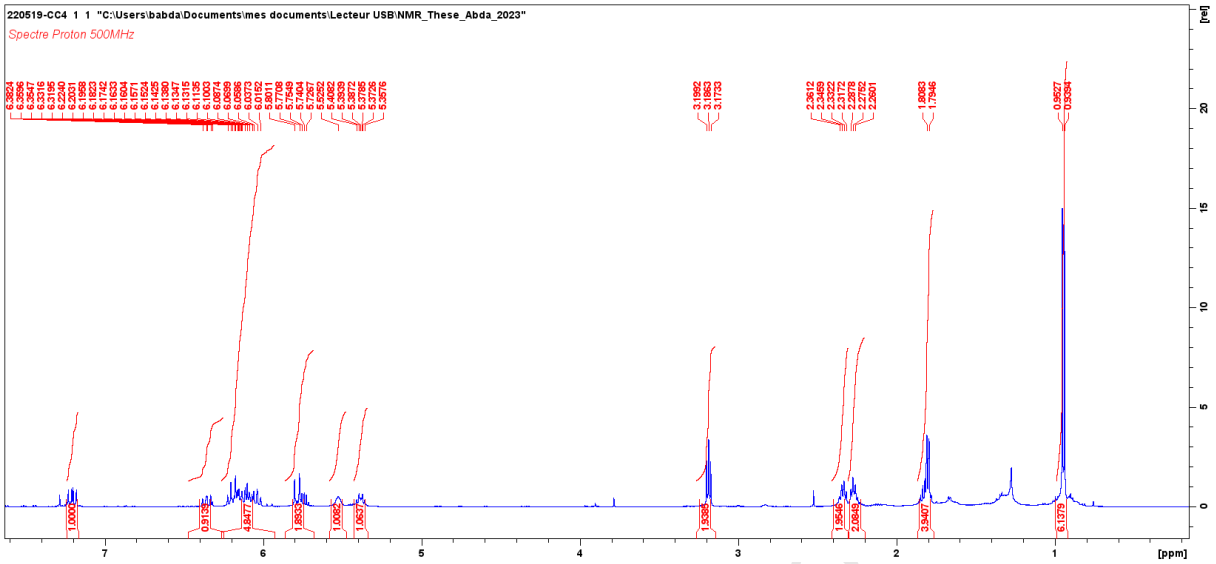

Fig. S67. ^{1}H-NMR (500 MHz, $CDCl_3$) spectrum of compound **6.**

Chelerythrine (7):

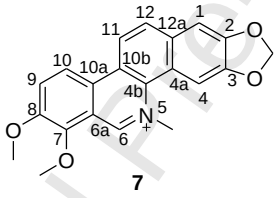

7

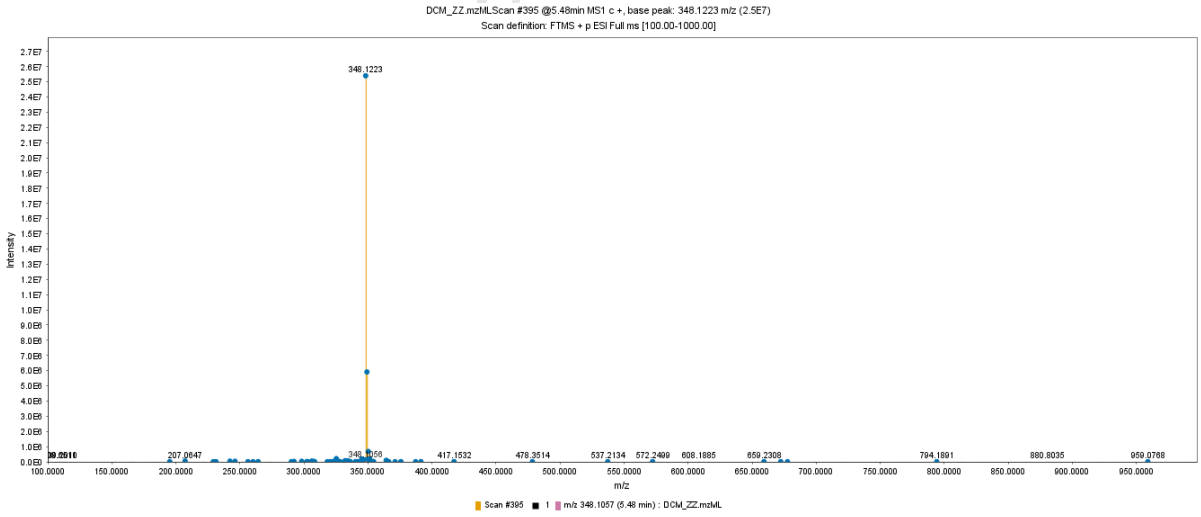

Fig. S68. HR-ESI-MS spectrum of compound **7.**

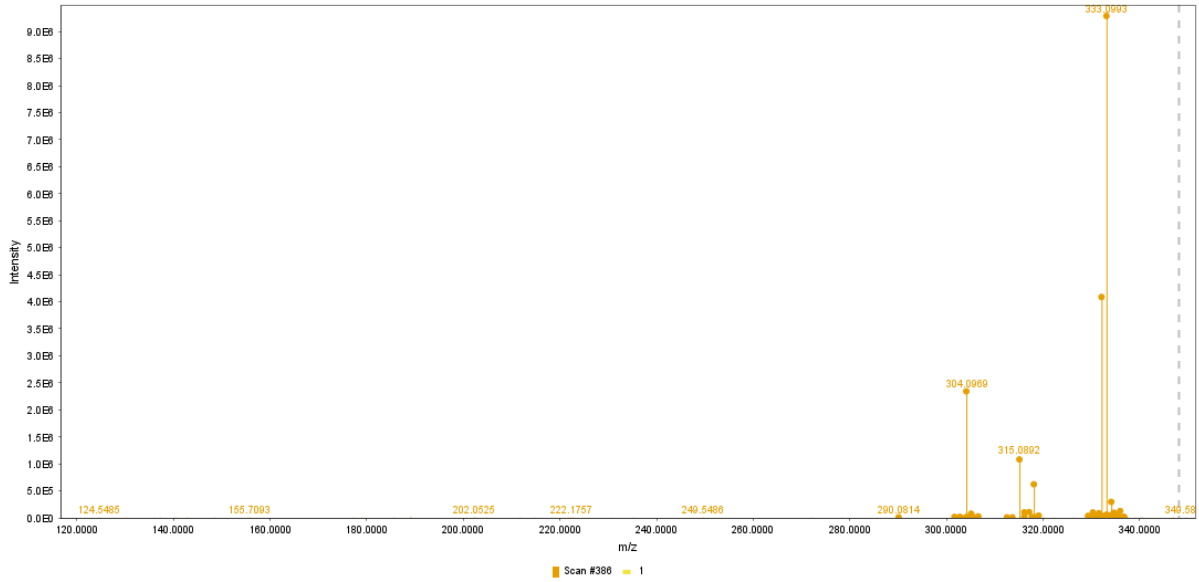

Fig. S69. HR-ESI-MS/MS spectrum of compound **7.**

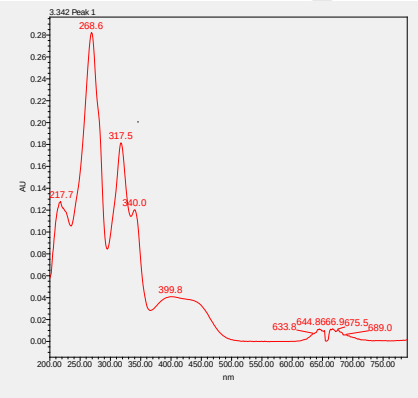

Fig. S70. UV spectrum of compound **7.**

Evodiamide (8):

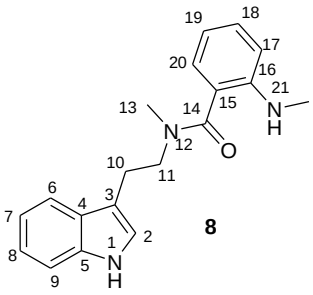

8

Yellow powder; UHPLC-UV: λ_{max} (AU) 222 (0.52), 260 (sh), 282 (0.15), 290 (0.14), 318 (0.11) nm; ^{1}H NMR (DMSO-d_6, 500 MHz) δ (ppm) 10.81 (1H, s, H-l), 7.31 (1H, d, H-9), 7.21 (1H, m, J = 7.5 Hz, H-18), 6.72-7.13 (5H, m, H-2, H-8, H-7, H-20, H-6), 6.59 (1H, d, J = 8.2 Hz, H-17), 6.56 (1H, dd, J = 7.1 Hz, H-19), 5.07 (1H, s, NH-21), 3.35 (3H, d, H-13), 2.81-3.06 (4H, m, H-5, H-6), 2.66 (3H, d, J = 4.9 Hz, 21-NH-Me); ^{13}C NMR (DMSO-d_6, 125 MHz) δ (ppm) 170.1 (C, C-1), 146.5 (C, C-16), 136.6 (C, C-5), 130.4 (CH, C-18), 127.5 (CH, C-20), 123.3 (CH, C-2), 121.4 (CH, C-8), 118.7 (CH, C-7), 115.5 (CH, C-19), 111.8 (CH, C-9), 110.5 (CH, C-17), 46.7 (CH2, C-11), 30.3 (2CH3, 21-NHMe, 12-N-Me), 24.6 (CH2, C-10); HR-ESI-MS: *m/z* 308.1756 $[M+H]^+$ (calcd for $C_{19}H_{21}N_3O$, 308.1754).

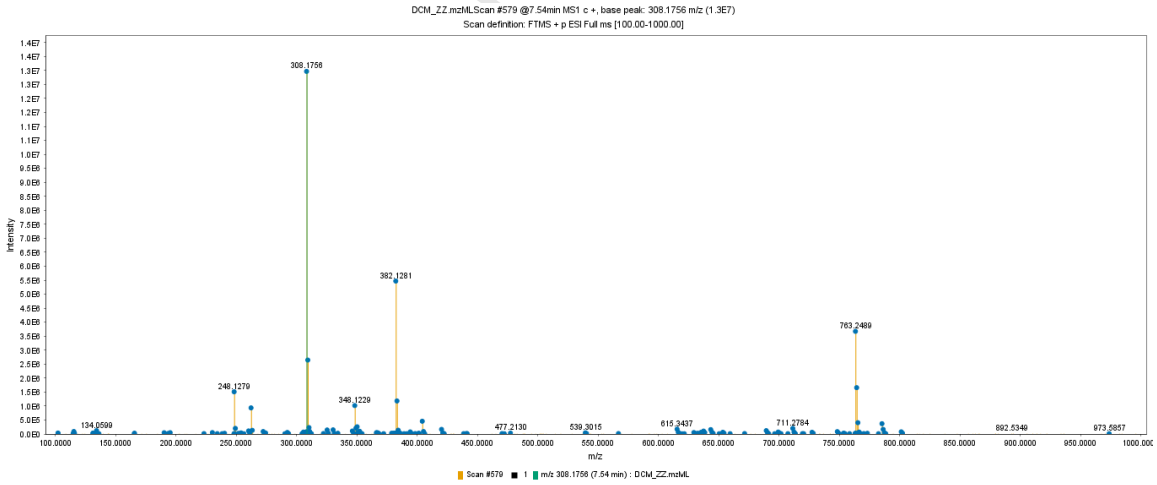

Fig. S71. HR-ESI-MS spectrum of compound **8.**

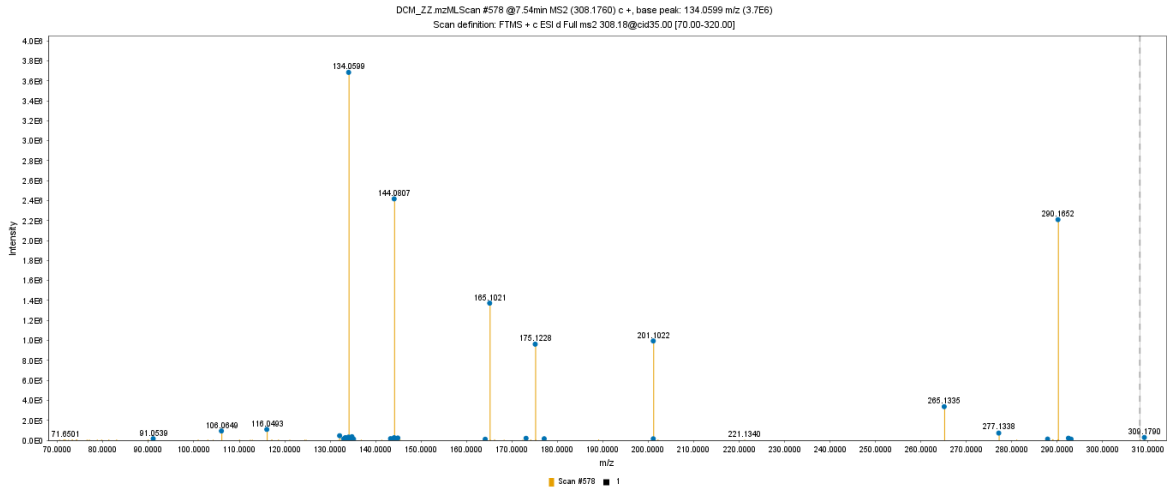

Fig. S72. HR-ESI-MS/MS spectrum of compound **8.**

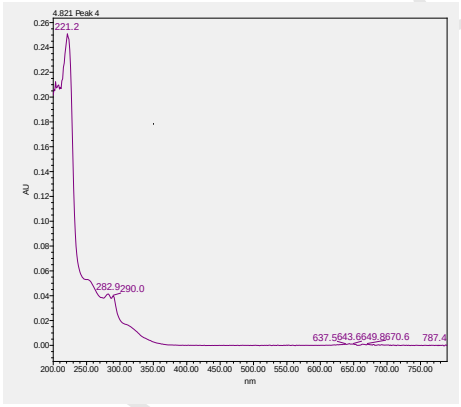

Fig. S73. The UV spectrum of compound **8.**

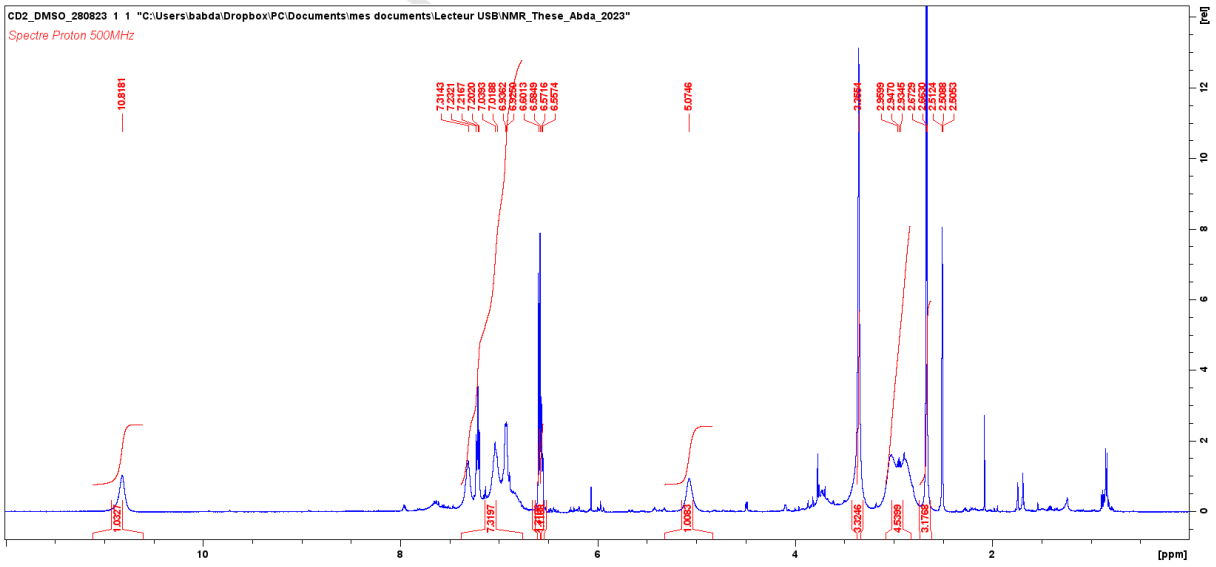

Fig. S74. ^{1}H-NMR (500 MHz, DMSO-d_6) spectrum of compound **8.**

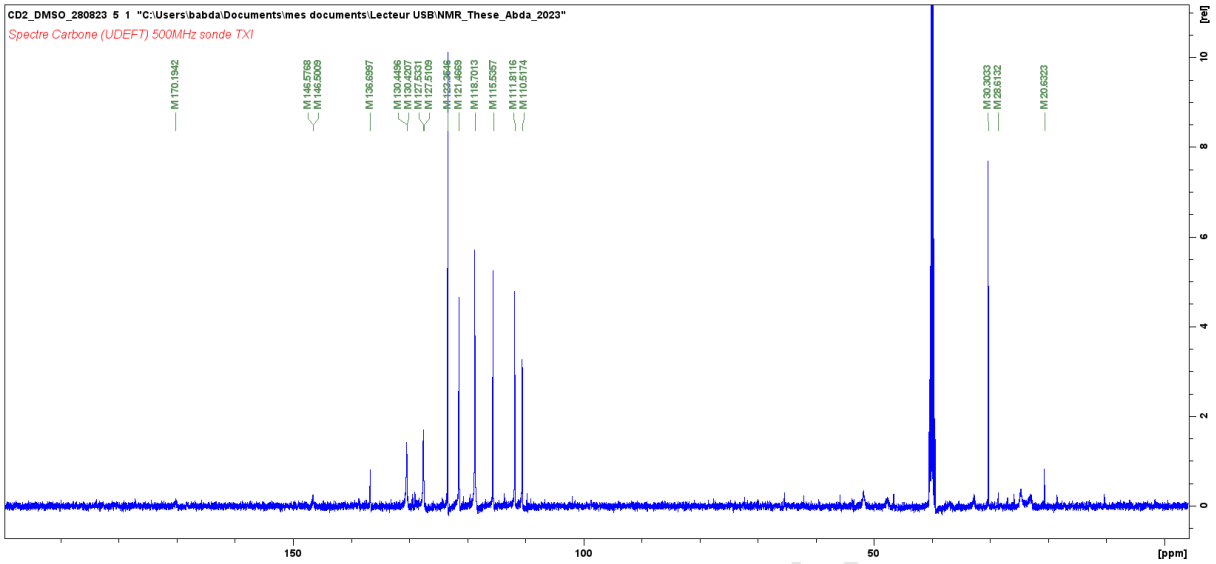

Fig. S75. ^{13}C-NMR (125 MHz, DMSO-d_6) spectrum of compound **8.**

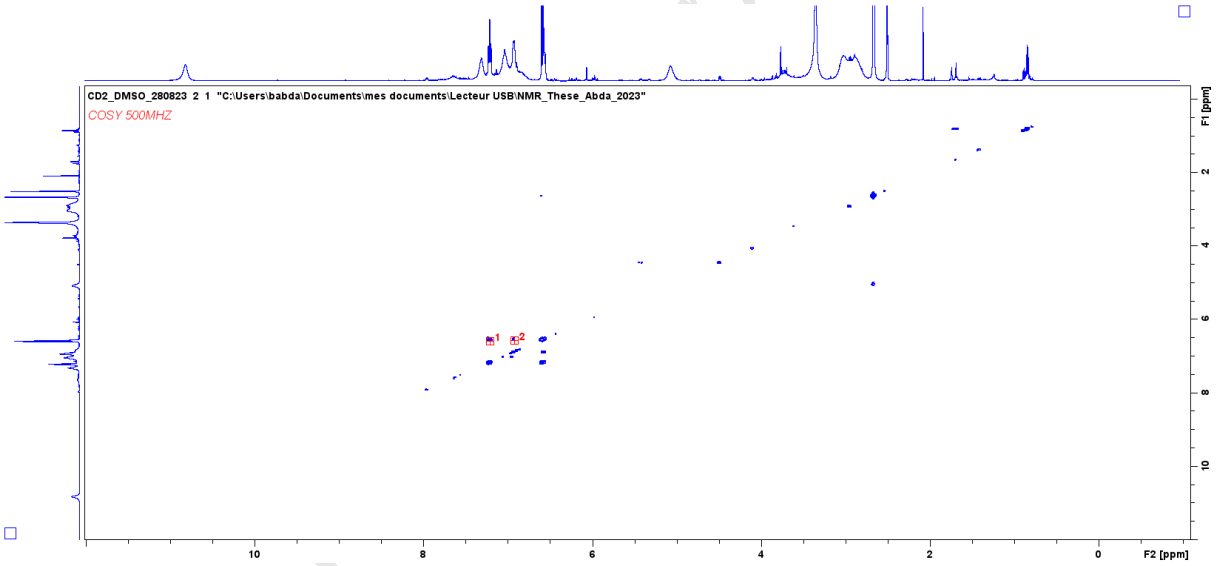

Fig. S76. ^{1}H-^{1}H COSY (500 MHz, DMSO-d_6) spectrum of compound **8.**

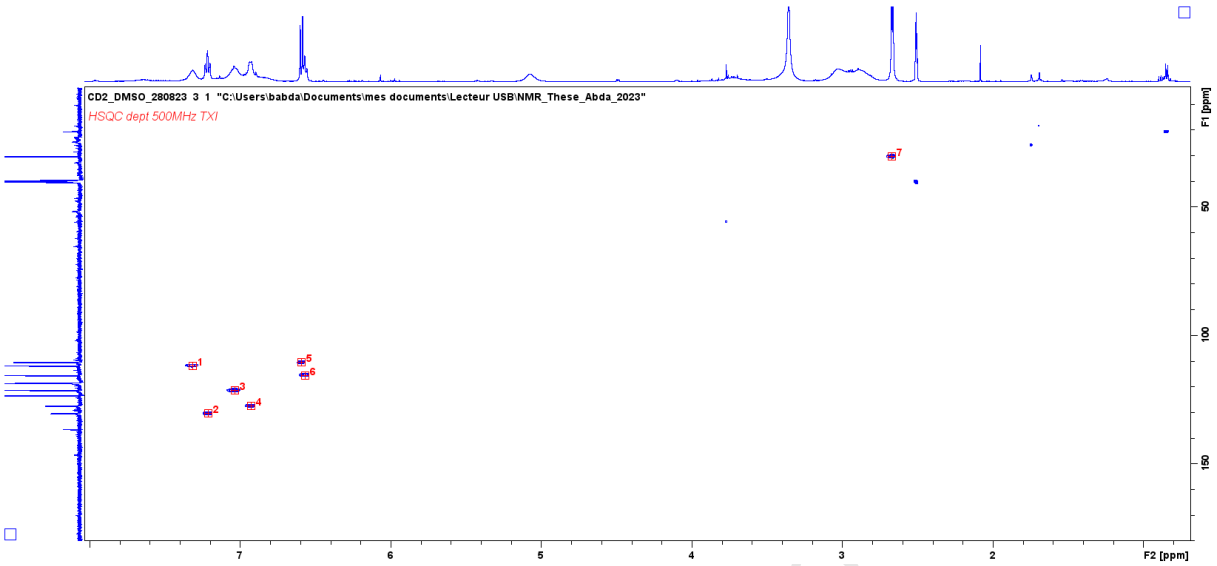

Fig. S77. HSQC-DEPT (500 MHz, DMSO-d_6) spectrum of compound **8.**

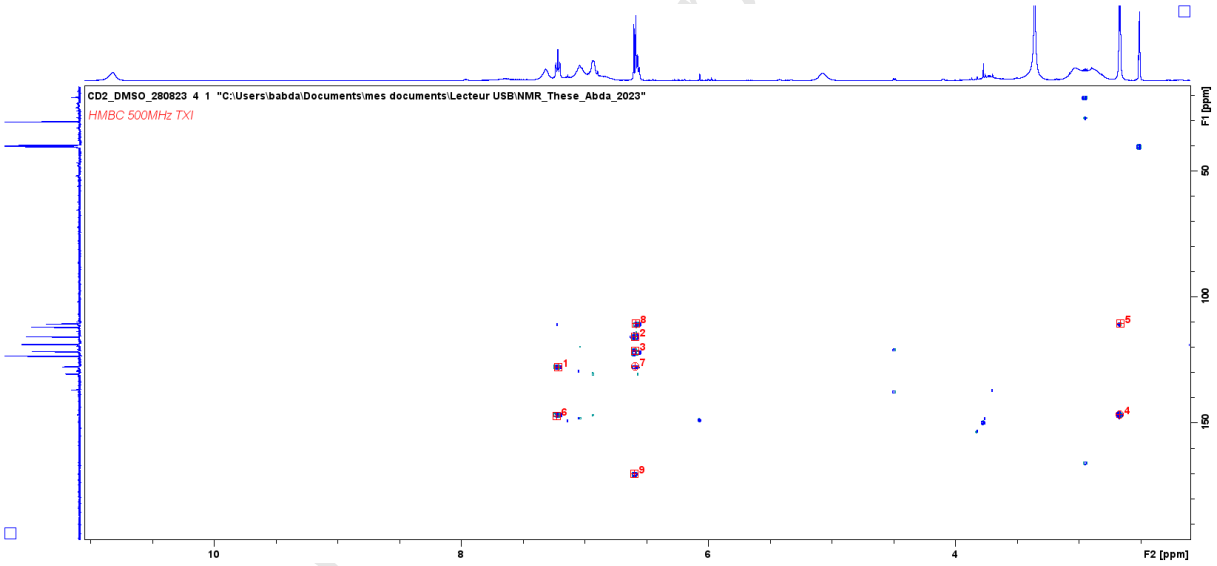

Fig. S78. HMBC (500 MHz, DMSO-d_6) spectrum of compound **8.**

Decarine (9):

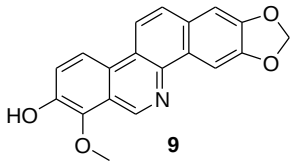

9

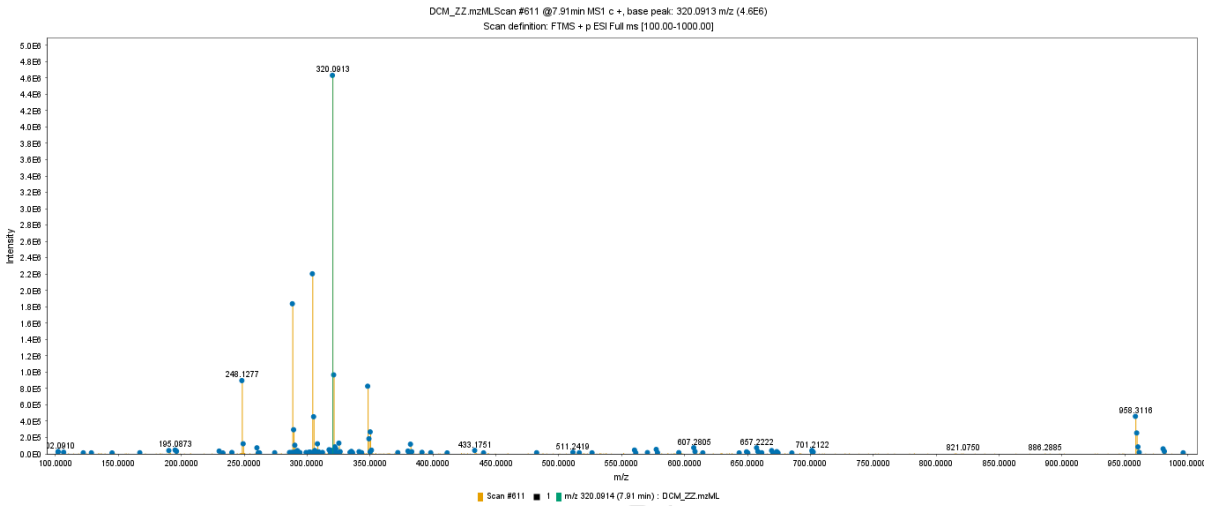

Fig. S79. HR-ESI-MS spectrum of compound **9.**

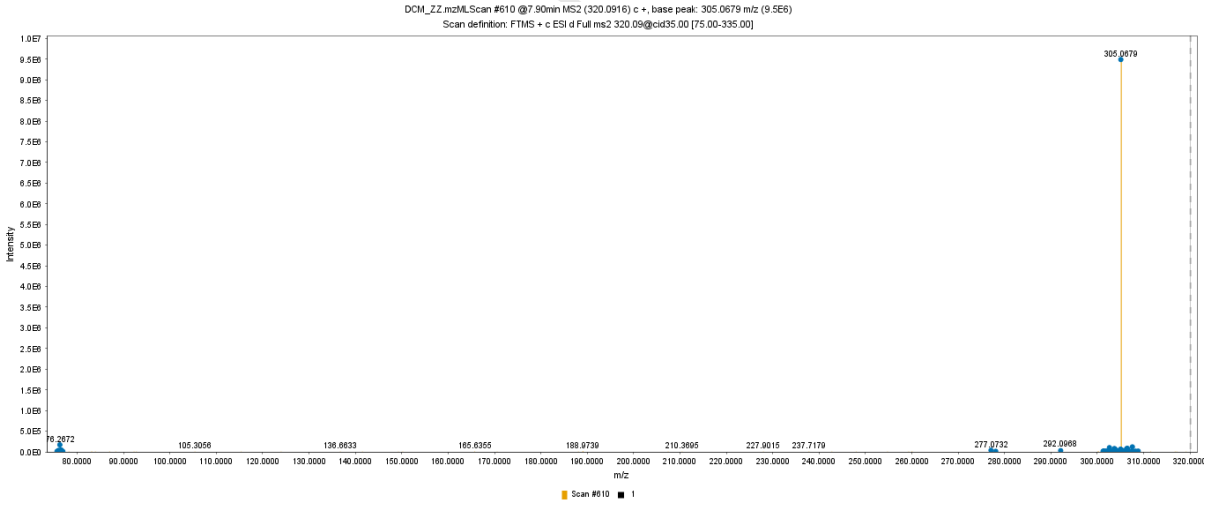

Fig. S80. HR-ESI-MS/MS spectrum of compound **9.**

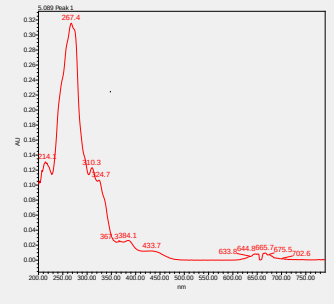

Fig. S81. UV spectrum of compound **9.**

6-Oxochelerythrine (10):

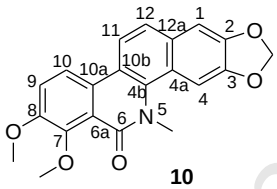

10

Brown prism; UHPLC-UV: λ_{max} (AU) 238 (0.78), 287 (1.09), 323 (0.30), 338 (0.29), 380 (sh) nm; ^{1}H NMR ($CDCl_3$, 500 MHz) δ (ppm) 8.01 (1H, d, J = 8.7 Hz, H-10), 8.01 (1H, d, J = 8.7 Hz, H-11), 7.55 (1H, s, H-4), 7.54 (1H, d, J = 9.8 Hz, H-12), 7.40 (1H, d, J = 9.0 Hz, H-9), 7.17 (1H, s, H-1), 6.11 (2H, s, C-2-O-CH2-O-C-3), 4.10 (3H, s, C-8-O-CH3), 4.00 (3H, s, C-7-O-CH3), 3.92 (3H, s, N-CH3); ^{13}C NMR ($CDCl_3$, 125 MHz) δ (ppm) 162.6 (C=O, C-6), 152.6 (C, C-7), 150.1 (C, C-8), 147.4 (C, C-2), 147.0 (C, C-3), 135.6 (C, C-4b), 131.6 (C, C-12a), 128.9 (C, C-10a), 123.3 (CH, C-12), 121.0 (C, C-4a), 119.7 (C, C-6a), 118.4 (CH, C-10), 117.8 (CH, C-11), 117.7 (CH, C-9), 117.1 (C, C-10b), 104.6 (CH, C-1), 102.4 (CH, C-4), 101.5 (CH_2, C-2-O-CH_2-O-C-3), 61.7 (CH_3, C-8-O-CH_3), 56.5 (CH_3, C-7-O-CH_3), 40.8 (CH_3, N-CH_3); HR-ESI-MS: *m/z* 364.1177 $[M+H]^+$ (calcd for $C_{21}H_{17}NO_5$, 364.1174).

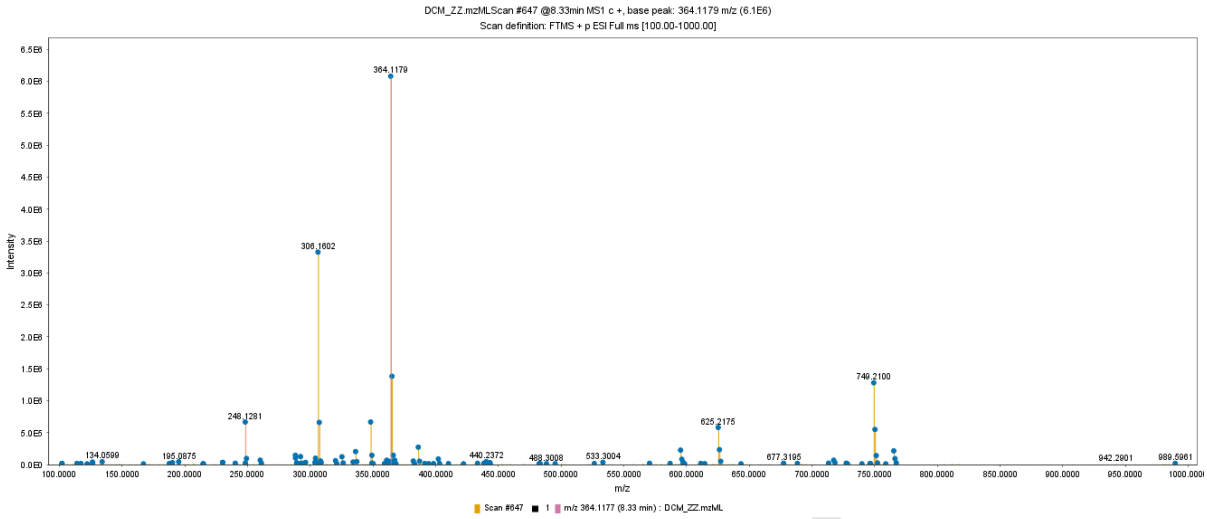

Fig. S82. HR-ESI-MS spectrum of compound **10.**

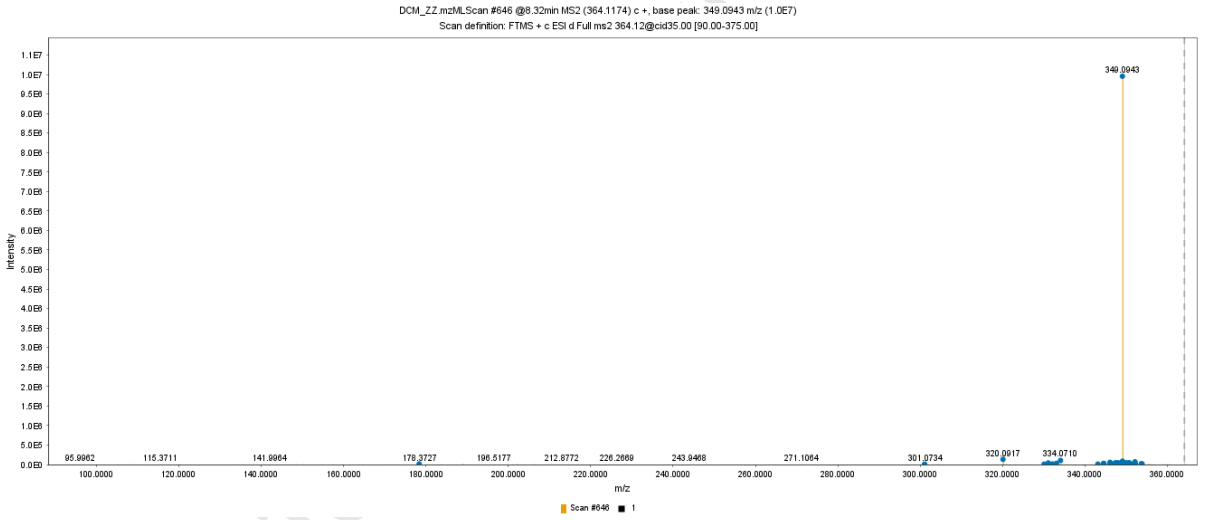

Fig. S83. HR-ESI-MS spectrum of compound **10.**

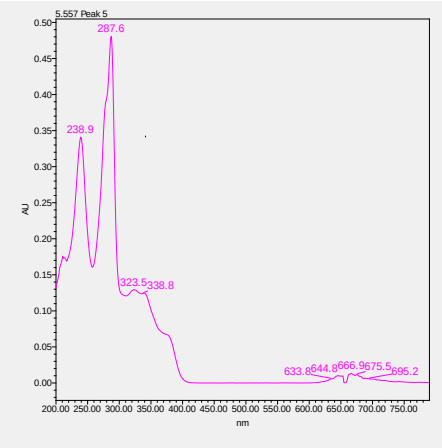

Fig. S84. UV spectrum of compound **10.**

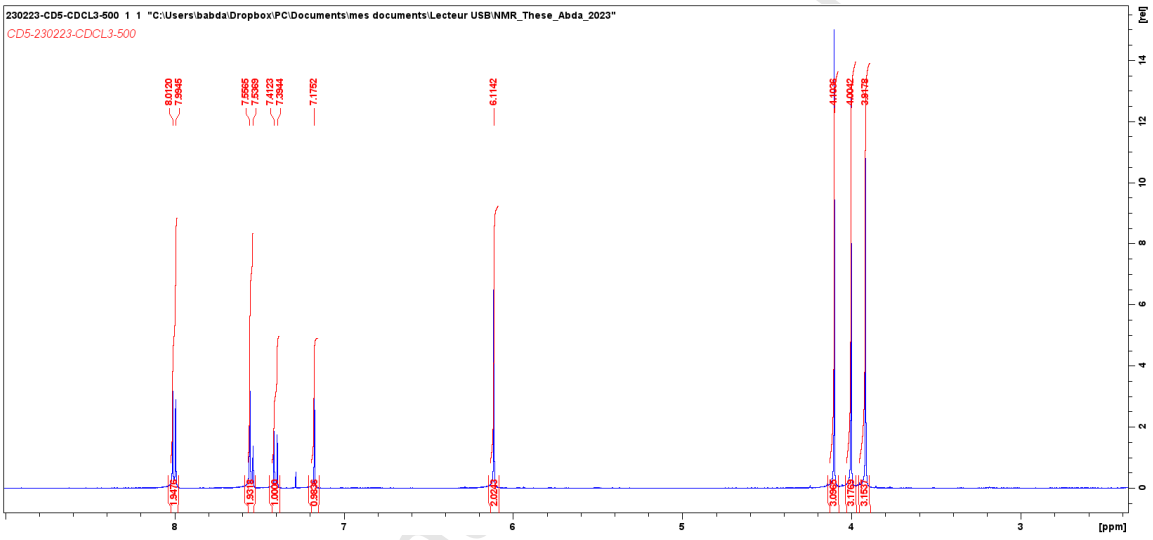

Fig. S85. ^{1}H-NMR (500 MHz, $CDCl_3$) spectrum of compound **10.**

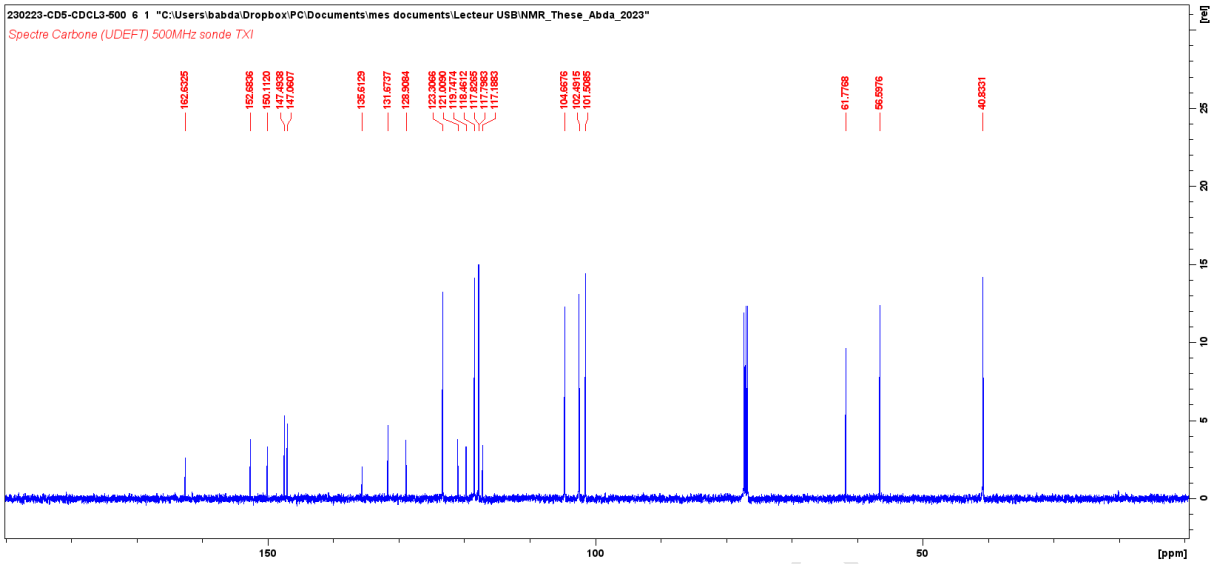

Fig. S86. ^{13}C-NMR (125 MHz, $CDCl_3$) spectrum of compound **10.**

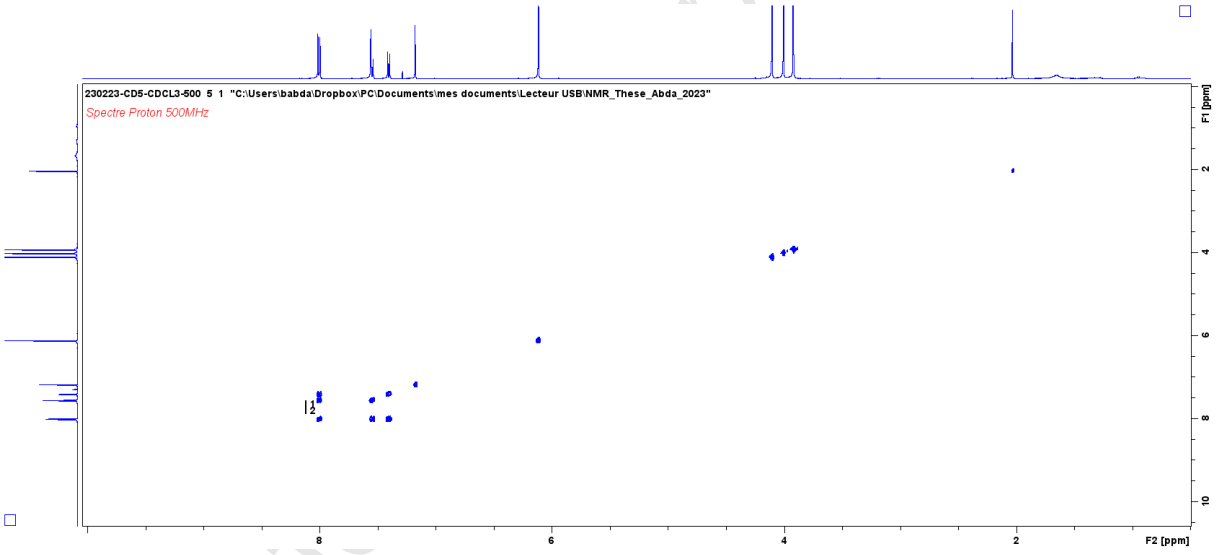

Fig. S87. ^{1}H-^{1}H COSY (500 MHz, $CDCl_3$) spectrum of compound **10.**

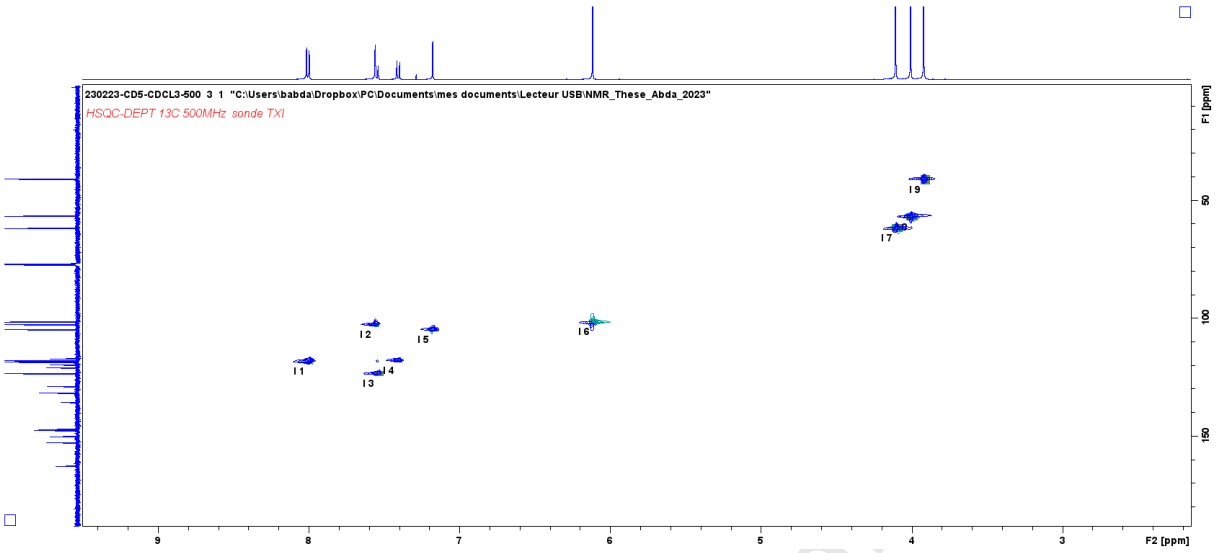

Fig. S88. HSQC-DEPT (500 MHz, $CDCl_3$) spectrum of compound **10.**

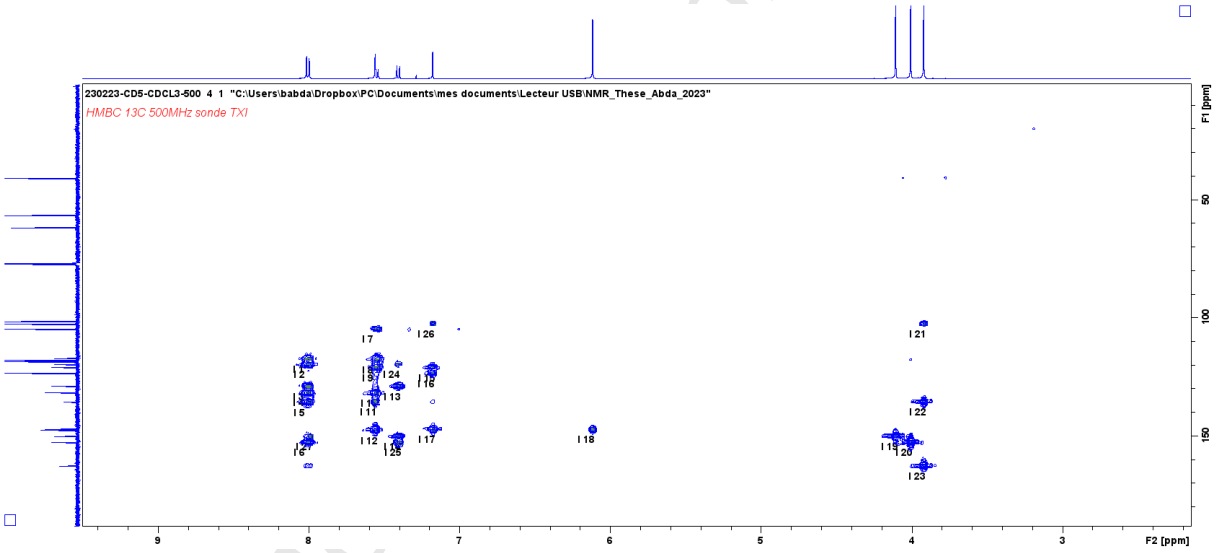

Fig. S89. HMBC (500 MHz, $CDCl_3$) spectrum of compound **10.**

Scoparone (11):

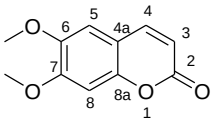

11

Yellow powder; UHPLC-UV: λ_{max} (AU) 229 (0.034), 260 (sh), 294 (0.01), 343 (0.02) nm; ^{1}H NMR ($CDCl_3$, 500 MHz) δ (ppm) 7.64 (1H, d, J = 9,4 Hz, H-4), 6.87 (1H, s, H-5), 6.87 (1H, s, H-8), 6.31 (1H, d, J = 9,4 Hz, H-3), 3.97 (3H, s, C-7-O-CH3), 3.94 (3H, s, C-6-O-CH3); ^{13}C NMR ($CDCl_3$, 125 MHz) δ (ppm) 161.4 (C=O, C-2), 152.8 (C, C-7), 150.0 (C, C-8a), 146.3 (C, C-6), 143.3 (CH, C-4), 113.5 (CH, C-3), 111.4 (C, C-4a), 107.9 (CH, C-5), 100.0 (CH, C-8), 56.4 (CH_3, C-7-O-CH3), 56.3 (CH_3, C-6-O-CH_3); HR-ESI-MS: *m/z* 207.0649 $[M+H]^+$ (calcd for $C_{11}H_{10}O_4$, 207.0646).

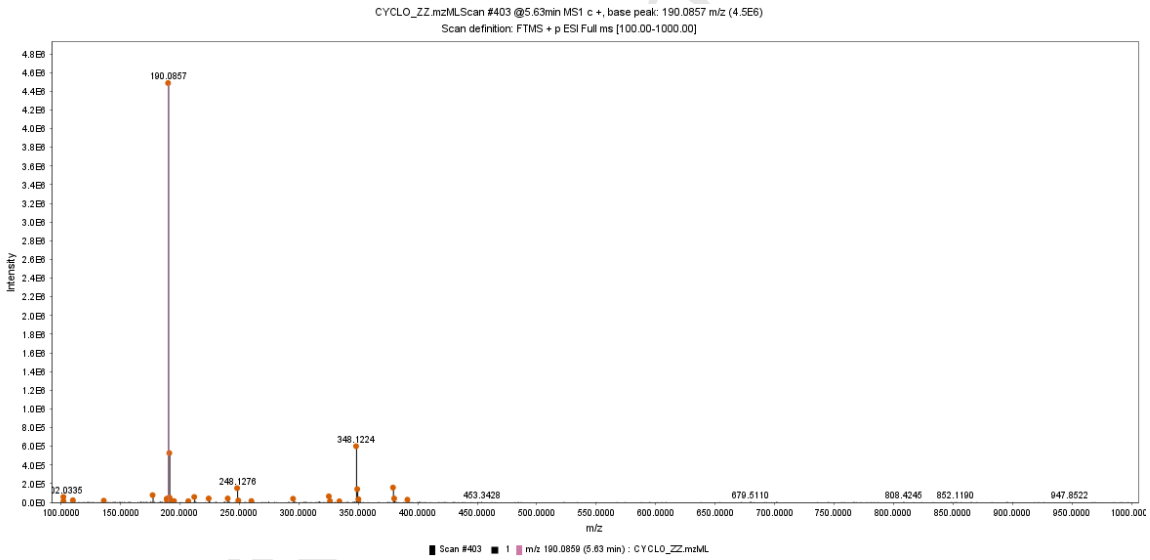

Fig. S90. HR-ESI-MS spectrum of compound **11.**

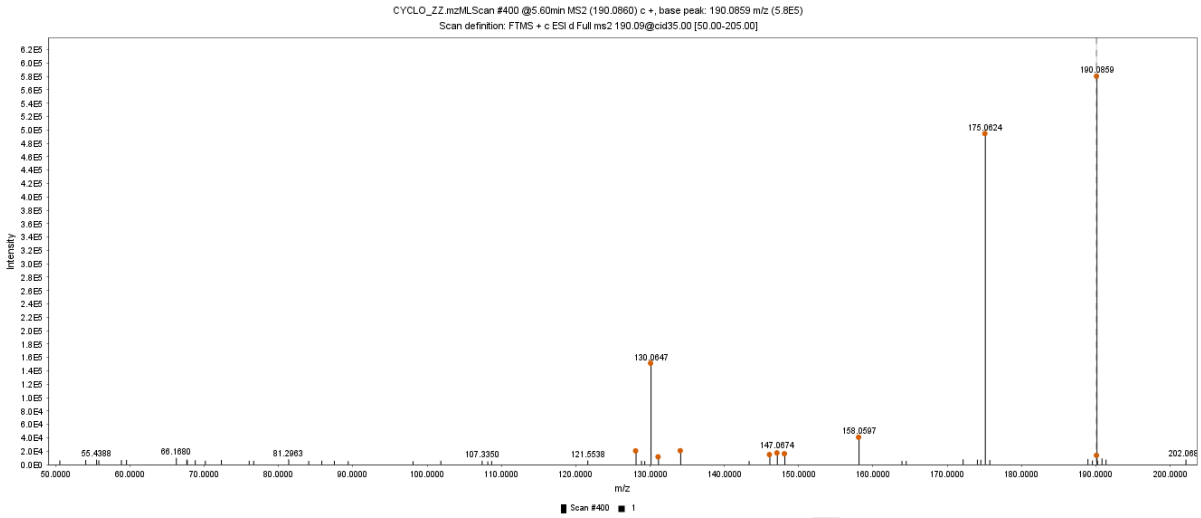

Fig. S91. HR-ESI-MS/MS spectrum of compound **11.**

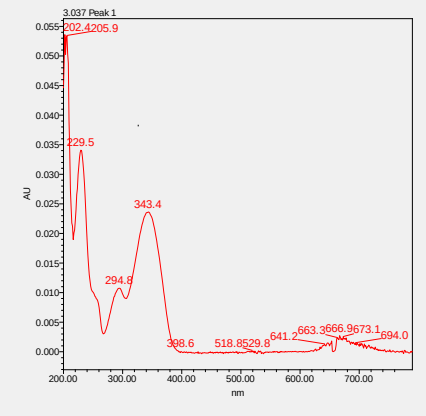

Fig. S92. UV spectrum of compound **11.**

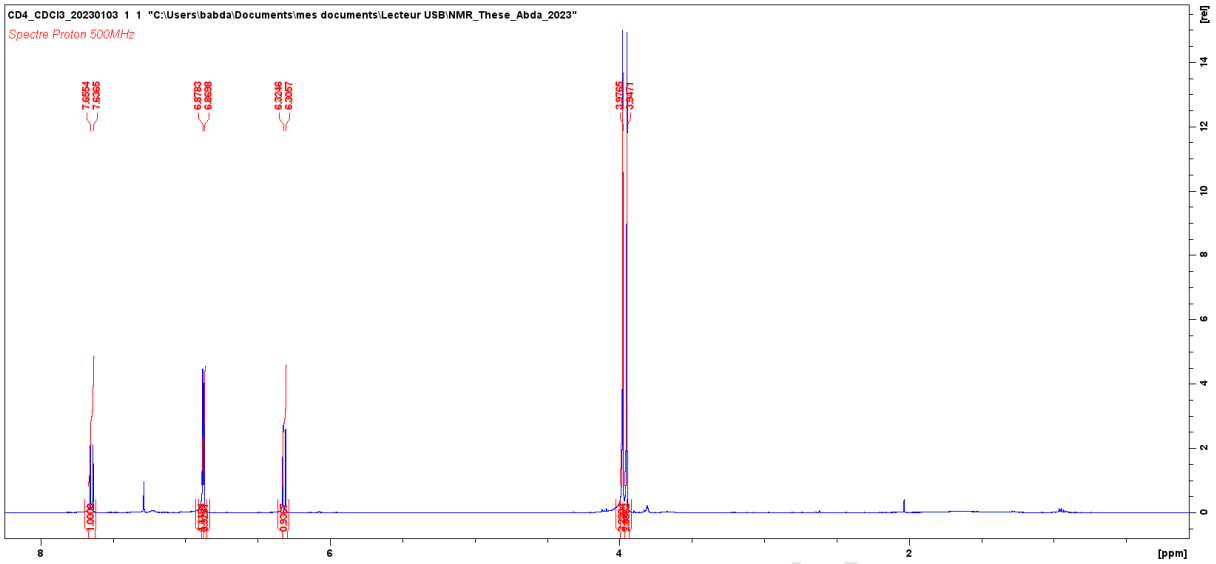

Fig. S93. ^{1}H-NMR (500 MHz, $CDCl_3$) spectrum of compound **11.**

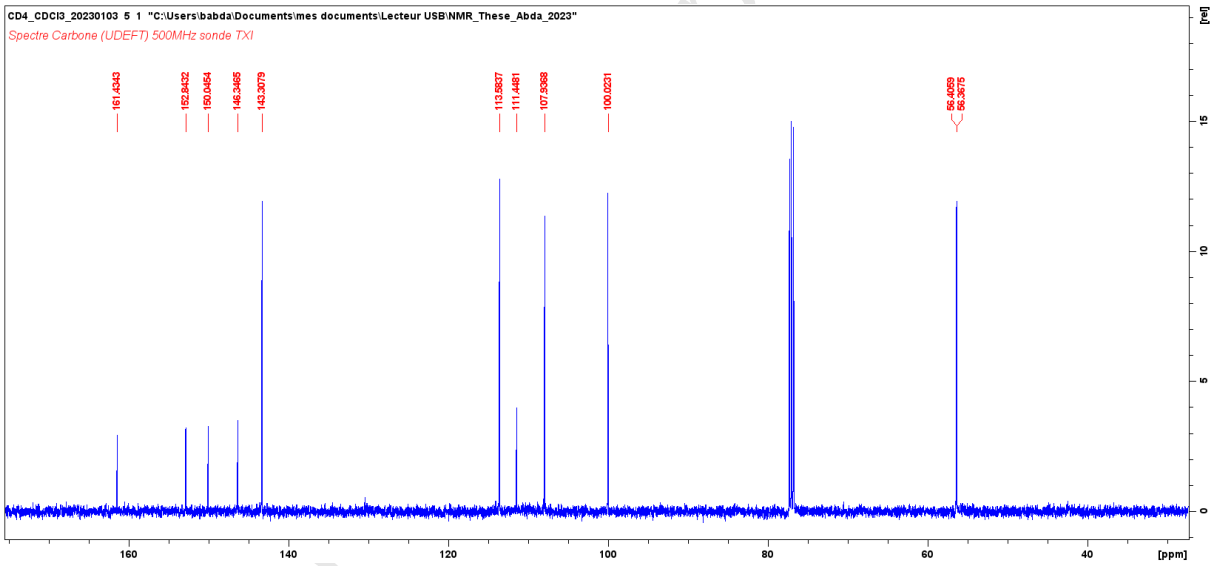

Fig. S94. ^{13}C-NMR (125 MHz, $CDCl_3$) spectrum of compound **11.**

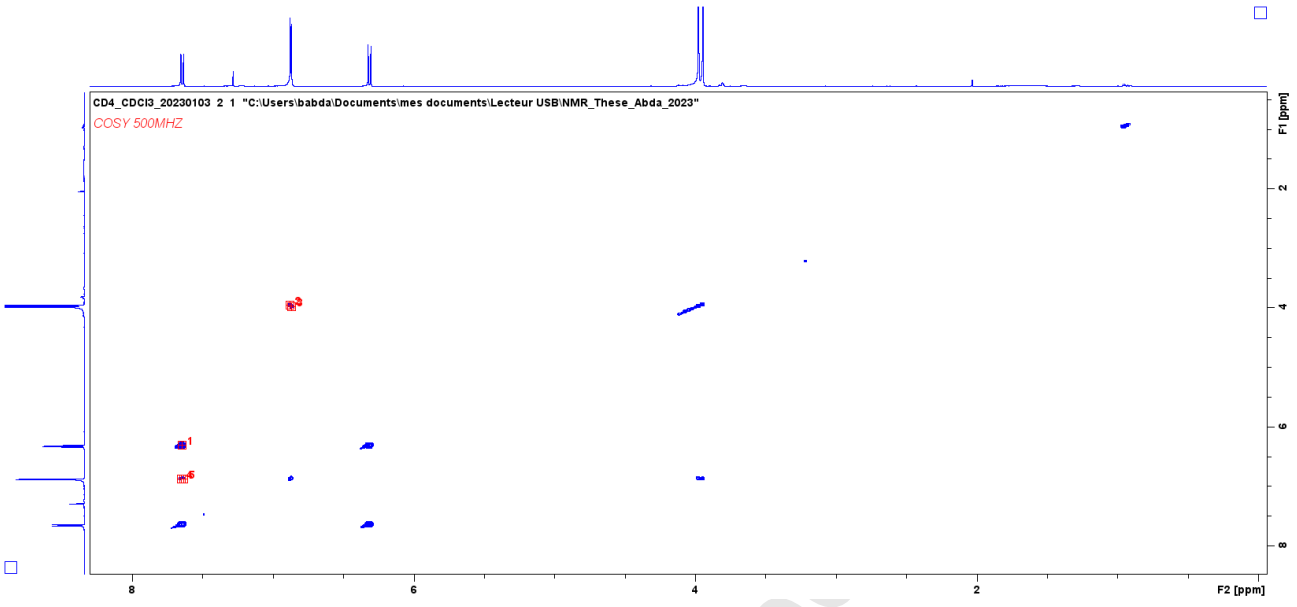

Fig. S95. ^{1}H-^{1}H COSY (500 MHz, $CDCl_3$) spectrum of compound **11.**

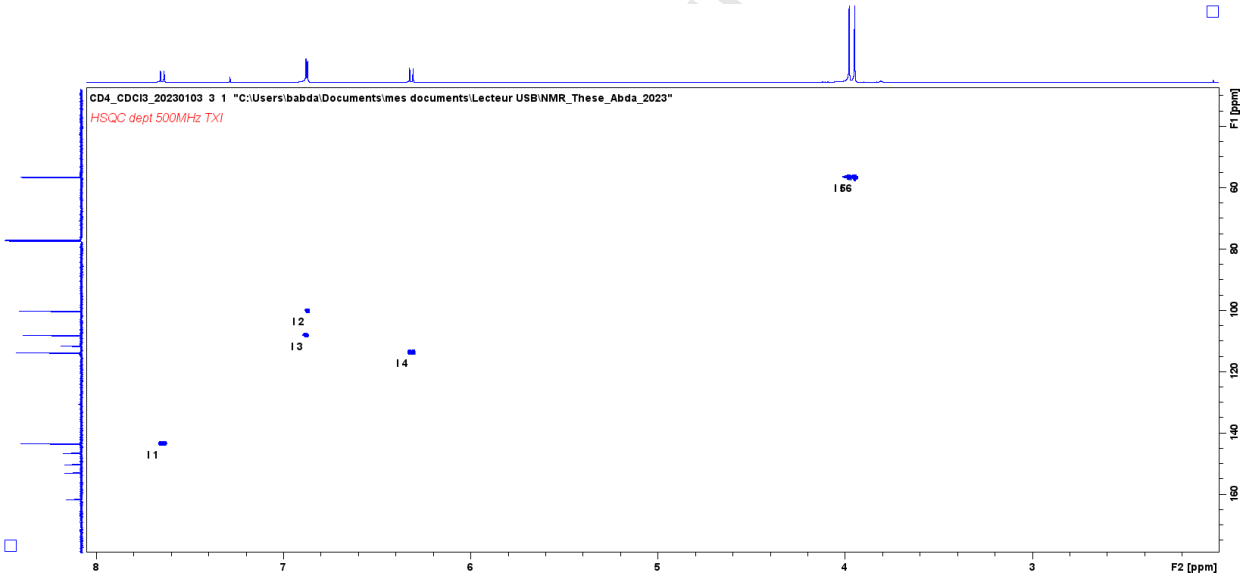

Fig. S96. HSQC-DEPT (500 MHz, $CDCl_3$) spectrum of compound **11.**

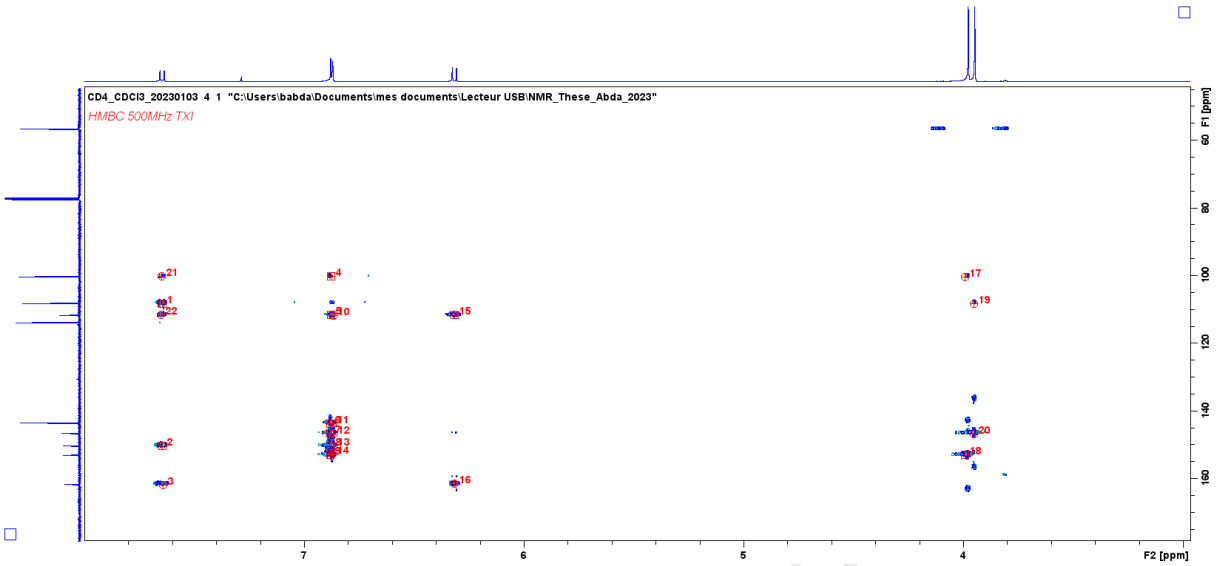

Fig. S97. HMBC (500 MHz, $CDCl_3$) spectrum of compound **11.**

4-methoxy-1-methylquinolin-2-one (12):

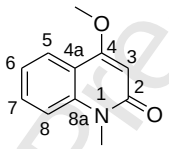

12

White needles; UHPLC-UV: λ_{max} (AU) 234 (2.55), 260 (1.05), 268 (1.05), 315 (0.9), 330 (sh) nm; ^{1}H NMR ($CDCl_3$, 500 MHz) δ (ppm) 7.99 (1H, dd, J = 7.9, 1.4 Hz, H-8), 7.60 (1H, dd, J = 7.9, 1.5 Hz, H-6), 7.36 (1H, dd, J = 8.5 Hz, H-5), 7.24 (1H, dd, J = 7.6, 1.0 Hz, H-7), 6.06 (1H, s, H-3), 3.97 (3H, s, C-4-O-CH_3), 3.69 (3H, s, N-CH_3); ^{13}C NMR ($CDCl_3$, 125 MHz) δ (ppm) 163.8 (C=O, C-2), 162.6 (C, C-4), 139.7 (C, C-8a), 131.2 (CH, C-6), 123.3 (CH, C-8), 121.6 (CH, C-7), 116.5 (C, C-4a), 114.0 (CH, C-5), 96.4 (CH, C-3), 55.8 (CH_3, C-4-O-CH_3), 29.0 (CH_3, N-CH_3); HR-ESI-MS: *m/z* 190.0862 $[M+H]^+$ (calcd for $C_{11}H_{11}NO_2$, 190.0861).

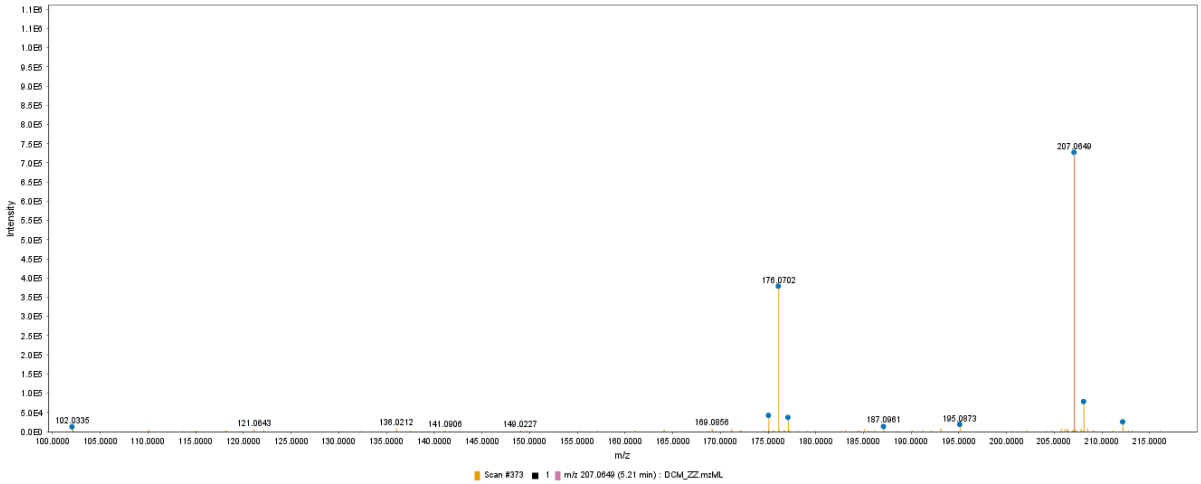

Fig. S98. HR-ESI-MS spectrum of compound **12.**

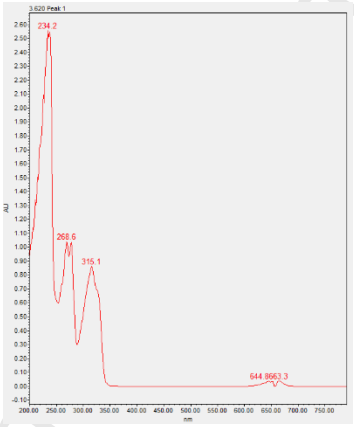

Fig. S99. UV spectrum of compound **12.**

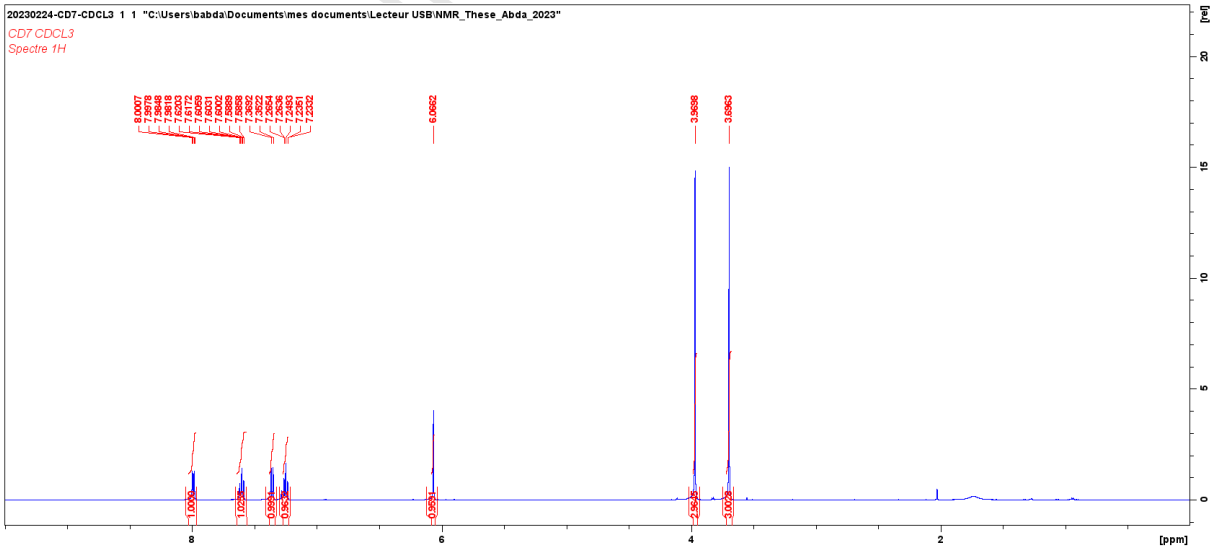

Fig. S100. ^{1}H-NMR (500 MHz, $CDCl_3$) spectrum of compound **12.**

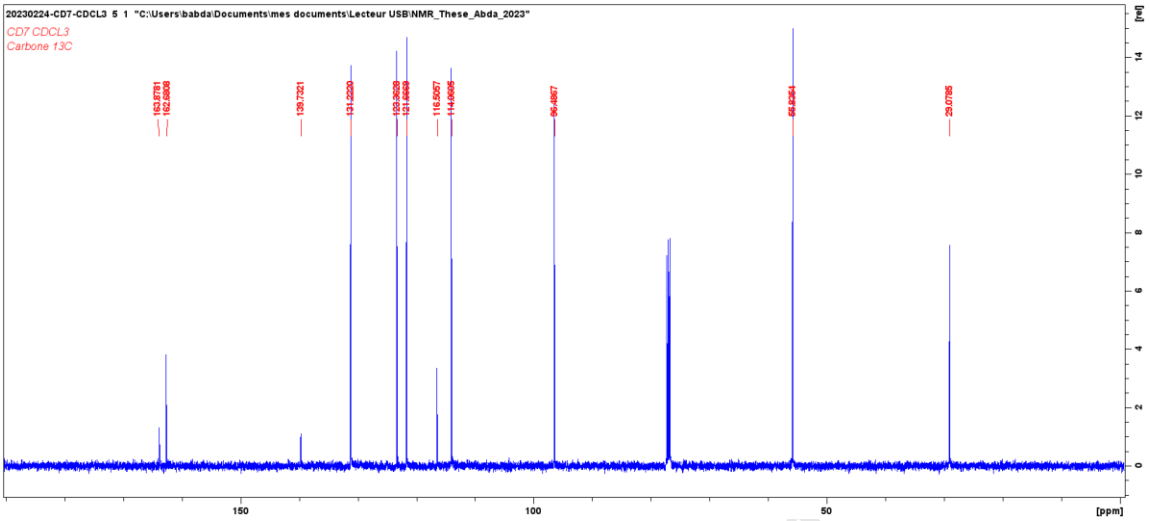

Fig. S101. ^{13}C-NMR (125 MHz, $CDCl_3$) spectrum of compound **12.**

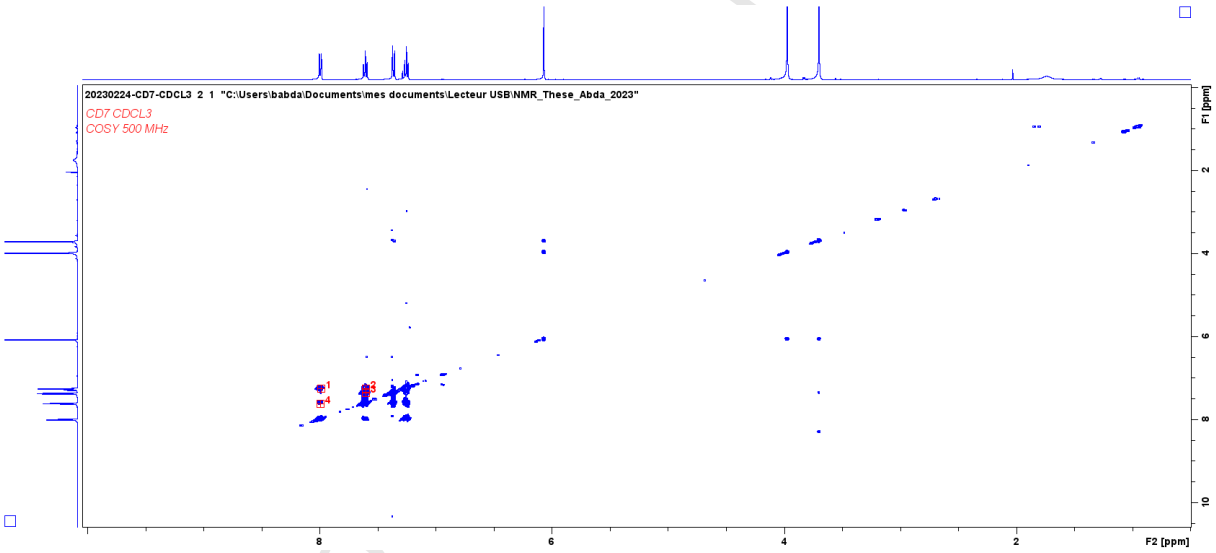

Fig. S102. ^{1}H-^{1}H COSY (500 MHz, $CDCl_3$) spectrum of compound **12.**

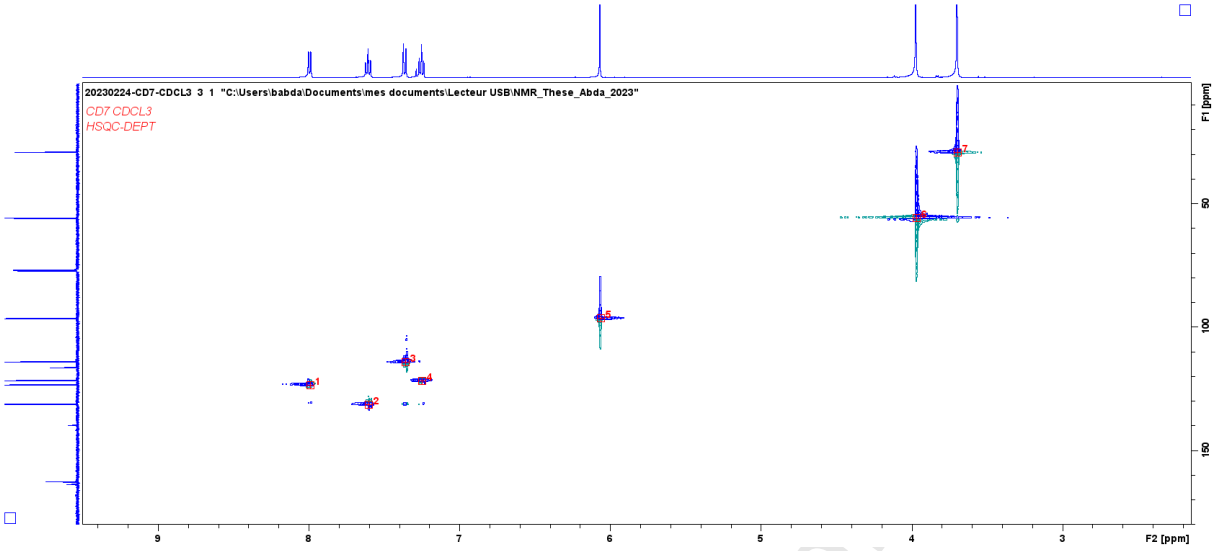

Fig. S103. HSQC-DEPT (500 MHz, $CDCl_3$) spectrum of compound **12.**

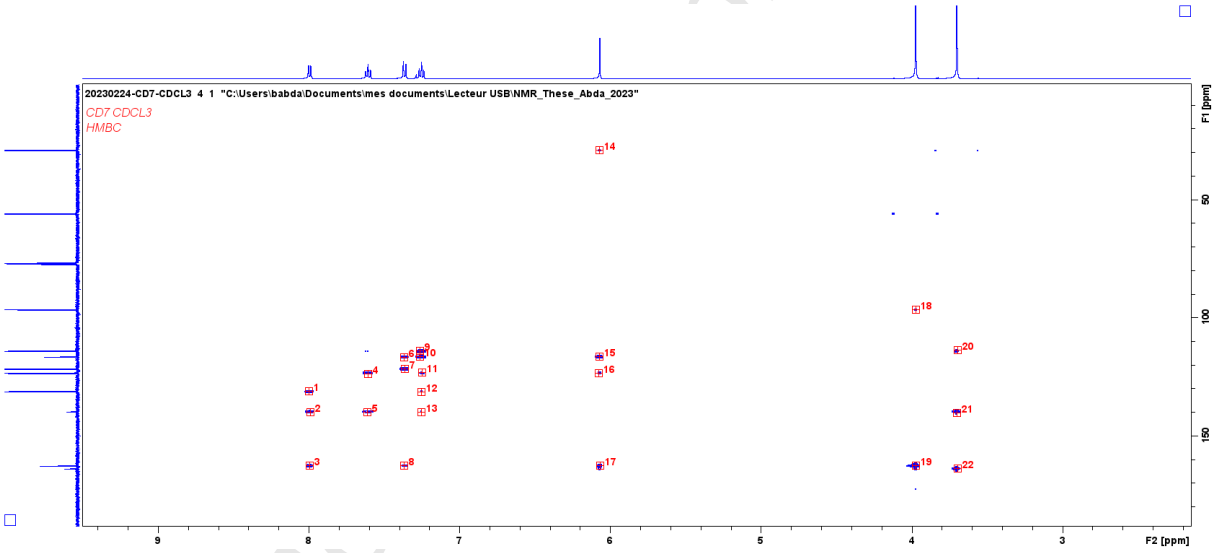

Fig. S104. HMBC (500 MHz, $CDCl_3$) spectrum of compound **12.**

Skimmianine (13):

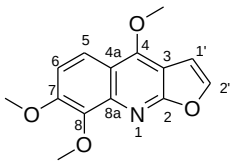

13

White crystal; UHPLC-UV: λ_{max} (AU) 246 (2.65), 319 (0.55), 328 (0.55) nm; ^{1}H NMR ($CDCl_3$, 500 MHz) δ (ppm) 8.03 (1H, d, J = 9.3 Hz, H-5), 7.60 (1H, d, J = 2.7 Hz, H-2'), 7.25 (1H, d, J = 9.4 Hz, H-6), 7.05 (1H, d, J = 2.7 Hz, H-1'), 4.44 (3H, s, C-4-O-CH_3), 4.13 (3H, s, C-7-O-CH_3), 4.04 (3H, s, C-8-O-CH_3); ^{13}C NMR ($CDCl_3$, 125 MHz) δ (ppm) 164.3 (C, C-2), 157.1 (C, C-4), 152.1 (C, C-8), 143.0 (CH, C-2'), 141.9 (C, C-7), 141.4 (C, C-8a), 118.1 (CH, C-5), 114.8 (C, C-4a), 111.9 (CH, C-6), 104.6 (CH, C-1'), 102.0 (C, C-3), 61.6 (CH_3, C-7-O-CH_3), 58.9 (CH_3, C-4-OCH_3), 56.7 (CH_3, C-8-O-CH_3); HR-ESI-MS: *m/z* 260.0913 $[M+H]^+$ (calcd for $C_{14}H_{13}NO_4$, 260.0908).

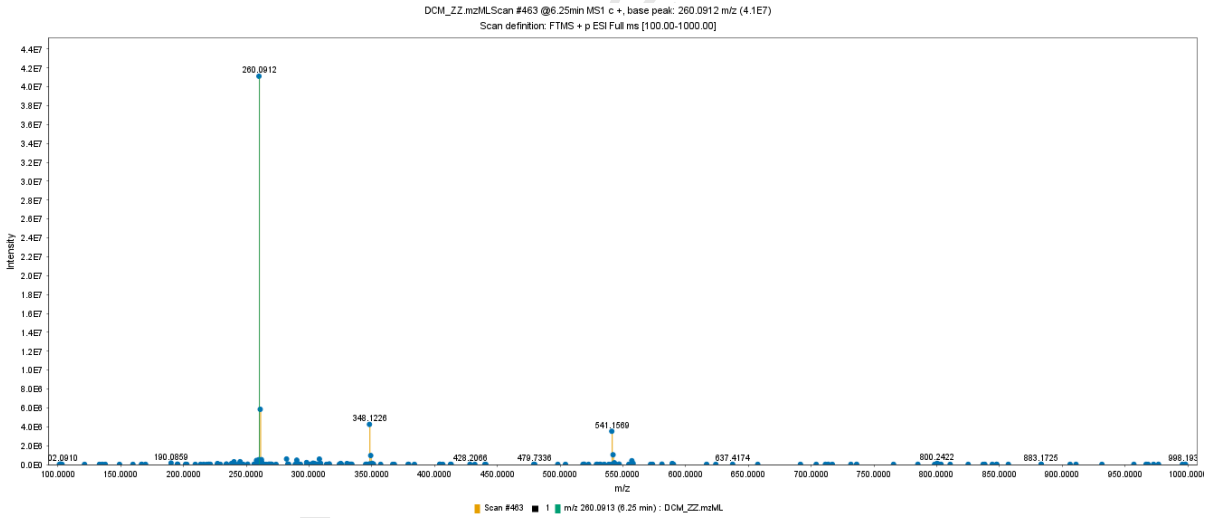

Fig. S105. HR-ESI-MS spectrum of compound **13.**

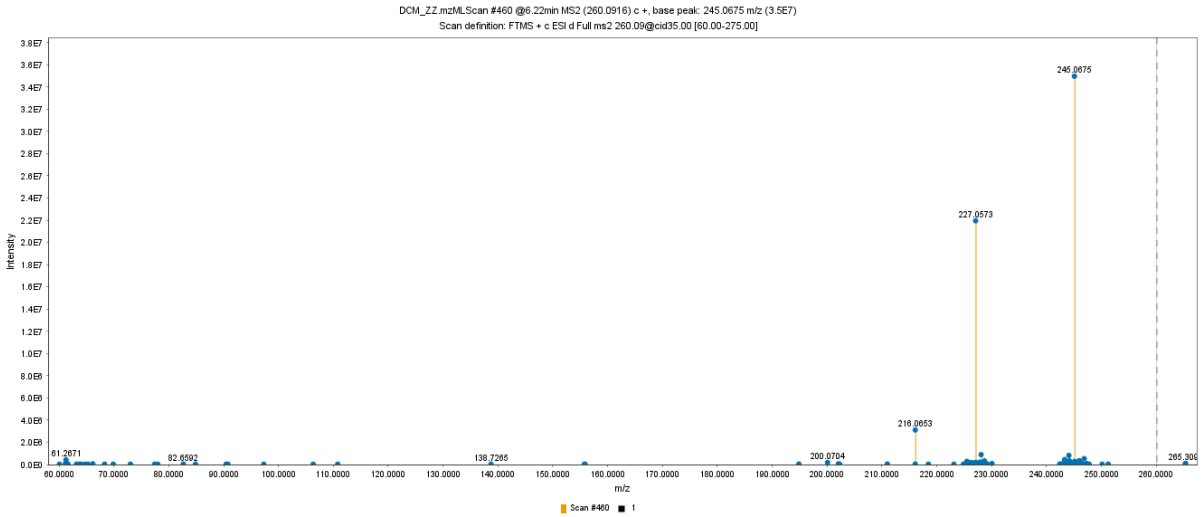

Fig. S106. HR-ESI-MS/MS spectrum of compound **13.**

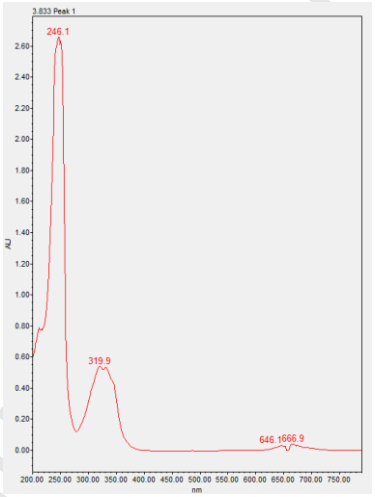

Fig. S107. UV spectrum of compound **13.**

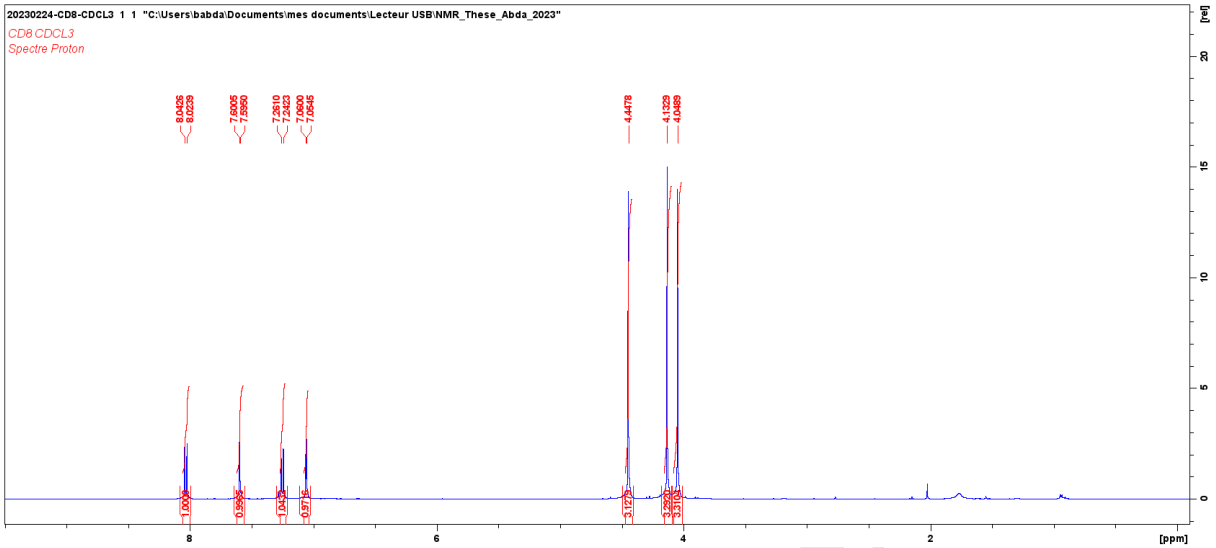

Fig. S108. ^{1}H-NMR (500 MHz, $CDCl_3$) spectrum of compound **13.**

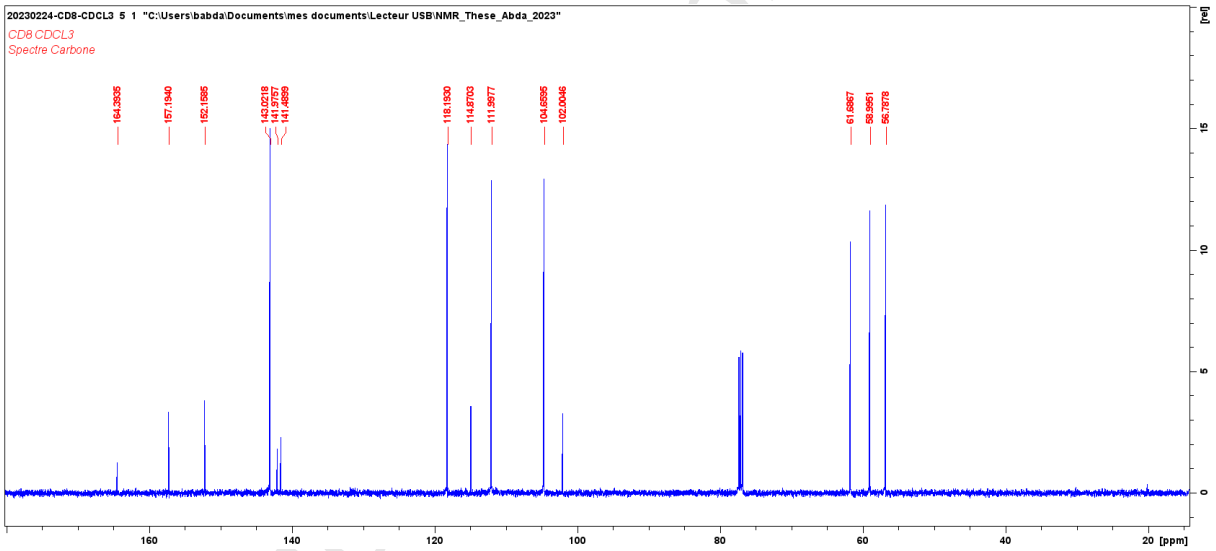

Fig. S109. ^{13}C-NMR (125 MHz, $CDCl_3$) spectrum of compound **13.**

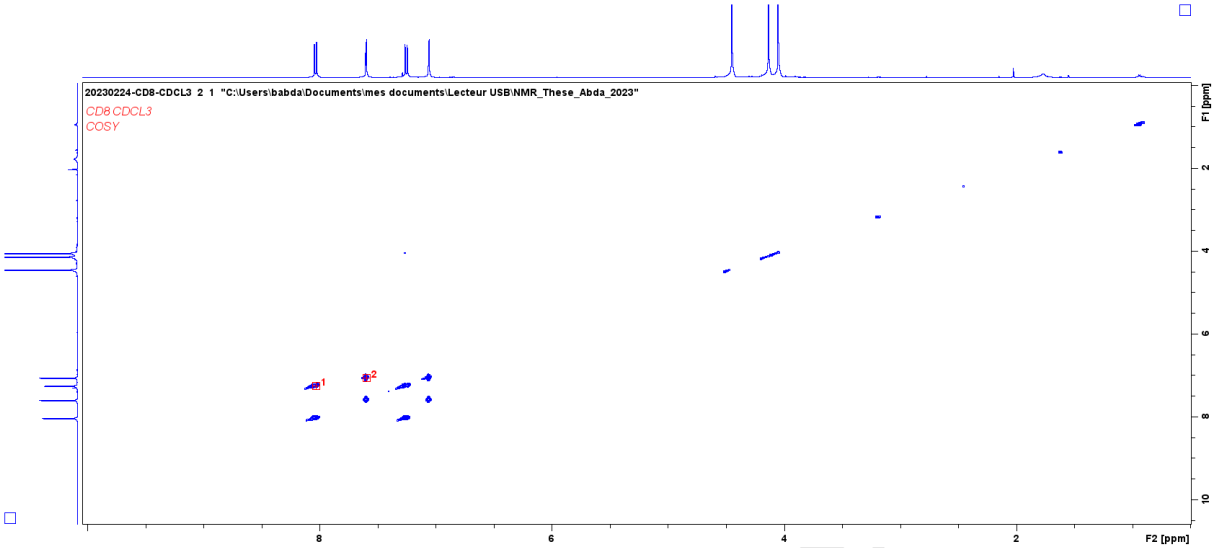

Fig. S110. ^{1}H-^{1}H COSY (500 MHz, $CDCl_3$) spectrum of compound **13.**

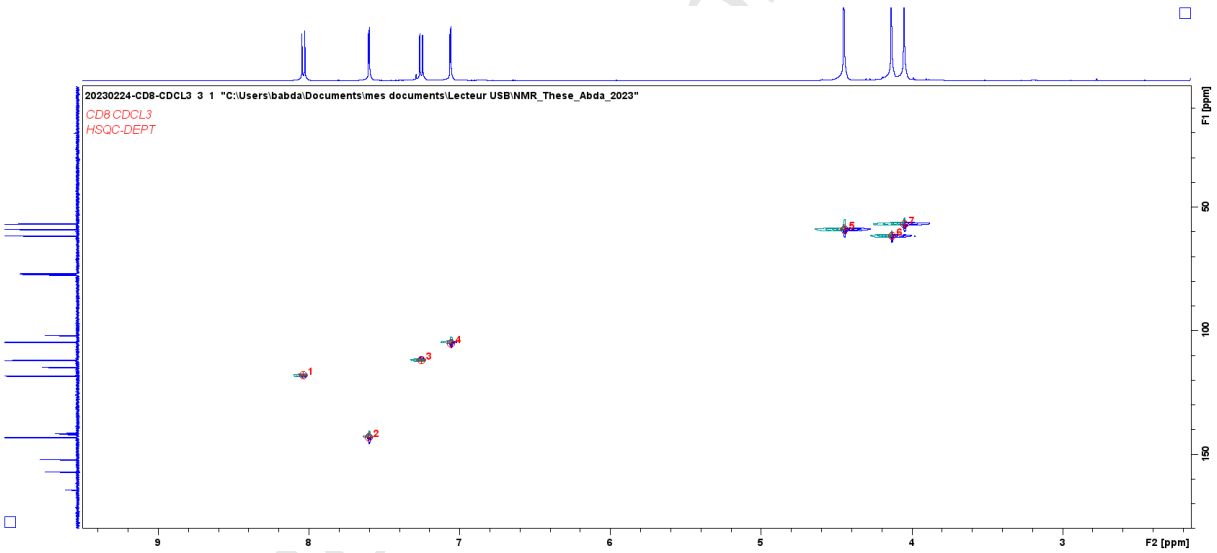

Fig. S111. HSQC-DEPT (500 MHz, $CDCl_3$) spectrum of compound **13.**

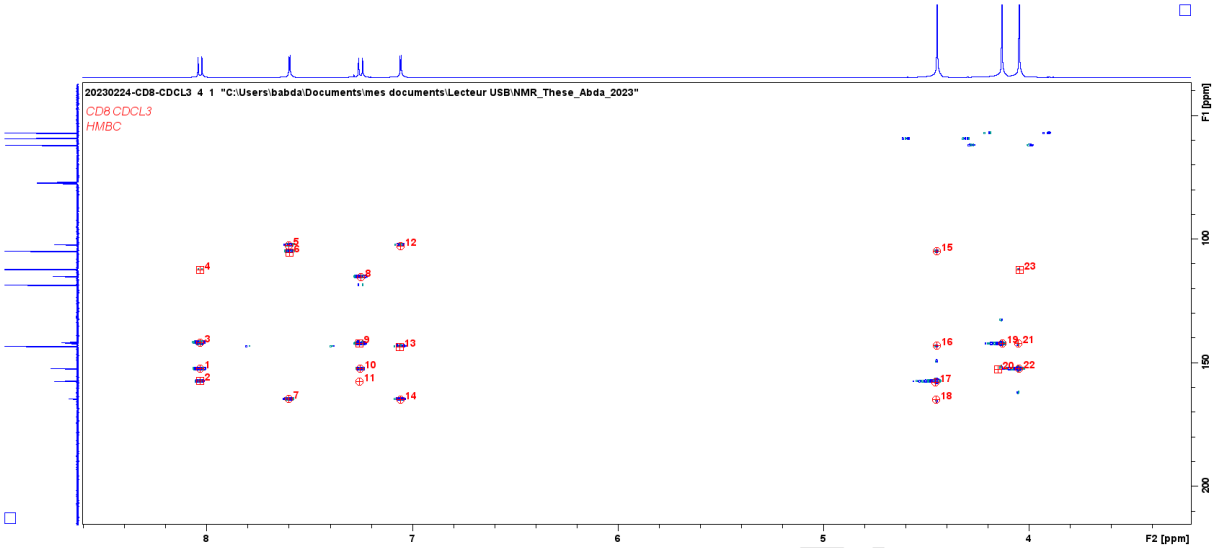

Fig. S112. HMBC (500 MHz, $CDCl_3$) spectrum of compound **13.**

γ-fagarine (14):

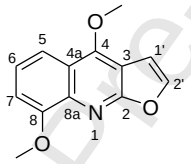

14

White crystal; UHPLC-UV: λ_{max} (AU) 249 (3.00), 310 (1.37), 328 (1.25), 348 (1.17) nm; ^{1}H NMR ($CDCl_3$, 500 MHz) δ (ppm) 7.87 (1H, dd, *J* = 8.6, 1.2 Hz, H-5), 7.67 (1H, d, *J* = 2.8 Hz, H-2'), 7.39 (1H, dd, *J* = 8.6, 0.9 Hz, H-6), 7.11 (1H, d, *J* = 2.8 Hz, H-1'), 7.09 (1H, dd, *J* = 7.7, 1.2 Hz, H-7), 4.48 (3H, s, C-4-O-CH_3), 4.09 (3H, s, C-8-O-CH_3); ^{13}C NMR ($CDCl_3$, 125 MHz) δ (ppm) 163.0 (C, C-2), 157.0 (C, C-4), 154.4 (C, C-8), 143.9 (C, C-2'), 137.2 (C, C-8a), 123.5 (CH, C-6), 119.6 (C, C-4a), 114.1 (CH, C-5), 107.8 (CH, C-7), 104.6 (CH, C-1'), 103.9 (C, C-3), 59.0 (C-4-O-CH_3), 55.9 (C-8-O-CH_3); HR-ESI-MS: *m/z* 230.0808 $[M+H]^+$ (calcd for $C_{13}H_{11}NO_3$, 230.0804).

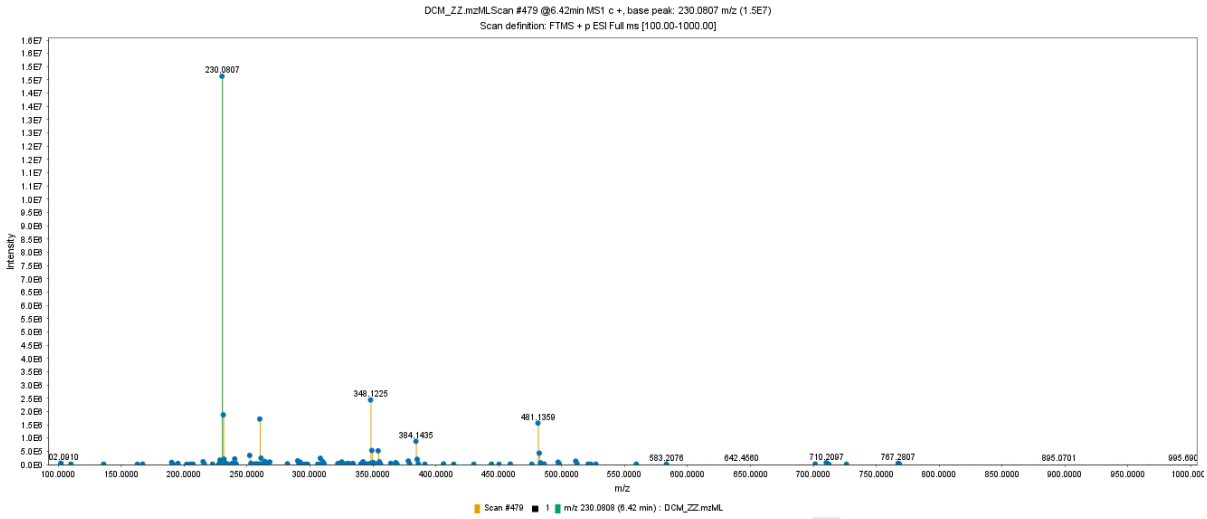

Fig. S113. HR-ESI-MS spectrum of compound **14.**

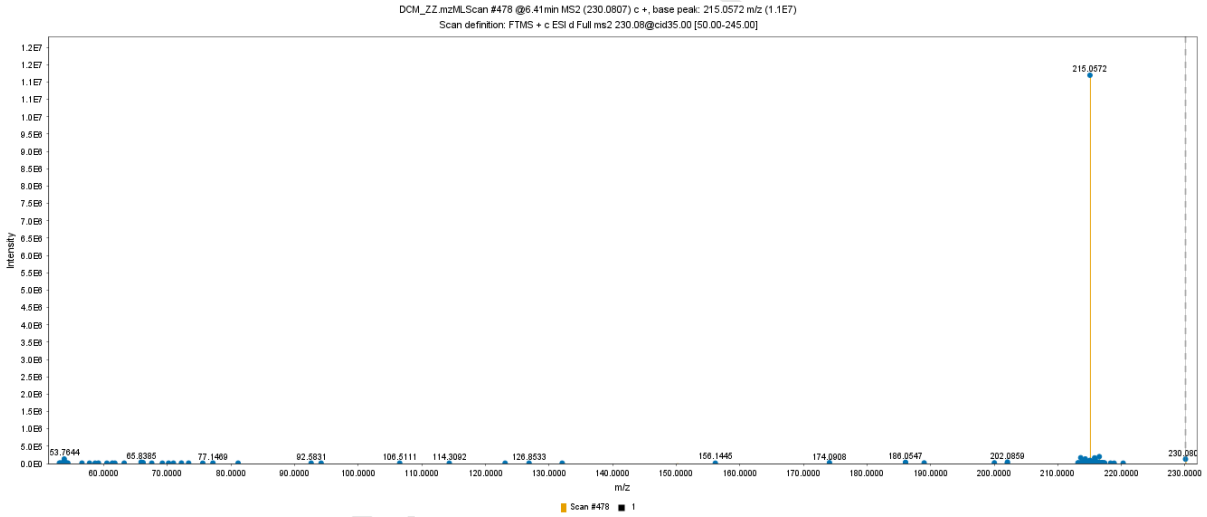

Fig. S114. HR-ESI-MS/MS spectrum of compound **14.**

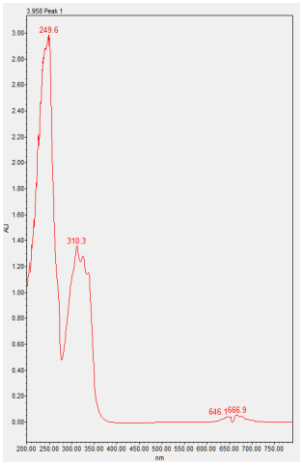

Fig. S115. UV spectrum of compound **14.**

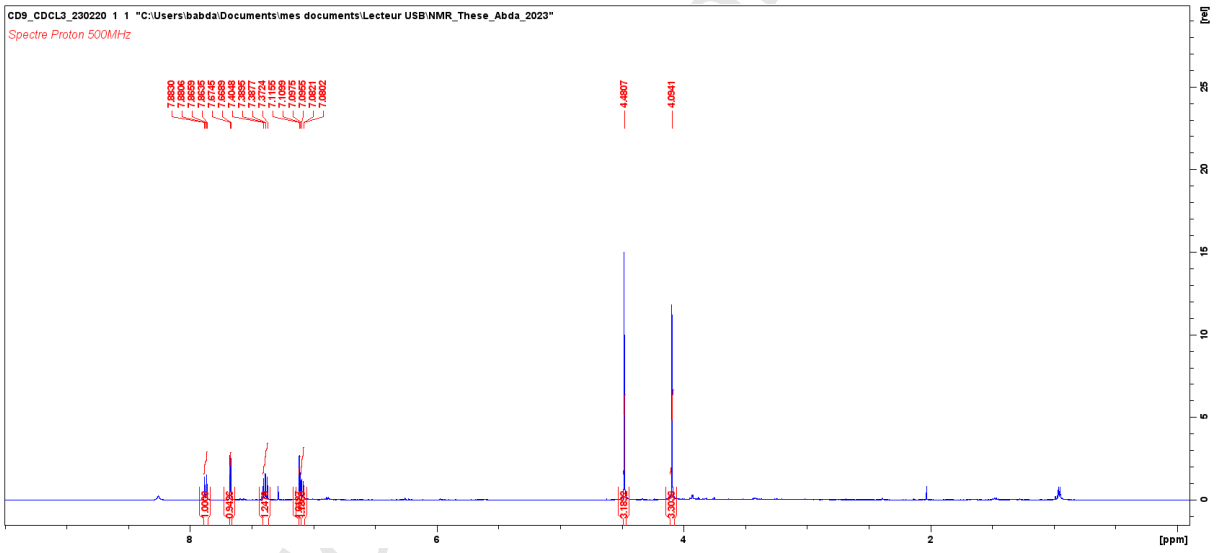

Fig. S116. ^{1}H-NMR (500 MHz, $CDCl_3$) spectrum of compound **14.**

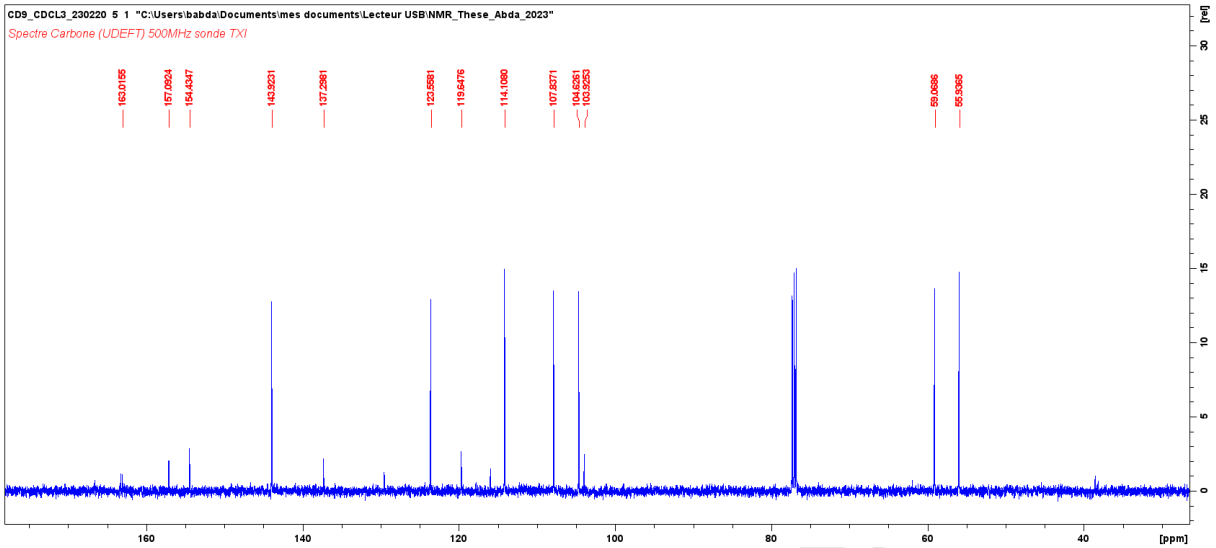

Fig. S117. ^{13}C-NMR (125 MHz, $CDCl_3$) spectrum of compound **14.**

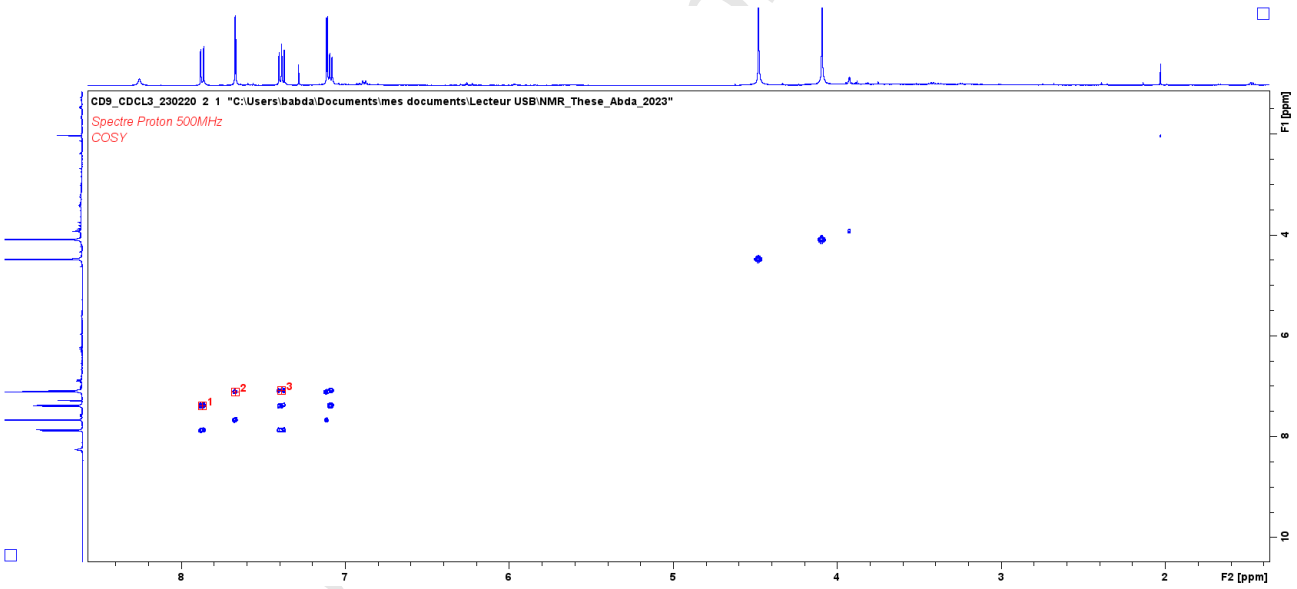

Fig. S118. ^{1}H-^{1}H COSY (500 MHz, $CDCl_3$) spectrum of compound **14.**

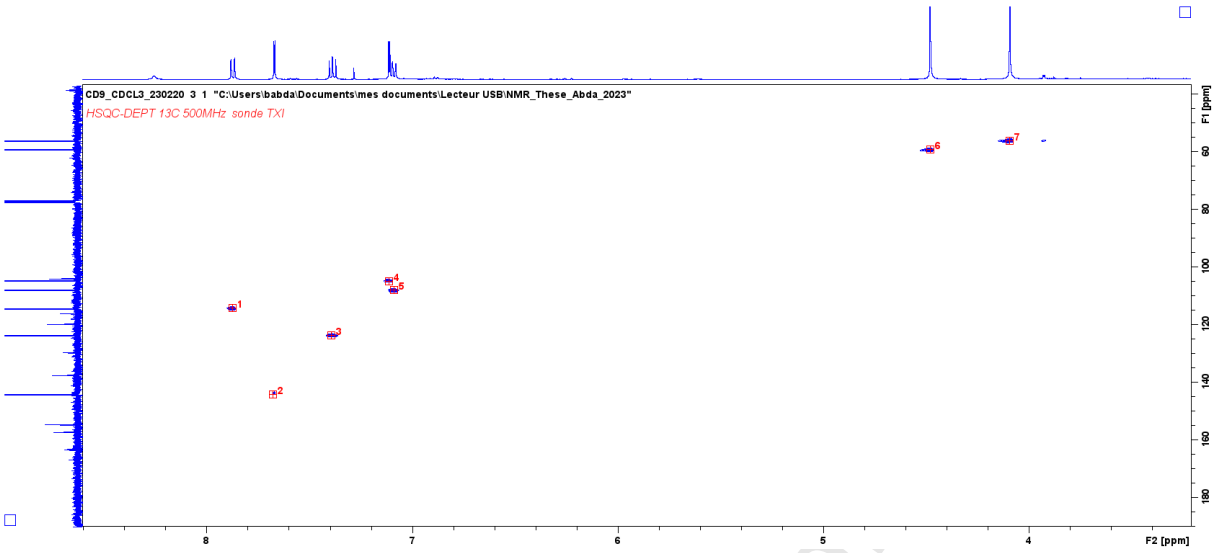

Fig. S119. HSQC-DEPT (500 MHz, $CDCl_3$) spectrum of compound **14.**

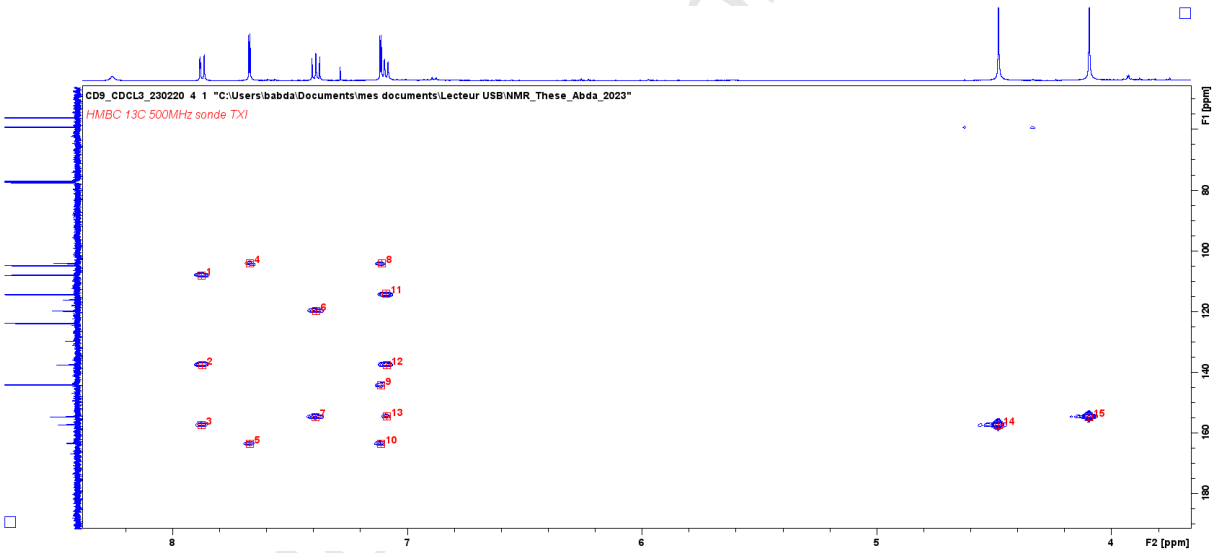

Fig. S120. HMBC (500 MHz, $CDCl_3$) spectrum of compound **14.**

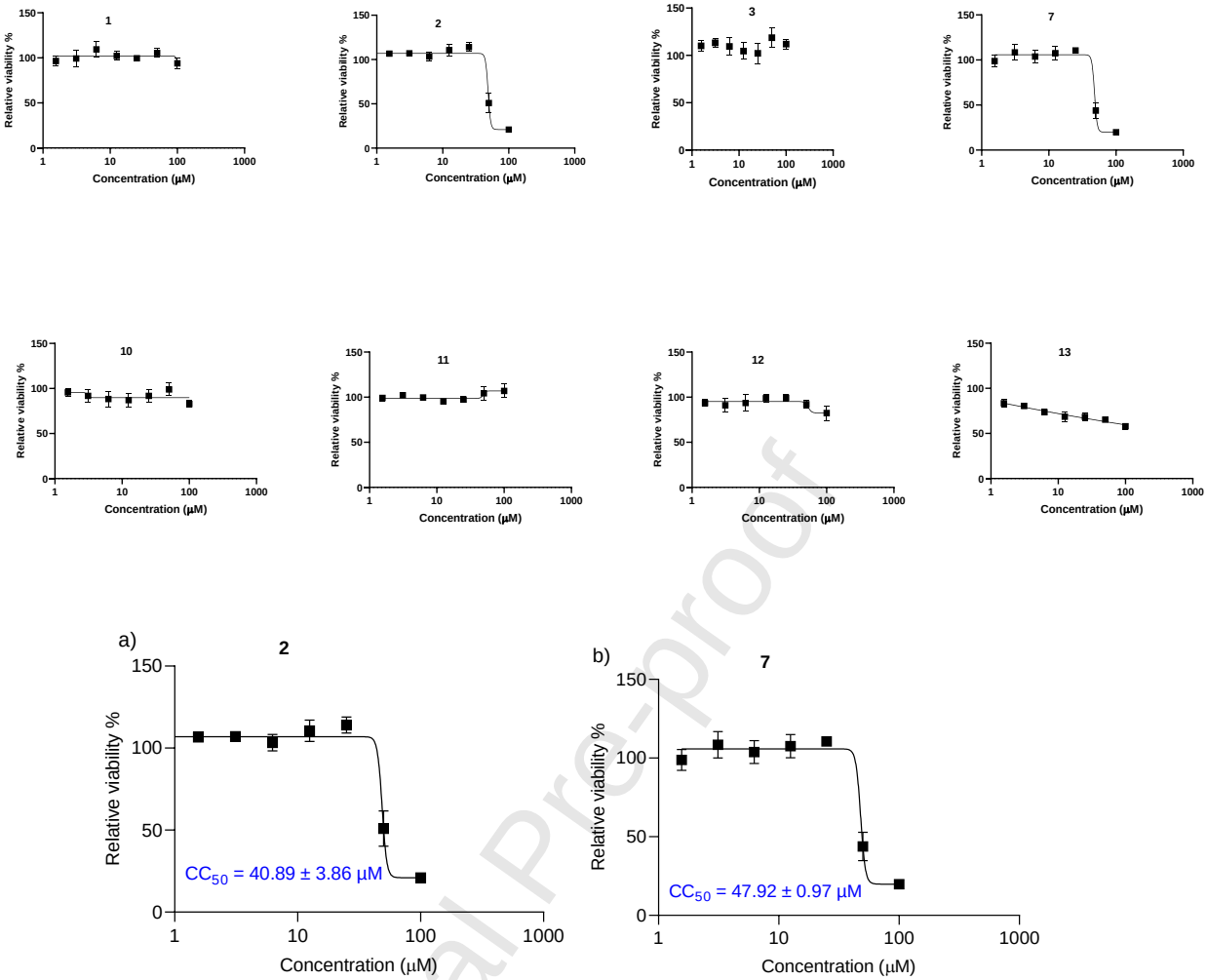

Fig. S121. Cytotoxicity evaluation of compounds **1**, **2**, **3**, **7**, **10**, **11**, **12**, and **13** on Huh-7 cells. For each sample, toxicity activity was determined with increasing concentrations. Huh-7 cells were incubated with each sample at the indicated concentrations for 24 h. The MTS assay was performed to monitor cell viability. Data are expressed relative to the control DMSO ($p < 0.001$, for 2 and 7). CC_{50} were only determined for compounds **2** and **7** and were expressed as mean ± SEM from three independent experiments, performed in triplicates.

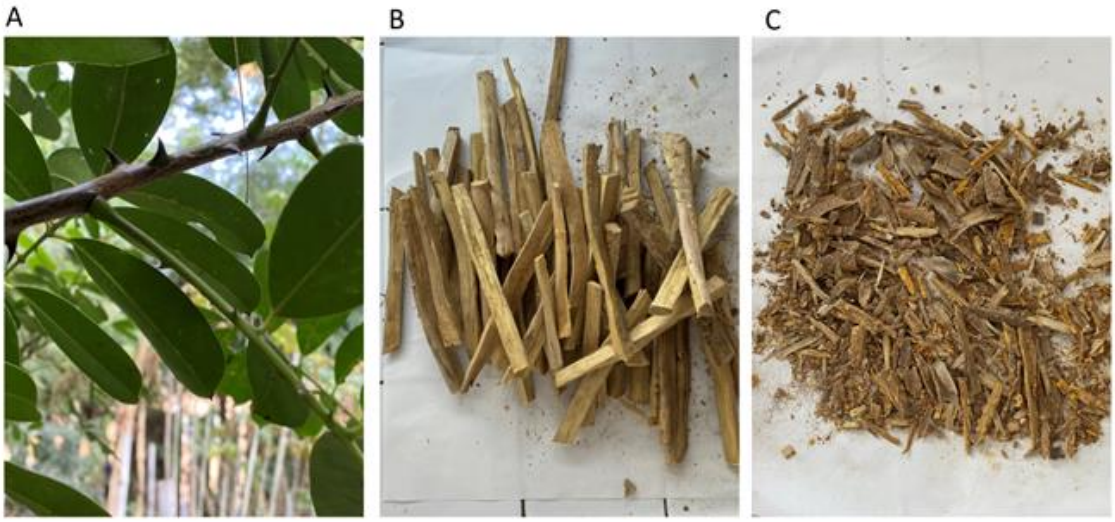

Fig. S122. Appearance of the (A) plant, (B) root and (C) root bark

Table S1. *Identification of chemical constituents in cyclohexane and dichloromethane extracts by comparison of the MS^2 data (Positive mode, HR-ESI-MS/MS) and matched with KEGG and PubChem databases by using Mzmine 3 (v3.3.0) software. Several levels of confidence were assigned (levels 1-4): level 1 (unambiguously identified metabolite, confirmed by at least two parameters of an authentic standard, such as retention time and MS/MS spectrum, purified compounds in the case of our study), level 2 (putatively annotated metabolite), level 3 (putatively annotated metabolite class) and level 4 (unidentified metabolite).*

Rt (min)	Isolated compounds	*m/z*	Major quasi-molecular ions	MS/MS fragments [*m/z*]	Molecular formula	Δ ppm	Δ mDa	Combined score (%)	RDBE	*w*	Area	Identification	Chemical class identified	Level of confidence
4.26		260.1275	$[M+H]^+$	66.1679	$C_{15}H_{17}NO_3$	-2.5	-0.6	75.17	8		6.9E3	-	Alkaloid	Level 3
4.51		206.0807	$[M+H]^+$	66.1679; 191.0573	$C_{11}H_{11}NO_3$	-2.4	-0.5	75.95	7		4.1E4	Edulitine	alkaloid	Level 2
4.56		356.1850	$[M+H]^+$	192.1014	$C_{21}H_{25}NO_4$	-1.9	-0.7	81.47	10		2.3E4	Glaucine	alkaloid	Level 2
4.67		260.1277	$[M+H]^+$	66.1679; 188.0702; 242.1171;	$C_{15}H_{17}NO_3$	-1.7	-0.4	82.89	8		2.8E4	Norsanguinine	Alkaloid	Level 2
4.76		679.5103	$[M+H]^+$	336.2277; 435.3328; 452.3604; 643.4906; 661.5000	$C_{35}H_{70}N_2O_{10}$	-0.1	-0.0	99.66	2		3.5E4	-	-	Level 4
4.76		701.4923	$[M]^+$	591.4539; 657.5030; 683.4820; 684.4858; 701.4905	$C_{47}H_{63}N_3O_2^+$	0.4	0.3	96.13	18		3.3E4	-	Alkaloid	Level 3
4.81		370.1645	$[M+H]^+$	149.0593; 165.0906; 188.0703; 206.0808; 290.0935; 321.1354; 337.1307; 352.1540	$C_{21}H_{23}NO_5$	-1.1	-0.4	88.55	11		1.3E5	Allocryptopine	Alkaloid	Level 2
4.92		302.1284	$[M+H]^+$	156.0804; 167.0601; 185.0707; 257.1073; 272.0819; 287.10491	$C_{19}H_{15}N_3O$	-1.4	-0.4	86.31	14		4.0E5	-	Alkaloid	Level 3
5.21	**11**	207.0649	$[M+H]^+$	n.f	$C_{11}H_{10}O_4$	-1.5	-0.3	85.01	7		4.7E4	Scoparone	Coumarin	Level 1
5.24		352.1538	$[M+H]^+$	294.1488; 309.1117; 321.1355; 337.1303;	$C_{21}H_{21}NO_4$	-1.6	-0.6	84.10	12		1.4E5	Ochotensine	Alkaloid	Level 2
5.45	**7**	348.1228	$[M]^+$	202.0531; 304.0970; 333.0994	$C_{21}H_{17}O_4N^+$	-2.2	-0.8	77.51	13		1.3E4	Chelerythrine	Benzo[c]phenanthridine alkaloid	Level 1

5.95	**12**	190.0862	$[M+H]^+$	130.0647; 158.0597; 175.0624	$C_{11}H_{11}NO_2$	-0.4	-0.1	98.90	7		3.8E5	4-methoxy-1-methylquinolin-2-one	Alkaloid	Level 1
6.25	**13**	260.0913	$[M+H]^+$	61.2607; 138.7265; 200.0703; 210.9619; 216.0653; 227.0572; 245.0674	$C_{14}H_{13}NO_4$	-1.8	-0.5	82.33	9		3.3E6	Skimmianine	Alkaloid	Level 1
6.42	**14**	230.0808	$[M+H]^+$	186.0546; 200.0266; 215.0572;	$C_{13}H_{11}NO_3$	-1.7	-0.4	82.83	9		1.4E6	γ fagarine	Alkaloid	Level 1
6.63		240.1954	$[M+H]^+$	93.06950; 121.1007; 156.1378; 167.1062; 222.1850	$C_{14}H_{25}NO_2$	-1.8	-0.4	82.06	3	2	1.6E5	-	Amide	Level 3
6.73		382.1280	$[M+H]^+$	201.0781; 305.1044; 323.0910; 336.1226; 354.1331	$C_{21}H_{19}NO_6$	-1.4	-0.5	85.99	13		2.1E5	Isoarnottianamide	Formamide	Level 2
6.94	**3**	248.1277	$[M+H]^+$	66.1679; 107.3148; 117.0332; 119.0488; 145.0281; 149.0594; 173.9689; 175.0385; 192.0651	$C_{14}H_{17}NO_3$	-1.8	-0.4	82.06	7	1	1.1E7	*Trans*-Fagaramide	Amide	Level 1
6.94		495.2480	$[M+H]^+$	175.0386; 248.1280	$C_{28}H_{34}N_2O_6$	-2	-1	80.03	13		6.9E6	Fagaramide dimer	Amide	Level 3
7.48	**4**	382.1281	$[M+H]^+$	201.0783; 305.1046; 323.0914; 336.12298; 354.1333	$C_{21}H_{19}NO_6$	-1.1	-0.4	88.53	13		9.0E5	Arnottianamide	Formamide	Level 1
7.50		763.2489	$[M+H]^+$	292.0733; 339.1098; 354.1330; 382.1282	$C_{42}H_{38}N_2O_{12}$	-1.1	-0.9	88.53	25		7.1E5	Arnottianamide or isoarnottianamide dimer	Formamide	Level 3
7.54	**8**	308.1756	$[M+H]^+$	91.0539; 106.0648; 116.0492; 134.0598; 165.1020; 201.1021; 265.1335; 290.1651	$C_{19}H_{21}N_3O$	-0.5	-0.2	94.72	11		1.2E6	Evodiamide	Alkaloid	Level 1
7.70		196.1693	$[M+H]^+$	66.1679; 95.0851; 123.0800; 140.1066	$C_{12}H_{21}NO$	-1.6	-0.3	83.9	3	2	1.3E5	*N*-(2-methylpropyl)octa-2,4-dienamide	Amide	Level 2
7.82		304.1443	$[M+H]^+$	118.0647; 144.0805; 161.0706; 187.0862; 261.1384; 287.1177	$C_{19}H_{17}N_3O$	-0.5	-0.2	94.65	13		6.9E5	Evodiamine	Alkaloid	Level 2
7.91	**9**	320.0914	$[M+H]^+$	76.2671; 277.0731; 305.0679	$C_{19}H_{13}NO_4$	-1.1	-0.4	88.78	14		5.3E5	Decarine	Alkaloid	Level 1
8.19		288.1129	$[M+H]^+$	66.1680; 167.0599; 227.2003; 243.0912; 273.0892	$C_{18}H_{13}N_3O$	-0.9	-0.3	90.87	14		1.8E5	Rutaecarpine	Alkaloid	Level 2
8.24		336.1228	$[M+H]^+$	276.1016; 291.1012; 304.0963; 321.0991; 323.7860	$C_{20}H_{17}NO_4$	-0.8	-0.3	92.3	13		9.1E4	-	Benzo[c]phenanthridine alkaloid	Level 3

8.33	**10**	364.1177	$[M+H]^+$	178.3727; 301.0734; 320.0917; 333.0993; 334.0709; 349.0942	$C_{21}H_{17}NO_5$	-0.8	-0.3	92.49	14		7.6E5	6-Oxochelerythrine	Benzo[c]phenanthridine alkaloid	Level 1
8.38		306.1601	$[M+H]^+$	134.0598; 161.0706; 175.0863; 199.0863; 263.1541; 289.1333	$C_{19}H_{19}N_3O$	0.0	0.0	99.6	12		6.4E5	-	Alkaloid	Level 3
8.51		318.2062	$[M+H]^+$	177.0543; 250.1433	$C_{19}H_{27}NO_3$	-0.6	-0.2	93.89	7	1	1.7E5	-	Amide	Level 3
8.58		222.1850	$[M+H]^+$	66.1680; 67.0537; 93.0695; 107.0851; 123.1164; 149.0957; 166.1223	$C_{14}H_{23}NO$	-1.2	-0.3	88.05	4	3	4.6E5	-	Amide	Level 3
8.63		288.2530	$[M+H]^+$	66.1680; 88.0753; 106.0859; 227.2002; 270.2424	$C_{16}H_{33}NO_3$	-1.2	-0.3	88.01	1	0	7.3E5	-	Amide	Level 3
8.96		408.1435	$[M+H]^+$	348.1226	$C_{23}H_{21}NO_6$	-1.7	-0.7	83.12	14		1.7E5	-	Benzo[c]phenanthridine alkaloid	Level 3
8.96		649.2436	$[M+H]^+$	304.0963; 333.0992; 348.1226	$C_{40}H_{32}N_4O_5$	-1.5	-1	85.03	27		1.8E5	-	Benzo[c]phenanthridine alkaloid	Level 3
9.37	**5**	224.2004	$[M+H]^+$	66.1679; 95.0489; 107.0852; 123.1165; 133.1008; 151.1114; 168.1380	$C_{14}H_{25}NO$	-2.3	-0.5	76.95	3	2	5.4E6	Pellitorine	Amide	Level 1
9.49		288.1956	$[M+H]^+$	88.0754; 106.0860; 227.2003; 270.2425	$C_{18}H_{25}NO_2$	-0.8	-0.2	92.02	7		6.2E4	-	Amide	Level 3
9.56		521.3364	$[M+H]^+$	213.0906; 248.1278; 347.1638; 375.1585; 420.2526; 448.2474; 503.3257	$C_{32}H_{44}N_2O_4$	-1.9	-1	80.63	12		3.0E5	-	Alkaloid	Level 3
9.69	**1**	593.1907	$[M+H]^+$	n.f	$C_{34}H_{28}N_2O_8$	-2	-1.2	80.33	22		2.6E5	-	Benzo[c]phenanthridine alkaloid	Level 1
9.78		471.3208	$[M+H]^+$	299.1639; 325.1430; 370.2373; 398.2320; 453.3104	$C_{28}H_{42}N_2O_4$	-2	-1	79.63	9		3.1E5	-	-	Level 4
10.05		532.1954	$[M+H]^+$	333.0991; 334.1070; 348.1225; 488.2059; 500.1690; 517.1723	$C_{30}H_{29}NO_8$	-2.3	-1.2	77.09	17		1.7E5	-	Benzo[c]phenanthridine alkaloid	Level 3
10.14		334.1070	$[M+H]^+$	290.0808; 302.0809; 304.0602; 318.0758; 319.0834	$C_{20}H_{15}NO_4$	-1.2	-0.4	87.75	14		3.7E5	Norchelerythrine	Benzo[c]phenanthridine alkaloid	Level 2
10.20	**6**	274.2162	$[M+H]^+$	66.1679; 93.0695; 107.0851; 119.0850; 133.1008; 168.1378; 175.1477; 201.1270; 224.8881	$C_{18}H_{27}NO$	-1.3	-0.4	86.66	6	5	3.6E6	γ sanshool	Amide	Level 1

10.43	**2**	350.1382	$[M+H]^+$	85.7472; 232.7949; 290.0938; 304.0970; 319.1203; 333.1125; 334.1076; 335.1148	$C_{21}H_{19}NO_4$	-1.5	-0.5	85.45	13		1.8E6	Dihydrochelerythrine	Benzo[c]phenanthridine alkaloid	Level 1
10.58		276.2319	$[M+H]^+$	93.0695; 107.0851; 121.1007; 135.1164; 177.1634; 194.1535; 206.1536; 220.1690	$C_{18}H_{29}NO$	-1.1	-0.3	88.57	5	4	5.1E5	Hazaleamide	Amide	Level 2
10.89		252.2318	$[M+H]^+$	66.1680; 93,0694; 119.0850; 133.1007; 161.1319; 179.1426; 196.1691	$C_{16}H_{29}NO$	-1.7	-0.4	83.5	3	2	2.4E5	-	Amide	Level 3
11.36		278.2475	$[M+H]^+$	93.0694; 107.0850; 121.1007; 135.0800; 152.1065; 167.1300; 177.1634; 205.1582; 222.1848	$C_{18}H_{31}NO$	-1.3	-0.4	86.85	4	3	2.9E5	-	Amide	Level 3
11.65		348.1227	$[M]^+$	85.2431; 304.0969; 315.0892; 318.0762; 319.0846; 333.0992; 349.1262	$C_{21}H_{18}NO_4^+$	-2.5	-0.9	74.63	14		1.6E6	-	Benzo[c]phenanthridine alkaloid	Level 3
12.06		564.2370	$[M+H]^+$	348.1224	$C_{35}H_{33}NO_6$	-1.9	-1.1	80.69	20		6.1E4	-	Benzo[c]phenanthridine alkaloid	Level 3
12.06		739.2638	$[M+H]^+$	196.0182; 303.2381; 533.1547; 616.3439; 634.3195; 701.9672	$C_{44}H_{38}N_2O_9$	-1.7	-1.2	83.33	27		8.8E4	-	Alkaloid	Level 3
12.26		398.2320	$[M+H]^+$	121.0278; 149.0230; 233.1169; 268.0965; 296.1278; 314.1383; 369.1930	$C_{24}H_{31}NO_4$	-1.5	-0.6	84.68	10		2.5E5	1-(3,4-diethoxybenzyl)-6,7-diethoxy-3,4-dihydroisoquinoline	Alkaloid	Level 2
12.33		280.2631	$[M+H]^+$	66.1680; 93.0695; 107.0850; 119.0850; 133.1007; 154.1221; 168.1378; 189.1633; 207.1739; 224.2005	$C_{18}H_{33}NO$	-1.5	-0.4	85.15	3	2	5.3E5	*N*-isobutyl-(2E,4E)-tetradecadienamide	Amide	Level 2
12.72		447.3938	$[M+H]^+$	275.2364; 346.3099; 374.3046; 389.3043; 429.3361	$C_{28}H_{50}N_2O_2$	-1.6	-0.7	83.67	5	4	8.1E4	-	diamide	Level 3
12.83		497.4091	$[M+H]^+$	224.2005; 269.1895; 323.2365; 351.2313; 396.3253; 424.3200; 479.3984	$C_{32}H_{52}N_2O_2$	-2.2	-1.1	78.27	8	7	2.2E5	-	diamide	Level 3
12.83		739.2638	$[M+H]^+$	205.2081; 334.3310; 348.1224	$C_{44}H_{38}N_2O_9$	-1.7	-1.2	83.33	27		1.7E5	-	Benzo[c]phenanthridine alkaloid	Level 3
13.22		256.2632	$[M+H]^+$	66.1680; 88.0753; 102.0909; 116.1065; 130.1221; 144.1378; 158.1534; 172.1693; 186.1849; 200.2005; 214.2157	$C_{16}H_{33}NO$	-1.2	-0.3	87.67	1	0	1.5E5	*N*-(2-methylpropyl)dodecanamide	Amide	Level 2
13.22		294.2788	$[M+H]^+$	70.3319; 95.0851; 109.1008; 133.1008; 182.1534;203.1795; 221.1896; 238.2161	$C_{19}H_{35}NO$	-1.2	-0.4	87.56	3	2	4.4E4	-	Amide	Level 3
13.28		547.4248	$[M+H]^+$	183.1165; 247.1478; 274.2162; 312.2318; 373.2521; 401.2469; 446.3412; 474.3357; 529.4141	$C_{36}H_{54}N_2O_2$	-1.9	-1	81.17	11	10	3.0E5	-	diamide	Level 3

w: number of double bonds on aliphatic chain of polyunsaturated amides and diamides

RDBE: Ring Double Bond Equivalents

-: no identification

n.f: no fragmentation (compound covered by another)

Graphical Abstract

Zanthoxylum zanthoxyloides (Lam.) B.Zepernick & Timler

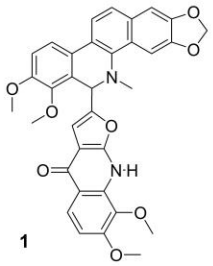

1

***L. mexicana mexicana*:**
IC_{50} = 0.14 µM

***T. brucei brucei*:**
IC_{50} = 0.36 µM

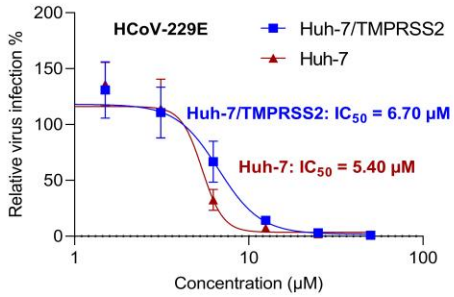

Highlights

- *Zanthoxylum zanthoxyloides* demonstrated antiparasitic and anti-coronavirus activities.
- An original benzophenanthridine alkaloid was isolated along with 13 known compounds.
- Zanthoxyloithrine, the novel alkaloid, showed promising antimicrobial activities.
- Dereplication and molecular network analyses were performed on the apolar extracts.
- Alkaloids and polyunsaturated amides were putatively identified by this dereplication.